Titre: Title:	Electrochemical Studies on the Biopigment Eumelanin
Auteur: Author:	Ri Xu
Date:	2020
Type:	Mémoire ou thèse / Dissertation or Thesis
Référence: Citation:	Xu, R. (2020). Electrochemical Studies on the Biopigment Eumelanin [Thèse de doctorat, Polytechnique Montréal]. PolyPublie. https://publications.polymtl.ca/5431/

POLYTECHNIQUE MONTRÉAL

affiliée à l'Université de Montréal

Electrochemical Studies on the Biopigment Eumelanin

RI XU

Département de génie physique

Thèse présentée en vue de l'obtention du diplôme de *Philosophiae Doctor*

Génie physique

Août 2020

POLYTECHNIQUE MONTRÉAL

affiliée à l'Université de Montréal

Cette thèse intitulée :

Electrochemical Studies on the Biopigment Eumelanin

présentée par **Ri XU**

en vue de l'obtention du diplôme de *Philosophiae Doctor*

a été dûment acceptée par le jury d'examen constitué de :

Jolanta-Ewa SAPIEHA, présidente

Clara SANTATO, membre et directrice de recherche

William SKENE, membre

Young Jo KIM, membre externe

ACKNOWLEDGMENTS

First, I would like to thank my supervisor, Clara Santato, for offering me the opportunity to do PhD research with financial support, conference experience, and supervision. I thank her for inspiring passion, initiative, presentation and rigor. I am grateful to the jury members, Prof. J. Sapieha, Prof. W. Skene and Prof. Y.-J. Kim, for their time, interest, and inspiring comments on my work. I believe the revision of the thesis has brought out the best in me with respect to doing science.

At the same time, I would like to thank Prof. Francesca Soavi, who has contributed her solid knowledge to my PhD work. I am also grateful to Prof. A. Pezzella for providing the eumelanin materials. I am grateful to both of them for providing hands-on experience and insights.

I am grateful to technical support from D. Gingras, P. Plamondon, Dr. J. Lefèbvre and Ms. M.-H. Bernier, P. Moraille, Y. Drolet, Christophe Clément, Mikaël Leduc, and Daniel Chartrand.

I am very grateful for mediating efforts by the coordinators of Engineering Physics, Prof. A. Rochefort, Prof. S. Francoeur and Prof. Y.-V. Peter. I am very grateful to the officers, professors, research fellows working on aspects of ethics in both Polytechnique and University of Montreal. Here I specially thank E. Smith, G. Patience, G. Guay, M. Villiard, G. De Langavant, J. Poupart, C. Roehrig.

I am thankful for the guidance on improving my mental health by Iona, Jee, and Dina. Here I specially thank my lover Jee for providing his unique artistic love, care, inspiration and new insights in my life.

I would like to thank all my colleagues who helped me: Prajwal, Jonathan, Eduardo, Federico, Côme, Julien, Shiming, Xiang, Martin, Fanny, Tania, Tian, Zhaojing, Abdelaziz, Fred, Dieudonné, Francis, Manuel, Dominique, Nicolò, Jo'Elen, Arun, Yang, Xin, Elizabeth and Ben. Among my friends, I especially wish to thank Annie, Erik, Natasha, Salim, Alfredo, Yanqi, Weifeng, Sorouche, Orlando and Mayada. I thank my family and my in-laws for their help and support and for making it possible for me to travel.

ABSTRACT

To meet the growing global energy demand, we need to fabricate energy storage devices for multiple future needs. Sustainability motivates the search for abundant, non-toxic, low-cost materials/chemicals for low-embedded energy and eco-friendly energy storage devices. Redox active organic materials extracted from natural sources (bio-sourced) are intriguing for such energy storage devices. The quinone-based brown-black biopigment eumelanin is a promising candidate for bio-sourced organic electrode materials. Eumelanin features interesting functional properties including broadband optical absorption, redox activity (electron transfer properties), and antioxidant properties (through metal ion chelation and radical scavenging). Among these functional properties, electron transfer is essential for energy storage as well as to exploit the antioxidant properties of the biopigment.

Natural eumelanin is composed of two building blocks, 5,6-dihydroxyindole (DHI) and 5,6-dihydroxyindole-2-carboxylic acid (DHICA). Natural eumelanin features chemical heterogeneity, which is recognized as the main challenge for studying its redox properties. In this work, we fabricated chemically controlled eumelanins from the building blocks, i.e. DHI-melanin, DHICA-melanin, and DHI-DHICA-melanin in controlled ratios. The main goal of this work is to shed light on the redox properties of eumelanin using electrochemical methods.

In Article 1 and Article 3, we conducted cyclic voltammetry and scanning electron microscopy (SEM) on eumelanin, aiming at understanding and further controlling its electrochemical properties based on the effect of metal ions, pH values of the electrolytes, etc. In Article 2, we studied the effect of light irradiation on the energy storage properties of eumelanin, aiming at enhancing its energy storage properties by the sustainable source solar light. Indeed, ca 50% enhanced capacity/capacitance of eumelanin is observed under light irradiation. In Article 3, the antioxidant/prooxidant dual properties of eumelanin are studied by exposing the samples to reactive oxygen species (ROS) and transition metal ions. Cyclic voltammetry, X-ray photoelectron spectroscopy (XPS) and SEM are used to characterize such effects. Article 3 aims at understanding the dual properties of eumelanin and proposing possible methods to suppress the prooxidant properties of eumelanin, which is reported to be the main cause of neurondegeneration-related diseases.

Finally, in General Discussion and Literature Review, to explain the proton-assisted electron transfer processes of eumelanin, we put forward the concept *local pH* that is induced by the applied potential. The local pH vs. pK_a values can be the key to explain the different electrochemical data of eumelanin in literature and this work, to build (supra)molecular structure-relationship properties, and to further synthesize eumelanin materials with controlled properties. Such a concept may also have an impact on investigating other materials with proton-assisted electron transfer processes.

RÉSUMÉ

Pour répondre à la demande énergétique mondiale croissante, nous devons fabriquer des dispositifs de stockage d'énergie pour de multiples besoins futurs. La durabilité motive la recherche de matériaux / produits chimiques abondants, non toxiques et bon marché pour des dispositifs de stockage d'énergie à faible consommation d'énergie et dont l'utilisation n'a pas d'impact négatif sur l'environnement. Les matières organiques actives redox extraites de sources naturelles (bio-sourcées) sont intrigantes pour de tels dispositifs de stockage d'énergie. L'eumélanine qui est un bio-pigment brun-noir à base de quinone est un candidat prometteur pour les électrodes organiques conçus à partir de matériaux provenant des bio-sources. L'eumélanine présente des propriétés fonctionnelles intéressantes, notamment l'absorption optique à large bande, l'activité redox (propriétés de transfert d'électrons) et des propriétés antioxydantes (par chélation des ions métalliques et piégeage des radicaux). Parmi ces propriétés fonctionnelles, le transfert d'électrons est essentiel pour le stockage d'énergie ainsi que pour exploiter les propriétés anti-oxydantes du biopigment.

L'eumélanine naturelle est composée de deux éléments de base, le 5,6-dihydroxyindole (DHI) et l'acide 5,6-dihydroxyindole-2-carboxylique (DHICA). Cependant, son hétérogénéité chimique est reconnue comme le principal défi pour l'étude de ses propriétés redox. Dans cette thèse de doctorat, nous avons fabriqué des eumélanines contrôlées chimiquement à partir leurs éléments constitutifs, à savoir DHI-mélanine, DHICA-mélanine et DHI-DHICA-mélanine dans des rapports contrôlés. L'objectif principal de ce travail est de faire la lumière sur les propriétés redox de l'eumélanine à l'aide de méthodes électrochimiques.

Dans l'article 1 et l'article 3, nous avons caractérisé l'eumélanine par les techniques de voltampérométrie et une microscopie électronique à balayage (SEM) dans le but de comprendre et de contrôler davantage ses propriétés électrochimiques basées sur l'effet des ions métalliques, les valeurs de pH des électrolytes, etc. À l'article 2, nous avons étudié l'effet de l'irradiation lumineuse sur les propriétés de stockage d'énergie de l'eumélanine, dans le but d'améliorer lesdites propriétés par la lumière solaire qui est considérée comme source d'énergie durable. En effet, une augmentation de la capacité / capacité d'environ 50% de l'eumélanine est observée sous irradiation lumineuse. Dans l'article 3, les doubles propriétés anti-oxydantes / pro-oxydantes de l'eumélanine sont étudiées en exposant les échantillons à des ROS (les espèces réactives de l'oxygène) et des

ions de métaux de transition. La voltampérométrie, la spectroscopie photo-électronique aux rayons X (XPS) et la SEM sont utilisées pour caractériser ces effets. L'article 3 vise à comprendre les propriétés duales de l'eumélanine et à proposer des méthodes possibles pour supprimer les propriétés pro-oxydantes de l'eumélanine, qui serait la principale cause des maladies liées à la neurodégénérescence.

Enfin, dans la discussion générale, pour expliquer les processus de transfert d'électrons assisté par protons de l'eumélanine, nous avons proposé le concept de *pH local* induit par le potentiel appliqué. Les valeurs locales de pH vs pKa peuvent être la clé pour expliquer les différentes données électrochimiques de l'eumélanine dans la littérature et ce travail, pour construire leur relation avec la structure supramoléculaire de l'eumélanine afin de synthétiser davantage les dispositifs bioélectroniques de ce type de matériau avec des propriétés bien contrôlées. Un tel concept pourrait également avoir un impact sur l'étude d'autres matériaux en considérant les processus de transfert d'électrons assistés par les protons.

TABLE OF CONTENTS

LIST OF TABLES

LIST OF FIGURES

LIST OF EQUILIBRIA AND REACTIONS

LIST OF EQUATIONS

LIST OF SYMBOLS

pH_{local}	Local pH
pH_{bulk}	Bulk pH (of the electrolyte)
HA	Weak acid
H^+	Proton
A^-	Anion of the weak acid
K_a	Association constant of an acid
pK_a	Negative logarithm of K_a
ΔE_{unb}	Unbuffered potential shift
$[A^-]_{initial}$	Initial concentration of anions
$[HA]_{initial}$	Initial concentration of the weak acid
E_b	Boundary potential
E_{bn}	Negative boundary potential
E_{bp}	Positive boundary potential
K_b	Association constant of a base
i	Electrochemical current
V	Electrochemical potential
t	Time
q	Capacity
C	Capacitance

i_{an}	Anodic current
i_{ca}	Cathodic current
q_{an}	Anodic capacity
q_{ca}	Cathodic capacity
q_{ox}	Oxidation capacity
q_{red}	Reduction capacity
Z	Electrochemical impedance
Re(Z)	Real part of the impedance
Im(Z)	Imaginary part of the impedance
E_{redox}	Redox potential
E_{app}	Applied potential
$E_{ox(onset)}$	Onset oxidation potential
$E_{ox(end)}$	End oxidation potential
$E_{red(onset)}$	Onset reduction potential
$E_{red(end)}$	End reduction potential
E^*	The potential corresponding to local pH = 7
A	The amount of product of degradation of 2-deoxy-D-ribose detected by thiobarbituric acid assay

LIST OF ABBREVIATIONS

PAET	Proton-assisted electron transfer
DHI	5,6-Dihydroxyindole
DHICA	5,6-Dihydroxyindole-2-carboxylic acid
DOPA	Dihydroxyphenylalanine
H2Q	Hydroquinone
SQ	Semiquinone
Q	Quinone
HQI	Protonated quinone imine
NHE	Normal hydrogen electrode
Ag/AgCl	Silver/silver chloride (reference) electrode
SCE	Saturated calomel electrode
MSE	Mercury sulfate electrode
ROS	Reactive oxygen species
THAM	Tris(hydroxymethyl)aminomethane
ORR	Oxygen reduction reaction
OER	Oxygen evolution reaction
PTFE	Polytetrafluoroethylene
SEM	Scanning Electron Microscopy
SE	Secondary Electron

BSE	Backscattered Electron
EIS	Electrochemical Impedance Spectroscopy
BE	Binding energy
KE	Kinetic energy
XPS	X-ray Photoelectron Spectroscopy
FE-ESEM	FEI Environmental Scanning Electron Microscope
AM	Air Mass
UV-vis	Ultraviolet-visible
ITO	Indium tin oxide
PD	Parkinson’s Disease
Dxrb	2-deoxy-D-ribose
SOD	Superoxide dismutase

LIST OF APPENDICES

CHAPTER 1 INTRODUCTION

1.1 Energy storage of eumelanin

1.1.1 Context: “green” electrochemical energy storage based on bio-sourced materials

The United Nations defines sustainability as “the ability to meet the needs of the present generation without compromising the ability of future generations to meet their own needs”. Global energy demand is predicted to rise by 1.3% each year until 2040, which would result in yearly increases in greenhouse emissions [1]. To find a compromise between the increasing energy demand and sustainable development goals, we need to develop sustainable energy conversion and storage devices. Such sustainable devices are based on components that are abundant, non-toxic, low-cost, and bio-sourced or synthesized in accordance with the principles of green chemistry. Examples of such components in energy storage include organic electrode materials and aqueous electrolyte solutions [2].

Organic electrode materials are based on redox-active organic compounds. Charge transfer (redox) properties of organic materials are the underpinning for their use in energy storage. With respect to inorganic electrode materials, they offer a diversity of chemical structures and mechanical flexibility [3]–[5]. Within organic materials, bio-sourced (i.e. extracted from natural sources) organic materials are receiving increasing attention [6]. Biodegradable and biocompatible materials are also increasingly investigated. Due to the chemical and physical disorder of bio-sourced materials, their functional properties, including charge transfer properties, are largely unknown.

Quinone-based materials are one of the promising candidates as bio-sourced electrode materials for energy storage [4], [7], [16]–[19], [8]–[15]. Melanin, a type of quinone-based material, has subcategories including eumelanin (brown-black), pheomelanin and neuromelanin.

Eumelanin, the material of interest in this thesis, has various intriguing properties, such as broadband UV–vis absorption, hydration dependence of the electrical response, redox activity and antioxidant behavior [20]–[24]. Eumelanin is made up of two building blocks, 5,6-dihydroxyindole (DHI) and 5,6-dihydroxyindole-2-carboxylic acid (DHICA) [25]–[27].

1.1.2 Fundamental properties of eumelanin

1.1.2.1 Types of eumelanin

Synthetic eumelanins polymerized from building blocks DHI and DHICA are chemically controlled eumelanins, called *DHI-melanin*, *DHICA-melanin* and *DHI-DHICA-melanin* (as a function of the ratio of the two building blocks in the final materials).

Sepia melanin is a type of natural eumelanin extracted from cuttlefish. Sepia melanin takes the shape of granules of various sizes at the microscale.

DOPA-melanin is a synthetic eumelanin polymerized from DOPA (dihydroxyphenylalanine) or tyrosine [28]. Polydopamine is polymerized from dopamine, which, unlike DOPA, does not have a -COOH functional group. Polydopamine has the same chemical structure as DHI-melanin [29].

1.1.2.2 Hydration dependence of the electrical response and redox properties of eumelanin

In ambient conditions, eumelanin absorbs water. The electrical response of eumelanin has a strong hydration dependence [21], [28], [30]–[32]. In eumelanin, quinones (Q, as the oxidized form of the building blocks) and hydroquinones (H2Q, as the reduced form, also called catechols or polyphenols) in the presence of water become semiquinones and protons (Figure 1.1). Semiquinone forms of eumelanin have been proposed as the main sources of mobile electronic charge carriers in eumelanin [32], [33]. Electronic transport is enabled by π-π interactions at the intramolecular and intermolecular levels.

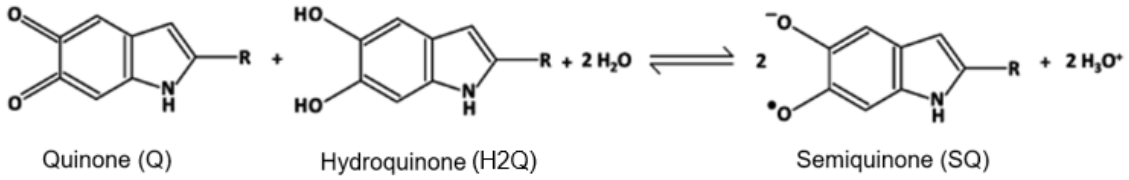

Figure 1.1 Comproportionation equilibrium in eumelanin. -R: -H (for DHI), or -COOH (for DHICA). Adapted from [32]. A comproportionation reaction is defined as a chemical reaction where two reactants, each containing the same chemical element but with a different oxidation number, form a product in which the element involved reaches the same oxidation number.

Eumelanin is redox-active. The quinone-based materials are reported to feature a 2-electron process between their redox forms Q and H2Q in aqueous solutions [34][7][15].

1.1.2.3 Disordered chemical structures and optical absorptions of eumelanin

A few chemical disorder models (related to molecular structures) and geometric disorder models (related to supramolecular structures) are proposed to explain the broadband optical absorption of eumelanin [20], [35], [36] (Section 3.8). The chemical disorder model hypothesizes different chemical species in eumelanin. For example, there are different building blocks (DHI or DHICA), coexisting redox forms, oligomers composed of different numbers of building blocks that are polymerized at different sites (Figure 1.2).

We may note from Figure 1.2 that the majority of the disorder models in the literature are merely DHI-based oligomers [37]. Indeed, DHI building blocks have multiple polymerization sites that enable the formation of chemically disordered oligomers. The convolution of the optical features of each chemical species makes the total optical absorption broad (Section 3.8) [35], [37]–[40]. The geometric disorder model hypothesizes that the oligomers of eumelanin are packed in different geometric forms. Therefore, excitonic coupling can occur and vary among these geometric disordered structures [41]–[45].

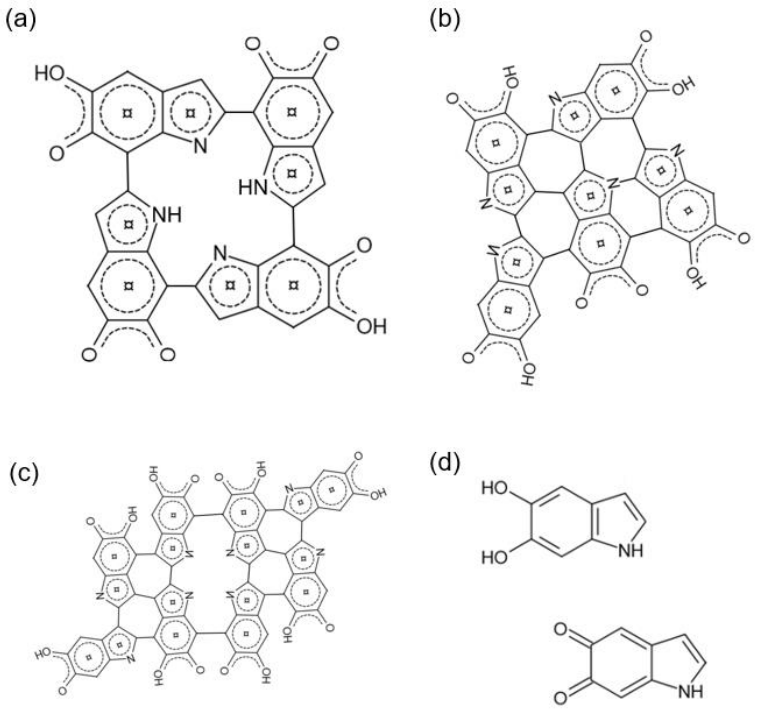

Figure 1.2 Proposed chemically disordered molecular structures of eumelanin [41]. (a) Tetrameric model [39][38]. (b) Pentameric model and (c) Octameric models [46][47] (d) Monomeric model [48].

1.1.2.4 Metal binding/chelation

Metal ions bind/chelate eumelanin at different sites [49]. For example, monovalent metal ions, such as Na^+, K^+, mainly bind the -COO^- (when available) and amine group [23], [50]. Mg^{2+} seems to preferably chelate quinone groups and -COO^- [23], [50]. Cu^{2+} and Fe^{3+} bind/chelate all three functional groups [23].

1.1.3 Energy storage devices based on eumelanin

Energy storage devices based on quinone-based materials are mainly divided into supercapacitor and batteries. As far as the voltammetric studies are concerned, there are eumelanins characterized by quasi-box shaped volrammetric features as well as with distinguishable electrochemical features (Section 7.4.2). Supercapacitors are usually fabricated using eumelanins featured by quasi-box shaped voltammograms (Section 1.1.3.2). Batteries make use of the eumelanin with distinguishable features, where the cell potential can be determined by the difference of redox potentials of anode and cathode materials (Section 1.1.3.1).

1.1.3.1 Electrochemical potentials of eumelanin

The literature reports various electrochemical potentials for eumelanin voltammograms (Section 2.2.1). Even with the same type of eumelanin, different electrochemical potentials are reported (Section 7.4.2). An important factor that affects the electrochemical potentials is the nature of the metal ions present in the electrolyte, especially multivalent metal ions. For example, monovalent cations such as Li^+, NH_4^+, Na^+ seem to contribute pseudocapacitive features and therefore electrodes to supercapacitors [51][16][52]. In the presence of Mg^{2+}, the voltammograms of Sepia melanin feature distinguishable potentials due to chelation (Section 2.2.8.2) [50].

1.1.3.2 Faradaic processes and pseudocapacitive materials for supercapacitors

Faradaic processes are electron transfer processes taking place at certain applied potentials [53]. Faradaic processes usually give distinct peaks in the cyclic voltammograms. Capacitive processes make use of materials that store charge through the electrostatic mechanism: electrical double layers form at the interface between the material and the electrolyte and are characterized by box-shaped cyclic voltammograms (Section 3.2.3.2). When redox-active materials are used as working electrodes, Faradaic processes are dominant. The redox-active materials that feature electrochemical signatures similar to capacitive materials can be termed *pseudocapacitive* [54]. In

such cases, the voltammograms are in *quasi-box shape* [16]. Kumar et al. reported on pseudocapacitive DOPA-melanin electrodes for supercapacitors [51].

1.1.3.3 Challenges for energy storage devices based on eumelanin

The main challenges for development of eumelanin-based energy storage devices are therefore: the unestablished electrochemical potentials, the improvement of capacity/capacitance, at the same time improving the cycling stability and potential limits of eumelanin [55]. *Cycling stability* means how much energy storage the material/device retains after thousands of cycles of charging-discharging. The best performance obtained with quinone-based materials so far is a supercapacitor based on polyaniline−benzoquinone−hydroquinone electrodes with high cycling stability (>50 000 cycles) and high pseudocapacitance (1500 F g^{-1}). In the case of supercapacitor based on eumelanin, there seems to be a trade-off between its capacitance and cycling stability [51]. Cycling stability is related to many factors, such as the possible changing structure of eumelanin under electrical bias, the adhesion properties to the current collector and the processability of eumelanin (Section 7.5).

1.2 Neuromelanin and its antioxidant/prooxidant dual behavior

1.2.1 The structure of neuromelanin

Pheomelanin is a yellow-red melanin featuring prooxidant behavior [56]. *Neuromelanin* has a core (pheomelanin)/shell (eumelanin) structure. Neuromelanin is mainly present in the neuron cells of the *substantia nigra* and *locus coeruleus* of the human brain [57]. Neuromelanin is proposed to have dual behavior towards neurodegeneration: antioxidant and prooxidant. The antioxidant eumelanin shell shields the prooxidant pheomelanin core, to protect neuron cells from oxidative stress [57]. Therefore, the antioxidant role of neuromelanin is mainly played by the shell material eumelanin [22]–[24].

1.2.2 Antioxidant and prooxidant dual properties

1.2.2.1 Definition of antioxidant and prooxidant properties

Oxidative stress is defined as “the imbalance between oxidants and antioxidants in favor of the oxidants produced at an elevated rate during pathophysiological conditions, potentially leading to damage” [58], [59]. *Antioxidant* compounds are natural or synthetic substances that may prevent or delay oxidative cell damage caused by physiological “oxidants” [60]–[62]. *Prooxidant*

compounds refer to biochemicals that induce oxidative stress or damage either by the generation of ROS or by inhibiting antioxidant systems [59], [60].

1.2.2.2 Reasons for dual properties of neuromelanin/eumelanin

Neuromelanin or eumelanin and other (hydro)quinone-based materials are reported to have antioxidant and prooxidant dual properties [59], [62]–[64]. The prooxidant properties of eumelanin are attributable for a variety of reasons. For example, one reason is that eumelanin reduces O_2 to generate $O_2^{\bullet-}$ and H_2O_2 [65]–[73]. The presence of a certain amount of H_2O_2 is important for human life [74], [75]. Fe^{3+} and Cu^{2+} have a synergetic effect with H_2O_2 and eumelanin. Taking Fe^{3+} for example, eumelanin can reduce Fe^{3+} to Fe^{2+} that generates $^{\bullet}OH$ by Fenton reaction ($Fe^{2+} + H_2O_2 \rightarrow Fe^{3+} + {}^{\bullet}OH + OH^-$) [76]–[82]. A certain amount of H_2O_2 and $^{\bullet}OH$ may cause neurodegeneration. On the other hand, neuromelanin can chelate metal ions and scavenge radicals to protect neuron cells, which are antioxidant properties [22], [23].

1.3 Motivations and objectives for the present work

Redox potentials are not only important for energy storage and antioxidant properties, but also for understanding various biological functions and designing electronic devices [83].

The main objective of this thesis is to study the redox properties of eumelanin by using electrochemical methods. By understanding the redox properties of eumelanin, we can suggest directions to improve its energy storage properties as well as optimize the use of its antioxidant/prooxidant dual properties.

1.3.1 To understand redox properties of eumelanin

To understand the electrochemical properties of eumelanin, a key step is to identify the different contributions of building blocks, i.e. DHI and DHICA. The 1st objective is to investigate the voltammetric properties of chemically controlled eumelanins and natural eumelanin in aqueous electrolytes, paying attention to the effects of metal ions (including monovalent cations NH_4^+, Na^+, K^+ and transition metal ions Cu^{2+}).

1.3.2 To investigate a sustainable method to improve energy storage properties

With respect to the need for sustainable energy conversion and storage devices, we propose to develop a sustainable method to improve the energy storage properties of eumelanin (Section 1.1.1). With its broadband optical absorption properties, eumelanin potentially absorbs a high amount of light energy and possibly converts it into electrochemical energy. The 2nd objective is to explore the possibility to enhance the energy storage properties of eumelanin under simulated solar light irradiation. The effect of light is to be explored by using various kinds of current collectors: two-dimensional (2D) transparent conductive glass and three-dimensional (3D) carbon paper.

1.3.3 To gain insights into antioxidant/prooxidant dual properties of neuromelanin/eumelanin

The antioxidant and prooxidant properties of eumelanin are related to its redox properties. For example, the antioxidant properties of eumelanins are based on their reductive properties for reactive oxygen species (ROS), i.e. their ability to be oxidized by H_2O_2 or $^{\bullet}OH$ [60], [84]. The antioxidant properties of quinone-based materials are proposed to be quantified by their oxidation capacity (anodic capacity) and oxidation potentials in cyclic voltammograms [85]–[88]. Cyclic voltammetry is a sensitive technique that can quantify the effect of transition metal ions at physiological (very low) concentrations [70], [78], [89].

To understand the mechanisms of how the antioxidant/prooxidant dual behavior of eumelanin take place is paramount to devising strategies on how to cope with neurodegeneration-related diseases [90].

The 3rd objective is to study the antioxidant vs. prooxidant behavior of neuromelanin using cyclic voltammetry [91]. In this work, we model neuromelanin by using chemically controlled eumelanin. The effects of transition metal ions and reactive oxygen species (ROS) (e.g. H_2O_2 and $^{\bullet}OH$) at their physiological concentrations, as well as their synergistic effects have to be considered [24], [62], [63].

1.4 Organization of the present work

The structure of the present thesis can be described as follows. Chapter 1 introduces the context and field together with the motivations and objectives of this thesis.

Chapter 2 critically reviews the literature, specifically on insights on synthesis and electrochemical properties of eumelanin.

Chapter 3 describes the chemical synthesis and storage conditions of the samples as well as the characterization techniques used in this thesis.

The principal results of the electrochemical properties of eumelanin are presented in the form of three peer-reviewed articles in Chapters 4, 5, and 6 in the following logical sequence of thought:

Chapter 4 (Article 1) investigated the effects of monovalent metal ions and transition metal ions on chemically controlled eumelanins and natural eumelanin.

Chapter 5 (Article 2), together with another published article [20], described the design, fabrication, and characterization of light-assisted eumelanin-based energy storage devices, based on the UV-Vis broadband light absorption and redox activity of eumelanin. In [20], 3D-networked carbon paper was used as the current collector for eumelanin, where great cycling stability in a light-assisted supercapacitor was achieved. In Chapter 5 (Article 2), 2D transparent ITO current collector was used to gain a deep understanding of the effect of light on energy storage properties of eumelanin.

In Chapter 6 (Article 3), chemically controlled eumelanins were used to model the biopigment neuromelanin in certain neuron cells of the *substantia nigra* and *locus coeruleus* of the human brain. The antioxidant/prooxidant dual properties of eumelanin (or neuromelanin), i.e. effects of transition metal ions, reactive oxygen species (ROS) (at physiological concentrations), and their synergetic effects were studied using cyclic voltammetry.

Please note that in Article 2 and Article 3, “eumelanin” is mostly written as “melanin”, and therefore “chemically controlled eumelanin” as “chemically controlled melanin”.

Chapter 7 hypothesizes the proton-assisted electron transfer (PAET) processes of eumelanin and predicts experimental data in literature and this work. In order to critically analyze the literature data of electrochemical potentials, we first need to build a hypothesis of mechanisms of the PAET

processes of eumelanin (Section 7.1) and, specifically, understand the relationship between electrochemical potentials and the composition of the electrolyte (Section 2.2.3). Afterwards, we critically discuss all the results in this work.

Chapter 8 includes the important findings of this work as well as impact and perspectives.

CHAPTER 2 LITERATURE REVIEW

This section critically reviews the literature. Section 2.1 reviews the polymerization as well as the supramolecular structure of eumelanin. The mechanism of polymerization of eumelanin (Section 2.1.1) provides a basic explanation of electrochemical polymerization in Section 2.2.4. From Section 2.2.3 and Section 2.2.8, we critically analyze the electrochemical properties of eumelanin in cyclic voltammograms reported in the literature. Reasons why electrochemical potentials reported in the literature are sometimes in disagreement are discussed in detail in Section 7.1 and Section 2.2.3. The electrochemical properties of eumelanin are largely impacted by the presence of O_2, as discussed in Section 2.2.6.

2.1 Chemical synthesis and molecular structure of eumelanin

The chemical synthesis of eumelanin comprises three parts. Tyrosine or DOPA is oxidized into DHI and DHICA monomers, here titled *Part 1 Synthesis* [92][93][94][95]. After that, DHI and/or DHICA polymerize to form oligomers, here titled *Part 2 Synthesis* (Section 2.1.1). The oligomers form certain (supra)molecular structures (10^{-9} m) then further assemble at the next two levels, at 10^{-8} m and 10^{-7} m scale, respectively, here titled *Part 3 Synthesis* [96]–[100] (Section 2.1.2). This section briefly introduces *Part 2* and *Part 3 Synthesis*. Part 1 Synthesis is related to further discussion for the rational design of eumelanin, discussed in Section 7.4.4.

2.1.1 Mechanism of synthesis of DHI oligomers and DHICA oligomers (Part 2 Synthesis)

To form eumelanin from DHI and DHICA, both reduced H2Q and oxidized Q need to coexist. The monomers/oligomers in H2Q form provide *nucleophilic polymerization sites* that donate electron pairs, whereas the monomers/oligomers in Q form give *electrophilic polymerization sites* that accept electron pairs. The nucleophilic and electrophilic polymerization sites form covalent bonds for the polymerization (Figure 2.1) [93].

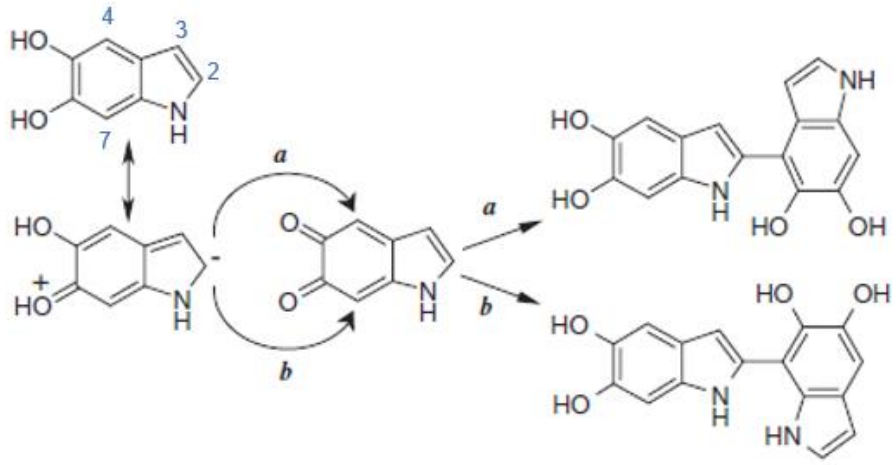

Figure 2.1 Mechanism of DHI polymerized into DHI-dimers. Adapted from [93].

DHI can have many possible polymerization sites including the free sites 2, 3, 4, 7. Sometimes, even site 1, i.e. the amine, is proposed as a polymerization site (Figure 1.2(b)). In the case of DHICA polymerization, the steric hindrance and repulsion forces between negatively charged functional groups such as $-COO^-$ and quinone groups decrease the number of polymerization sites and the polymerization rate (Figure 1.2 and Figure 2.2) [93]. Indeed, the polymerization rate of DHICA oligomers is much lower than that of DHI oligomers [101].

2.1.2 Supramolecular structure of DHI-melanin and DHICA-melanin (Part 3 Synthesis)

DHI oligomers are synthesized in planar structures. They form assemblies mainly by π-π stacking that favors electron transport [37], [102] (Figure 2.2). More examples of the planar structure of DHI oligomers are provided in Figure 1.2.

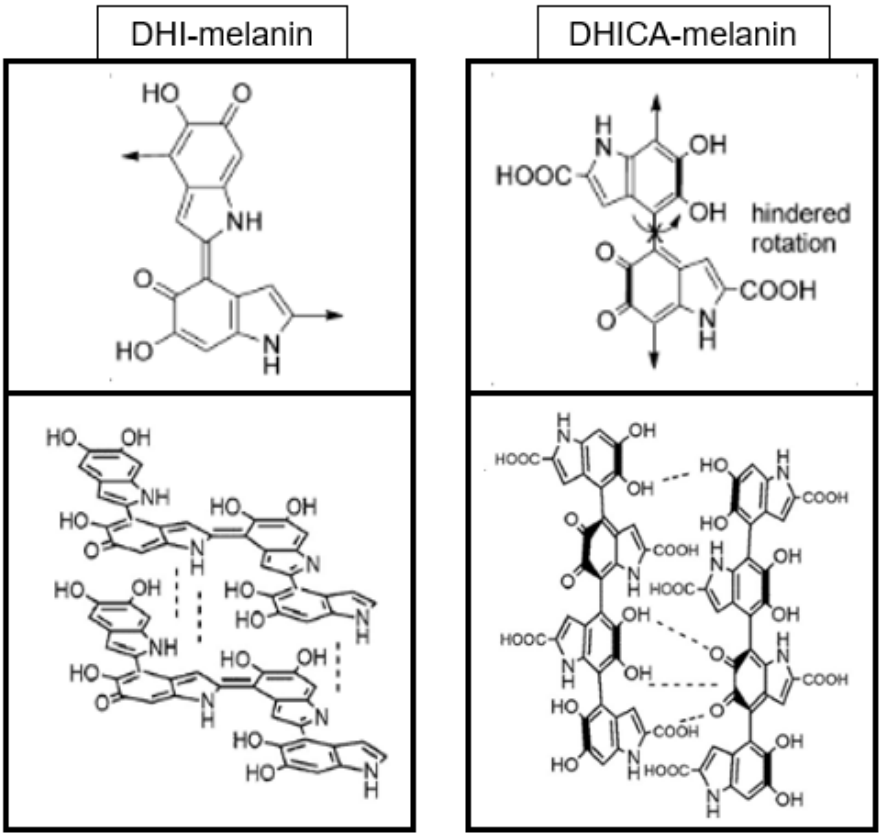

Figure 2.2 Supramolecular structures proposed for DHI- and DHICA-melanin. Adapted from [103].

DHICA mainly polymerizes into non-planar structured oligomers due to steric hindrance by carboxyl groups and quinone groups (Figure 2.2 and Section 2.1.1). These oligomers assemble into rod-shaped aggregates by hydrogen-bonding interactions. Due to the limited polymerization sites, DHICA-melanin is expected to have monomer-like behavior (Section 7.4.2). Due to the non-planar structure, DHICA-melanin is expected to have weaker electronic transport properties than DHI-melanin and therefore lower voltammetric current (Figure 6.3). The rod-shaped structure of DHICA-melanin can confine radicals in restricted spaces between DHICA oligomers, which makes DHICA-melanin a better radical scavenger than DHI-melanin (Section 7.6.1.2) [103]–[105].

2.2 Electrochemical properties of eumelanin

2.2.1 Unestablished electrochemical potentials of eumelanin

A few types of eumelanin have shown distinguishable voltammetric features as well as broad features. Examples include DOPA-melanin [36], [51], [106]–[108], Sepia melanin [16], [50], [66], [106] (Section 2.2.5, Section 2.2.6 and Section 2.2.7.3). The main reason can be the chemical heterogeneity of each type of eumelanin.

Among the cases of eumelanins with distinguishable potentials, challenges remain to establish a structure-property relation for eumelanin. There are typically 3-4 distinguishable potentials. At first, attempts are made on studying the dependence of potential on the pH value of the electrolyte. Young et al. obtained an empirical relation, E (vs. SCE) = 0.42 – 0.05 pH, based on the broad anodic peak potentials of methyl-DHI-melanin obtained at 50 mV/s in pH range 2 - 8 at 25 °C [92]. The saturated calomel electrode (SCE) is a reference electrode, where

$$E \text{ (V vs. SCE, } pH_{bulk}) = E \text{ (V vs. NHE, } pH_{bulk}) - 0.25 \qquad \text{Eq. 2.1}$$

However, the relation obtained by Young does not fit the potentials of eumelanin reported in other literature [36], [50], [66], [106], [107]. With contrary results, Serpentini et al. reported that the electrochemical potentials of eumelanin do not depend on the pH values of the electrolytes [107].

Kim et al. compared the voltammograms of Sepia melanin in HNO_3 (pH 0) and $Mg(NO_3)_2$ (pH 7) for the effect of Mg^{2+} [50]. They deduced that the multivalent metal ion Mg^{2+} results in distinguishable electrochemical potentials. However, such a comparison is not made at the same pH. Their Fourier Transform Infrared (FTIR) spectra demonstrate that the chelation of multivalent metal ions to eumelanin is related to the oxidation of eumelanin and the reverse process of its chelation is related to its reduction [50][52].

Tian et al. obtained three redox potentials for Sepia melanin in the presence of monovalent metal ions Li^+, Na^+ and K^+. The effect of the monovalent metal ions on eumelanin was studied using X-ray Photoelectron Spectroscopy (XPS). Based on the XPS results, the authors assigned the potential at ca -0.7 V vs. Ag/AgCl to be related to $-COO^-$; the potential at ca -0.5 V is assigned to be related to amine groups; the potential between -0.31 V/0.4 V is assigned to be related to quinone groups [106].

Based on the above, the unanswered question is how we can gain insights into the electrochemical potentials of eumelanin. In this thesis, we made a basic hypothesis for the redox properties of eumelanin (Section 7.1 and Section 2.2.3). In the rest of Section 2.2, we critically analyze the electrochemical potentials in the literature based on this hypothesis.

2.2.2 Effect of monovalent metal ions

Like H^+, metal ions are attracted to an electrode by the negative bias. In addition, Li^+, Na^+ and K^+ are reported to insert between the oligomer sheets of eumelanin at certain negative potentials [52], [109]. Here we call such potentials *insertion potentials* of metal ions. The insertion of the metal ions may increase the distance between the oligomer sheets of eumelanin. If the insertion potential is close to the onset/end redox potential, the monovalent metal ions may assist the electron transfer process. For example, Li^+ seems to insert into Sepia melanin at -0.45 V vs. Ag/AgCl (Figure 2.9) [106]. This may have promoted the tautomerization of HQI/H2Q and related redox activities (Section 2.2.7.2). If the insertion potential is not close to the onset/end redox potential, the insertion of the metal ions may simply affect the capacitive current. For example, the first Na^+ insertion potential occurs at ca -0.7 V and the second Na^+ at -0.8 V vs Ag/AgCl [110]. The first is observed with a decrease of capacity in the galvanostatic discharge plot, where the oligomer sheets with higher distances do not favor electronic transport (Section 3.3) [110]. Based on the above, redox potentials of eumelanin may not be affected by the monovalent metal ions at potentials more positive than their insertion potentials.

2.2.3 Effect of unbuffered electrolyte on local pH

From the literature data, we notice a significant difference in redox potentials of eumelanin in the buffered and the unbuffered electrolytes. This section follows Section 7.1, discusses the effect of the unbuffered electrolyte and predicts the electrochemical potentials in unbuffered electrolytes (Section 2.2.3.1 to Section 2.2.3.3). Furthermore, there are unbuffered and buffered potential ranges to be calculated for buffered electrolytes in literature and this work (Section 2.2.3.4).

2.2.3.1 Estimation of the potential shift in unbuffered electrolyte

We tentatively give a quantitative estimation of the electrochemical potentials in an unbuffered electrolyte, by the comparison of H_2O and $NaCH_3COO/CH_3COOH$ buffered electrolyte.

The reason that $NaCH_3COO/CH_3COOH$ can buffer the bulk pH of the electrolyte is due to its capability to dissociate protons by

$$CH_3COOH \rightleftharpoons CH_3COO^- + H^+ \qquad \text{Equilibrium 2.1}$$

We can generalize the chemical symbols as a weak acid HA with equilibrium

$$HA \rightleftharpoons H^+ + A^- \qquad \text{Equilibrium 2.2}$$

An additional amount of H^+ can be consumed/generated due to the equilibrium of the association constant of the buffering weak acid

$$K_a(\text{buffer}) = \frac{[H^+][A^-]}{[HA]} \approx \frac{[H^+][A^-]_{initial}}{[HA]_{initial}} \qquad \text{Eq. 2.2a}$$

or

$$pK_a(\text{buffer}) = pH_{bulk} - \log([A^-]_{initial}/[HA]_{initial}) \qquad \text{Eq. 2.7b}$$

where K_a (CH_3COOH) = 1.76×10^{-5}. H_2O can also be regarded as a very weak acid, where

$$H_2O \rightleftharpoons H^+ + OH^- \qquad \text{Equilibrium 2.3}$$

and $K_a(H_2O) = 10^{-14}$. The ratio $K_a(CH_3COOH)/K_a(H_2O) = 1.76 \times 10^9$. It means that the capability of H_2O to dissociate H^+ is 9 orders of magnitude lower than CH_3COOH. Therefore, higher applied potentials (more positive or more negative vs. NHE) are needed to obtain the same local pH values in an unbuffered electrolyte with respect to a buffered electrolyte. According to the linear relationship of pH_{local} and the applied potential (Eq. 7.5b), we tentatively estimate the potential shift caused by unbuffered electrolytes as ca 9×0.059 V = 0.53 V. Such a potential shift is named here an *unbuffered potential shift*, noted as ΔE_{unb}.

2.2.3.2 pK_a of buffer vs. pK_a of eumelanin

The definitions of pK_a of buffer and eumelanin are the same, indicated in Eq. 2.7b. In buffer, A^- is the anion CH_3COO^-, whereas in eumelanin, A^- are the deprotonated functional groups.

In the cyclic voltammetry measurements, the functional groups of eumelanin and buffer anions are placed in different situation. Here we would like to clarify their situations upon the change of

electrical potential bias. When the potential bias is increased towards more positive potentials, the $[H^+]$ surrounding the working electrode decreases, and $[CH_3COO^-]$ increases gradually. Eumelanin is fixed on the current collector as working electrode. When potential scans over the potential corresponding to the pK_a value of a functional group according to Eq. 7.5a, deprotonation of the functional group occurs. The reverse situation happens when the potential bias is decreased towards more negative potential.

2.2.3.3 The direction of the unbuffered potential shift

From Eq. 7.5b, we understand that the applied potential causes the change of the local pH from the potential where $pH_{local} = pH_{bulk}$, i.e. 0 V vs. NHE (Section 7.1.4.2). Therefore, the direction of the unbuffered potential shift ΔE_{unb} is expected to point from 0 V vs. NHE to both negative and positive directions. At $pH_{local} = pH_{bulk}$, $\Delta E_{unb} = 0$. At $pH_{local} < pH_{bulk}$, the unbuffered potential shift is negative, i.e. $\Delta E_{unb} < 0$, and vice versa.

For example, At bulk pH 7, for the potential corresponding to pK_a 6.3, $\Delta E_{unb} < 0$, whereas the potentials corresponding to the rest of the pK_a values have $\Delta E_{unb} > 0$ (Figure 2.3). At bulk pH 13, as all the pK_a values are lower than the bulk pH, all the onset potentials have $\Delta E_{unb} < 0$. At bulk pH 5.6, all the pK_a values are higher than the bulk pH, therefore all the onset potentials have $\Delta E_{unb} > 0$ (Figure 2.3).

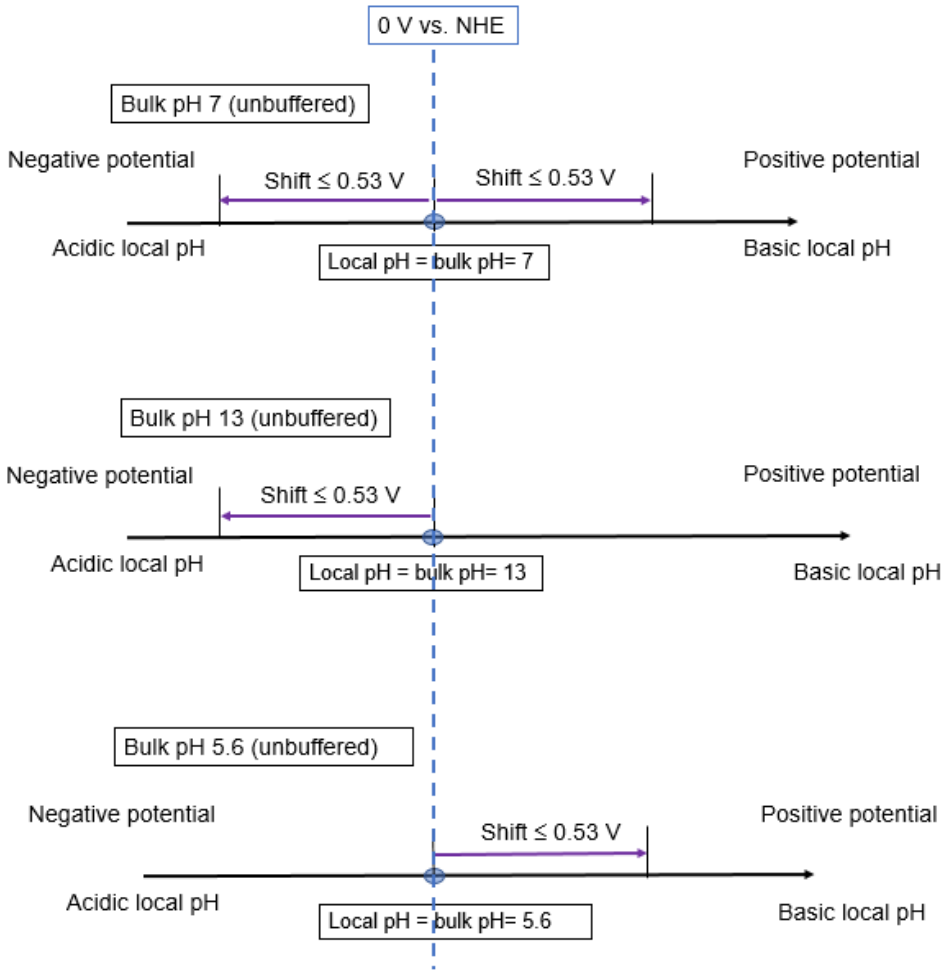

Figure 2.3 Directions of the unbuffered potential shifts at different bulk pHs.

Last but not least, for a small change of the local pH from pH_{bulk}, the unbuffered potential shift ΔE_{unb} can be smaller than 0.53 V, because the amount of H^+ or OH^- that H_2O needs to dissociate is small (Equilibrium 2.3). By data analysis, we obtain empirical values as follows. Within ca 3 pH units of difference from $pH_{local} = pH_{bulk}$, $\Delta E_{unb} < 0.53$ V. For example, in an unbuffered electrolyte at bulk pH 7, pK_a(SQ/H2Q) 6.3 is expected to have its onset oxidation potential shift negatively but still close to its counterpart potential in buffered electrolytes (Section 2.2.5.2). Based on the above discussions, we estimated the potentials in unbuffered electrolytes in Table 2.1.

Table 2.1 Expected onset oxidation or reduction potentials or potential range (vs. Ag/AgCl) of eumelanin in unbuffered electrolytes at different bulk pHs calculated from the pK_a

values. The values that appear in literature data analysis often are highlighted. HQI is protonated quinone imine (Section 7.1.3).

Material and reference	Equilibrium of functional groups	pK_a	Potential (range) at bulk pH 5.6	Potential (range) at bulk pH 7	Potential (range) at bulk pH 8	Potential (range) at bulk pH 13
DHI-melanin, DHI, DHICA, DOPA [111][112] [49][113]	HQI/H2Q (HQI can tautomerize and oxidize into SQ)	6.3	-0.16 V/0.37 V but close to -0.16 V	-0.24 V/-0.77 V but close to -0.24 V	-0.30 V/-0.83 V	-1.13 V
DHI-melanin, DHI, DHICA [111][112] [49][113]	SQ/H2Q (1)	9.4	0.55 V	-0.06 V/ 0.47 V	-0.12 V/ 0.41 V	-0.94 V
A DHI-melanin sample* [49][112]	SQ/H2Q (2)	10.7	0.66 V	0.58 V	0.52 V	-0.34 V/-0.84 V
	Q/SQ (1)	11.7	0.69 V	0.61 V	0.55 V	-0.28 V/-0.81 V
	Q/SQ (2)	12.8	0.75 V	0.67 V	0.61 V	-0.21 V/-0.74 V but close to -0.21 V
DHI, DHICA	Q/SQ (monomer)	13.2	0.78 V	0.70 V	0.64 V	-0.19 V/-0.72 V
DOPA [114][115]	SQ/H2Q (DOPA)	8.7	0.51 V	-0.10 V/ 0.43 V	-0.16 V/ 0.37 V	-0.98 V
	Q/SQ (DOPA)	9.9	0.58 V	-0.03 V/ 0.50 V	-0.09 V/ 0.44 V	-0.91 V

2.2.3.4 The potential shift in other buffered electrolytes

With the same logic as unbuffered shift, we estimate that there is similar potential shift for other buffered electrolytes. If their pK_a of their weak acid is above ca 5, the potential shift is ca [0.059 (pK_a (other weak acid) – 5)] V. For example, tris(hydroxymethyl)aminomethane (THAM) has pK_a 7.8, its potential shift vs. acetate buffer is therefore ca $0.059 \times (7.8 - 5) = 0.17$ V.

2.2.3.5 The limited buffered potential range by the concentration of buffer

In a buffered electrolyte, the *effective buffered potential range* is limited. Such potential range can be calculated as follows.

We use $NaCH_3COO$ with initial concentration $[A^-]_{initial}$ and CH_3COOH of initial concentration $[HA]_{initial}$ to compose a $NaCH_3COO$ buffer as an example.

We would like to name the potential dividing the buffered and the unbuffered ranges as the *boundary potential*, noted as E_b. At 0 V vs. NHE, $pH_{local} = pH_{bulk}$ (Section 7.1.4.2). The E_b at negative potential vs. NHE is named *negative boundary potential* E_{bn} and correspondingly *positive boundary potential* E_{bp} at positive potential vs. NHE.

At negative potential vs. NHE, H^+ is attracted to the interface of electrode/electrolyte by the electrostatic force. CH_3COOH is consumed to generate H^+. Therefore, at E_{bn}, CH_3COOH is totally transformed into H^+, that is,

$$pH_{local}\ (E = E_{bn}) = -\log[HA]_{initial} \qquad \text{Eq. 2.8}$$

At positive potential vs. NHE, CH_3COO^- is attracted to the interface of electrode/electrolyte. Notably, it is $CH3COO^-$ that deprotonates the majority of eumelanin. Therefore, at E_{bn}, CH_3COOH is totally consumed to generate CH_3COO^- that has a concentration of $([A^-]_{initial} + [HA]_{initial})$. Such concentration of CH_3COO^- gives a local pH equivalent to

$$pH_{local}\ (E = E_{bp}) = 14 - \log([A^-]_{initial} + [HA]_{initial}) \qquad \text{Eq. 2.9}$$

After then, the boundary potentials can be calculated through Eq. 2.8 and Eq. 2.9 (Figure 2.4). We calculated the boundary potentials for the buffered electrolytes in literature and this work in Table 2.2. To apply Eq. 2.8 and Eq. 2.9 to every type of buffered electrolyte, "HA" here is representative of the chemical that provides protons, such as NaH_2PO_4 for phosphate buffer, and "A^-" represents the chemical that balances the amount of proton (Equilibrium 2.2), such as Na_2HPO_4 for phosphate buffer. The initial concentrations $[HA]_{initial}$ and $[A^-]_{initial}$ for Eq. 2.8 and Eq. 2.9 are calculated according to Eq. 2.7b.

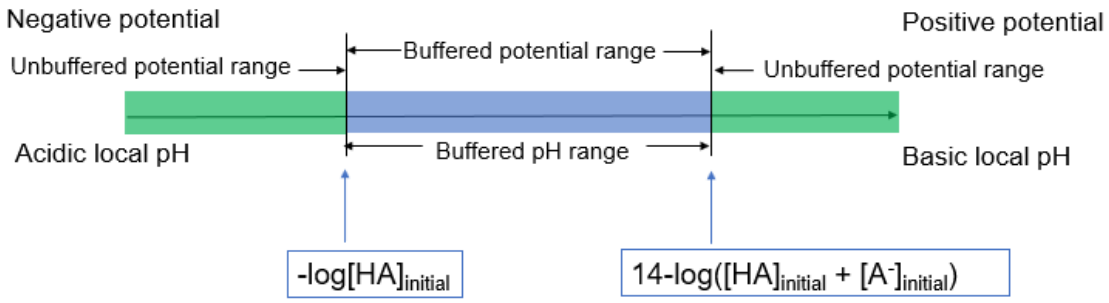

Figure 2.4 The relation between the buffered vs. unbuffered potential range in a buffered electrolyte prepared by HA and A^-. The local pH values at boundary potentials are limited by the initial concentrations of the weak acid $[HA]_{initial}$ and salt $[A^-]_{initial}$ composing the buffered electrolyte.

For the buffered electrolytes other than acetate electrolytes, the potential shift needs to be taken into consideration to calculate the buffered potential range (Section 2.2.3.4).

In the unbuffered potential range, it is water that generates OH^- or H^+. In this case, the A^- or H^+ of the weak acid of the buffer is accumulated on the working electrode. If the bias is more positive than E_{bp}, the local pH is expected to be higher than the local pH corresponding to E_{bp}. Conversely, if the bias is more negative than E_{bn}, the local pH is expected to be lower than the local pH corresponding to E_{bn}, but with a certain difference expected from the generation of OH^- or H^+ from the water (Section 2.2.3.1 and Section 2.2.3.3).

Table 2.2 Calculated boundary potentials between the buffered and unbuffered potential ranges for literature data and this work according to Eq. 2.8 and Eq. 2.9, and considering potential shifts of the buffering salts (Section 2.2.3.4). The initial concentrations are calculated according to Eq. 2.7b. Potential vs. Ag/AgCl is used in this table.

For which case in which table	Composition of buffered electrolyte	$[HA]_{initial}$	$[A-]_{initial}$	Negative boundary potential E_{bn}	Positive boundary potential E_{bp}
Case 2 in Table 2.3	½ THAM buffer bulk pH 7.4 + ½	0.042 M for THAM +	0.017 M for THAM +	-0.7 V	0.3 V

	phosphate buffer bulk pH 7	0.042 M for phosphate	0.058 M for phosphate		
Article 1 and 2	$NaCH_3COO$ bulk pH 5	0.14 M	0.25 M	-0.44 V	0.31 V
Article 3	$NaCH_3COO$ bulk pH 7	5.7×10^{-5} M	0.01 M	-0.36 V	0.10 V

*THAM: tris(hydroxymethyl)aminomethane

2.2.4 Electrochemical polymerization of eumelanin

This section analyzes the electrochemical potentials for the polymerization of eumelanins in Table 2.3 and discusses the mechanisms of its electrochemical polymerization.

2.2.4.1 Case 1: Electrochemical polymerization by reductive polymerization

Table 2.3 Electrochemical polymerization of eumelanin based on the constant potential technique.

Case number	Ions in electrolyte and bulk pH	Precursor, concentration of precursor and literature reference	Current collector	Electrochemical technique and its parameters (potential is vs. Ag/AgCl)
1	Na^+ (0.1 M) (Unbuffered) pH 13	Hydroxyindole-like products, DHI and DHICA (ca 0.2 mM) [36]	Au (111)	Constant potential (-0.96 V for 120 min)
2	H^+ and Na^+ 0.017 M for THAM* and 0.058 M for phosphate (Buffered) pH 7	DHI (1 mM) [105]	ITO	Constant potential (0.5 V for 120 min)

*THAM: tris(hydroxymethyl)aminomethane

In Case 1 [36] of Table 2.3, the synthetic potential (-0.96 V vs. Ag/AgCl) is close to the predicted potential (-0.94 V vs. Ag/AgCl) for SQ/H2Q where local pH = 9.4 (Table 2.1b). In the electrolyte of bulk pH 13, all the precursors are expected to be in the oxidized form Q [116]. The polymerization at the interface, therefore, needs to generate the H2Q form of eumelanin to combine with the Q form (Section 2.1.1). We here define the type of polymerization where the oxidized form Q is dominant and the reduced forms H2Q need to be generated for the polymerization, as the *reductive polymerization*.

2.2.4.2 Case 2: Electrochemical polymerization by oxidative polymerization

In Case 2 [105] of Table 2.3, the buffered potential range is limited (ca -0.7 V/0.3 V) (Table 2.2 and Section 2.2.3.4). The applied synthetic potential is 0.5 V vs. Ag/AgCl, much higher than the *positive boundary potential* ca 0.3 V. Therefore, the local pH induced by 0.5 V (unbuffered) can be higher than the local pH at 0.3 V (buffered) (Section 2.2.3.4). At 0.3 V, the local pH is ca 13.1,

where oxidation SQ/Q occurs (Eq. 7.5a). Therefore, at the interface, Q is generated to polymerize with H2Q (Section 2.1.1). We call this polymerization, where oxidized forms are generated from reduced forms in order to polymerize, *oxidative polymerization*.

2.2.5 Data analysis of electrochemical potentials in voltammograms of eumelanin

In this section, we critically analyze the onset/end redox potentials in the voltammograms available in literature.

2.2.5.1 Case 3: Electrochemically polymerized DOPA-melanin

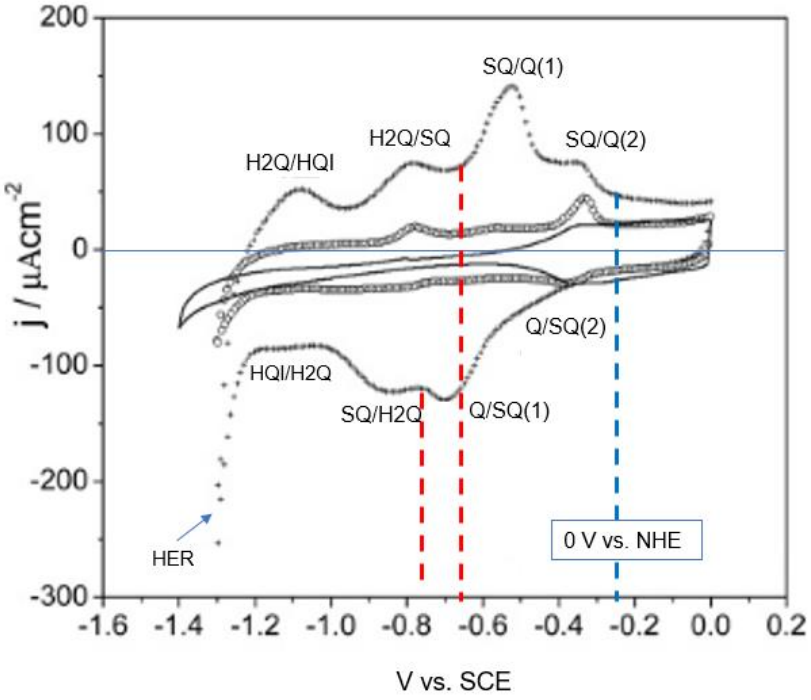

Figure 2.5 Case 3: Voltammograms of DOPA-melanin on Au(111) in unbuffered NaOH (0.1 M) at bulk pH 13 at 200 mV/s (Table 2.4). The voltammogram with the highest current (plotted with "+") is the object of discussion. The material is electrochemically synthesized for 120 min before the cyclic voltammetry (Case 1 in Table 2.3). The voltammogram plotted with "◯" is for the eumelanin electrochemically synthesized for 5 min. The voltammogram plotted with a solid line is the bare Au(111) current collector. Adapted from [36].

In Case 3 [36], the onset oxidation and reduction potentials are as expected for the unbuffered electrolytes (Figure 2.5 and Table 2.4). We find two redox couples Q/SQ, corresponding to pK_a ca 11.7 for redox couple Q/SQ(1) and ca 12.8 for redox couple Q/SQ(2) (Table 2.1). Peak SQ/Q(2) is not reversible, probably due to the oxidative polymerization (Section 2.2.4 and Section 7.5.1).

Table 2.4 Electrochemical potentials of eumelanin in Case 3 [36] (Figure 2.5). Potential vs. Ag/AgCl is used.

Oxidation features: onset/end potentials, functional groups and pK_a	Reduction features: onset/end potentials, functional groups and pK_a
-1.14 V/-0.90 V (H2Q/HQI pK_a 6.3)	-1.05 V/-1.14 V (HQI/H2Q pK_a 6.3)
-0.90 V/-0.60 V (H2Q/SQ pK_a 9.4)	-0.70 V/-1.05 V (SQ/H2Q pK_a 9.4)
-0.60 V/-0.38 V (SQ/Q(1) pK_a 11.7)	-0.52 V/ -0.70 V (Q/SQ(1) pK_a 11.7)
-0.38 V/ -0.21 V (SQ/Q(2) pK_a 12.8)	-
Hydrogen evolution reaction (HER) -1.15 V/-1.25 V	HER -1.15 V/-1.25 V

2.2.5.2 Case 4: DOPA-melanin with electrochemical features of DOPA precursors

In Case 4 (Figure 2.6 [107]), when we try to compare the literature experimental data with the expected data for bulk pH 5.6 in unbuffered electrolytes (Table 2.1), we find two redox couples HQI/H2Q and one redox couple SQ/H2Q. The last redox couple, Q/SQ (expected with an onset oxidation potential ca 0.69 V), is missing. We tentatively assume that the bulk pH 5.6 could be changed to bulk pH ca 8 before the voltammetry measurements, due to the experimental methods in the article [107]. The electrolyte was composed of KCl and HCl and was “flushed with argon for 5 hours before the voltammetry was conducted”. The HCl component most likely became HCl

gas and evaporated from the electrolyte accelerated by the argon flush. When the bulk pH rises above ca 6.3, the eumelanin sample can be deprotonated by the electrolyte and provide protons to form HCl that can evaporate to further basify the electrolyte. The bulk pH may be close to 8 when measurements are conducted, where the last onset oxidation potential is 0.55 V for SQ/Q (pK_a ca 11.7) (Table 2.1). The hypothesis of basified bulk pH can also be proved by the fact that, in the same article, the peak potentials at bulk pH 2, 5.6 and 10 do not show shifts by bulk pH as expected in Eq. 7.1a. It means that the bulk pH values of electrolytes employed in this article were probably close to ca pH 8 when voltammetry measurements were conducted [107].

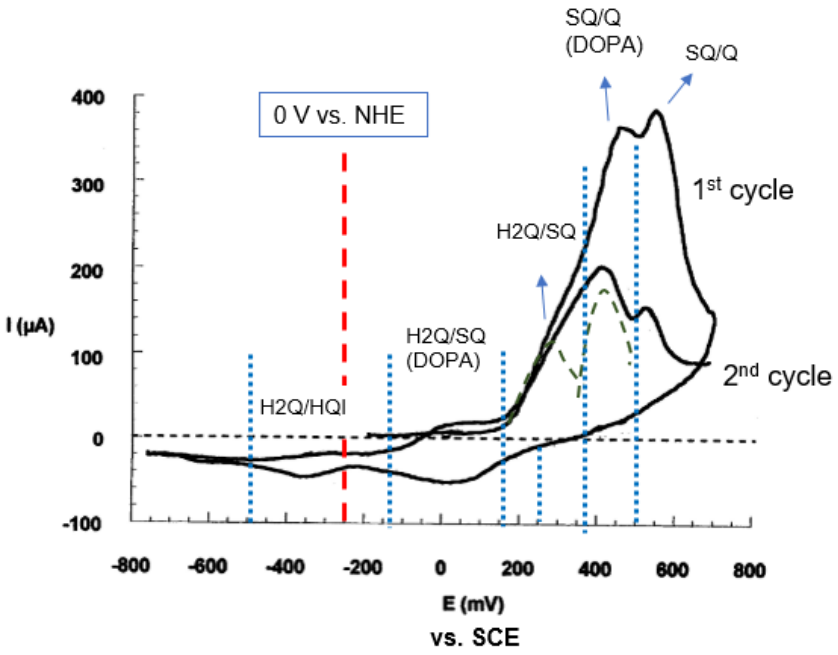

Figure 2.6 Case 4 (Table 2.5): Voltammogram of DOPA-melanin on carbon paste in unbuffered KCl at ca bulk pH 8 at 0.1 mV/s. Adapted from [107].

According to expected data for bulk pH 8 in an unbuffered electrolyte (Table 2.1), the redox features of Case 4 are assigned in Table 2.5. Peak H2Q/SQ of eumelanin (pK_a 9.4) and peak SQ/Q(DOPA) (pK_a 9.9) are convoluted due to their close pK_a values. DOPA-melanin synthesized by the method in [107] may include DOPA precursors considering peaks attributable to the presence of peak H2Q/SQ(DOPA) and SQ/Q(DOPA). The material is further oxidatively polymerized in cyclic voltammetry, shown by the irreversible oxidative current between 0.2 V and 0.7 V vs. SCE from the first to the second cycle (Section 7.5.1). The reduction peaks of both SQ/H2Q of eumelanin and SQ/H2Q(DOPA) are convoluted. The current during anodic sweep

below ca 0 V is reductive (negative current) probably due to the presence of a small amount of O_2 despite the use of Argon (Section 2.2.6).

Table 2.5 Electrochemical potentials of eumelanin in Case 4 [107] (Figure 2.6). Potential vs. Ag/AgCl is used.

Oxidation features: onset/end potentials, functional groups and pK_a	Reduction features: onset/end potentials, functional groups and pK_a
-0.45 V/-0.15 V (H2Q/HQI pK_a 6.3)	-0.15 V/-0.45 V (HQI/H2Q pK_a 6.3)
-0.09 V/0.25 V (H2Q/SQ(DOPA) pK_a 8.7)	0.3 V/-0.2 V (SQ/H2Q pK_a 9.4 and SQ/H2Q(DOPA) pK_a 8.7)
0.25 V/0.42 V (H2Q/SQ pK_a 9.4)	
0.42 V/0.55 V (SQ/Q(DOPA) pK_a 9.9)	-
0.55 V/0.75 V (SQ/Q pK_a 11.7)	-

2.2.6 Effect of oxygen reduction reaction (ORR)

Most of the cases of literature data are impacted by oxygen reduction reaction (ORR) due to the presence of O_2. In this section, we discuss the effect of ORR before analyzing the voltammograms under the effect of ORR (Section 2.2.7 and Section 2.2.8). Due to the scope of this thesis, we do not discuss the onset potentials of ORR and its related reactions (Section 8.4).

2.2.6.1 Possible reasons for the presence of O_2

The O_2 source for ORR can come from *oxygen evolution reaction (OER)*, where H_2O is oxidized into O_2 at a given positively biased potential,

$$2H_2O \rightarrow O_2 + 4H^+ + 4e^- \quad (1.23 \text{ V vs. NHE}) \qquad \text{Reaction 2.1}$$

Other reasons for the presence of O_2 include not degassing properly (Section 2.2.5.2). Indeed, degassing O_2 from the electrolyte to a given high degree can be difficult. Methods used for degassing in this work are described in Section 3.2.4.

2.2.6.2 Reactions involved in the presence of O_2

Below a certain potential, O_2 is reduced into H_2O_2, namely *oxygen reduction reaction (ORR)*,

$$O_2 + 2H^+ + 2e^- \rightarrow H_2O_2 \quad (0.7 \text{ V vs. NHE}) \qquad \text{Reaction 2.2}$$

The potential noted after the reaction is referred to its thermodynamic potential at bulk pH 0.

Above a certain potential, the generated H_2O_2 is oxidized into O_2, namely *H_2O_2 oxidation*,

$$H_2O_2 \rightarrow O_2 + 2H^+ + 2e^- \quad (0.7 \text{ V vs. NHE}) \qquad \text{Reaction 2.3}$$

A possible example of H_2O_2 oxidation is in Figure 2.9.

2.2.6.3 Positive/negative currents and acidification/basification of the electrolytes

This section discusses the impacts of ORR and its related reactions. First of all, this section explains why some current during anodic sweep below a certain potential is negative, as in Case 4 (Section 2.2.5.2) and Case 6 (Section 2.2.7.2) in the literature. Secondly, it can explain why some cathodic current is much higher than anodic current, as in Case 6 (Section 2.2.7.2) and Case 7 (Section 2.2.8.1). Thirdly, the basification and acidification of the electrolytes by these reactions will shift the redox potentials, as in Case 6 (Section 2.2.7.2).

When ORR occurs, O_2 is reduced by the current collector (or the working electrode material eumelanin as catalyst) to generate H_2O_2 (Reaction 2.2 and Figure 2.7(a)). In such a reaction, O_2 takes electrons from the current collector and/or eumelanin. Therefore, the current shown in the voltammogram is reductive (negative). Such a reaction also basifies the electrolyte (Reaction 2.2). The magnitude of current density therefore depends on the concentration of O_2, shown also in Case 5 (Section 2.2.7.1).

When H_2O_2 oxidation occurs, electrons emitted flow to eumelanin and/or the current collector, and oxidative (positive) current in the voltammogram is expected (Reaction 2.3 and Figure 2.7(b)). For the same reason, OER is shown with oxidative current (Reaction 2.1 and Figure 2.7(c)). Both these

reactions acidify the electrolyte. From the reactions, we understand that the degree of basification/acidification is proportionate to the amount of reduction capacity/oxidation capacity.

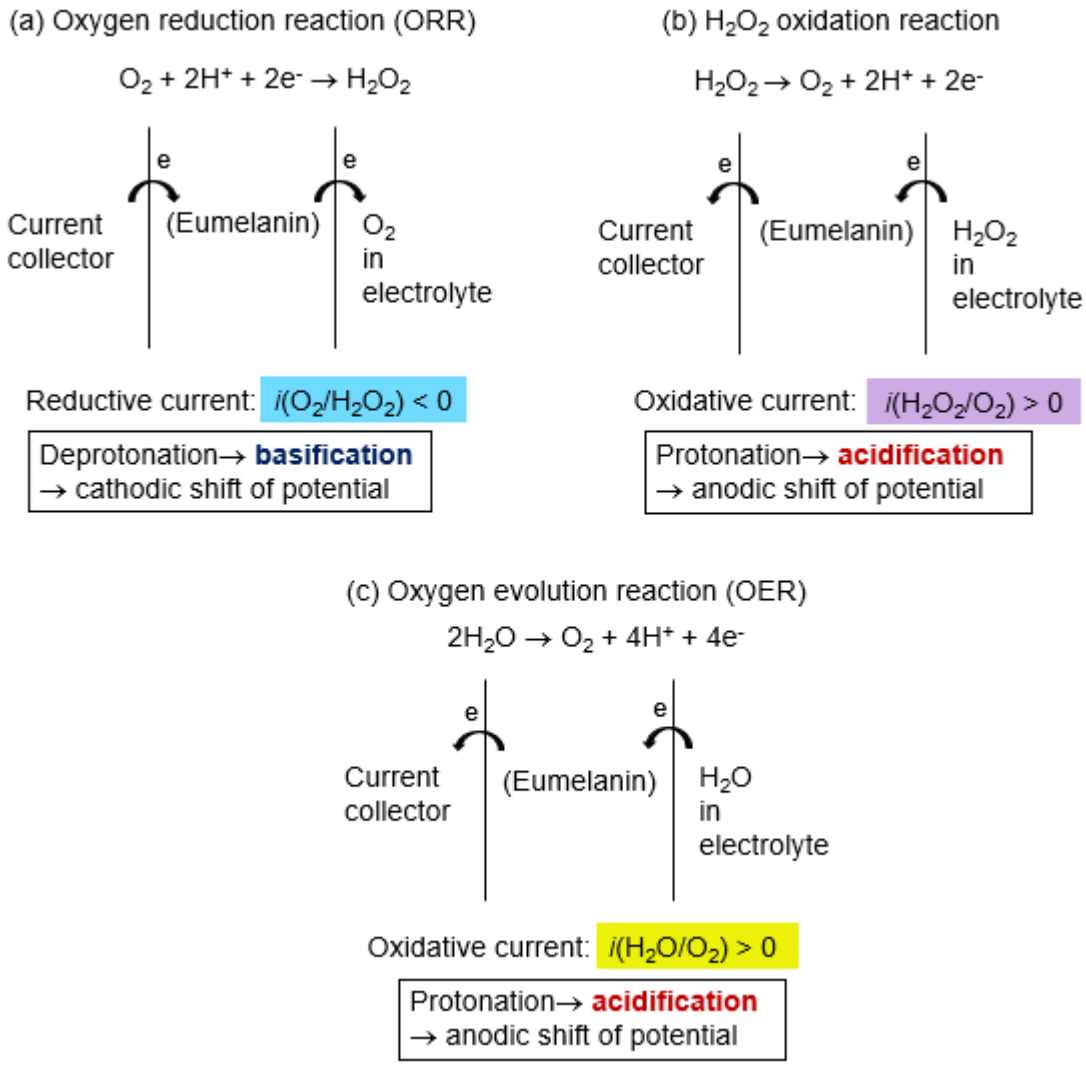

Figure 2.7 Voltammetric current and protonation/deprotonation for (a) oxygen reduction reaction (ORR) (b) H_2O_2 oxidation reaction and (c) oxygen evolution reaction (OER). Eumelanin is reported as the catalyst for ORR (a).

2.2.7 Data analysis of electrochemical properties under the effect of ORR

2.2.7.1 Case 5: voltammograms of eumelanin chelated with Fe^{3+} in absence and presence of O_2

Before analyzing the cases in the literature, we would like to note the ORR features related to the catalytic activity of certain functional groups of eumelanin as the *ORR (features or peaks) by deprotonated form/protonated form*. By analyzing Case 5, we would like to point out that, first, the redox potentials remain the same as in the absence of O_2 (Figure 2.8). For example, at bulk pH 13, the ORR features at ca -0.5 V, -0.8 V and -1.0 V vs. SCE are catalyzed by Q/SQ, SQ/H2Q and HQI/H2Q, respectively (Figure 2.8 (b)). These potentials are consistent with the redox potentials of eumelanin in the absence of O_2 (Figure 2.8 (a)).

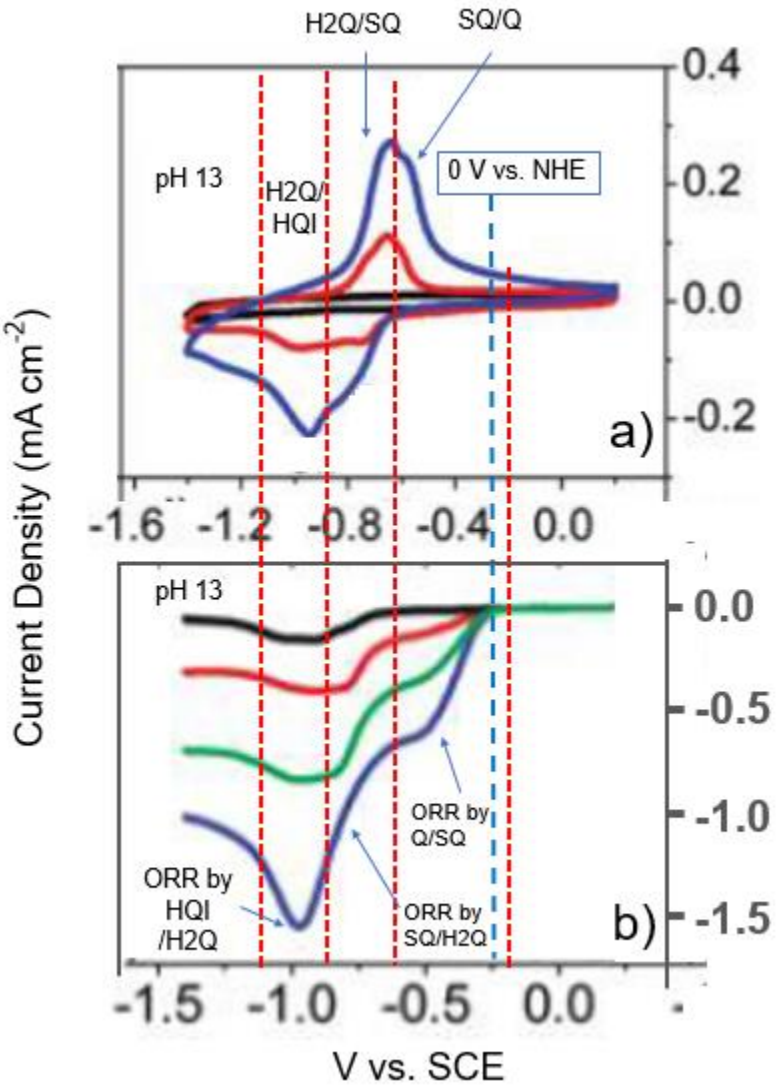

Figure 2.8 Case 5: Voltammograms of eumelanin chelated with Fe^{3+} at 200 mV/s in unbuffered NaOH at bulk pH 13, (a) in absence of O_2 and (b) in presence of O_2, at different O_2 concentrations: ca 0 M (black), 2.75×10^{-4} M (red), 7×10^{-4} M (green), and 1.2×10^{-3} M (blue). The eumelanin is electrochemically synthesized from eumelanin precursors solubilized in NaOH pH 13 with Fe^{3+} content present in the precursor solution (ca 1 ppm). Adapted from [66].

Secondly, the higher the concentration of O_2 is in the electrolyte, the higher the reduction current will be (Figure 2.8(b)). When the concentration of O_2 is high, the reduction current (negative current) is so high that the oxidation current of eumelanin seems negligible (Case 6 (Figure 2.9)).

Last but not least, the synthetic method in Case 5 is similar to Case 1 except that it is synthesized in the presence of Fe^{3+} (ca 1 ppm) (Section 2.2.4). Therefore, the voltammogram of Case 5 can be compared to Case 3, where Fe^{3+} is not present (Figure 2.8(a) and Figure 2.5). We analyze here the effect of Fe^{3+} on the electrochemical potentials and supramolecular structure of eumelanin based on discussions in Section 7.3.2 and Section 7.2.3.4. Compared to Figure 2.5, oxidation features H2Q/SQ and SQ/Q are both convolutions of peaks. For oxidation H2Q/SQ, the onset potentials of the convoluted peaks range from -0.9 V to -0.7 V vs. SCE. For oxidation SQ/Q, the convoluted peaks have onset potentials ranging between -0.6 V and -0.2 V vs. SCE. Those potentials that are more positive than Case 3 (Table 2.4) can be explained by the anodic shifts due to the chelation of Fe^{3+} to the $-COO^-$ functional group of eumelanin (Section 7.3.1.2). Due to such chelation, $-COO^-$ and amine groups on DHICA molecules are located inside the rod-shaped structure. Therefore, the deprotonation of H2Q/HQI does not occur easily, leading to very low current of oxidation feature H2Q/HQI (Figure 2.8(a)) (Section 7.2.3.4).

2.2.7.2 Case 6: ORR catalyzed by natural and synthetic eumelanins

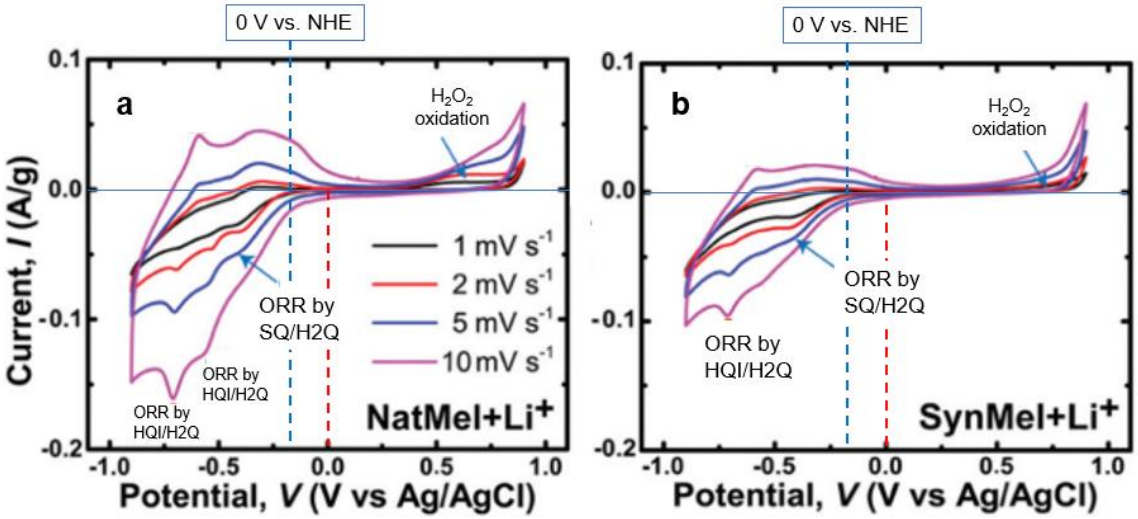

Figure 2.9 Case 6: voltammograms of (a) natural Sepia melanin and (b) synthetic DOPA-melanin in unbuffered Li_2SO_4 (1 M). The actual bulk pH may be ca 11. Polytetrafluoroethylene (PTFE) is used as the binder for eumelanin on the Ag nanowire current collector. Adapted from [106].

By analyzing Case 6, we further conclude that the redox potentials will undergo a significant shift due to the basification by ORR (Section 2.2.6.3). In Figure 2.9, Ag/AgCl is the reference electrode (Eq. 7.4).

In Case 6 (Figure 2.9), a comparison of ORR catalyzed by natural eumelanin and synthetic DOPA-melanin is made in the presence of Li^+. With DOPA-melanin, ORR has two main features at ca -0.4 V and ca -0.7 V vs. Ag/AgCl, assigned to the catalytic activity of SQ/H2Q and HQI/H2Q, respectively (Figure 2.9(b)). With respect to DOPA-melanin, Sepia melanin shows an extra ORR feature at ca -0.5 V that can be also assigned to the catalytic activity of HQI/H2Q. The extra ORR feature by HQI/H2Q is explained by the spaces between the oligomeric sheets of Sepia melanin. The small size of Li^+ allows Li^+ to enter the spaces at a certain negative potential to promote the reduction of HQI/H2Q, instead of H^+ [106]. The reason that Li^+ can be attracted to the working electrode at this negatively biased potential instead of H^+ can be that the concentration of H^+ (less than 10^{-7} M) is much lower than Li^+ (1 M) (Section 2.2.2 and Section 2.2.3.1). Last but not least, according to the positions of the redox potentials, we deduce that the electrolyte is basified by the ORR to ca bulk pH 11. The oxidation feature at ca 0.7 V may be due to H_2O_2 oxidation (Section 2.2.6.2).

2.2.7.3 Case studies of influence of ORR in this work

For DHI-melanin, a noisy reductive current is observed below ca -0.2 V in the presence of Na^+. This phenomenon is attributed to a very small amount of O_2 in the electrolyte due to incomplete degassing of O_2 (Figure S2(c) in Appendix A).

Reductive current is also observed during anodic sweep in presence of Cu^{2+} below ca -0.1 V, probably also related to ORR (Figure 4.4).

Reductive current is also observed in the case of the addition of Fe^{3+} in the electrolyte, which is probably related to ORR due to the small amount of O_2 added (Figure 7.9). The current above 0.17 V vs. Ag/AgCl is more oxidative (positive) than the current before adding Fe^{3+}, probably related to H_2O_2 oxidation (Reaction 2.3).

2.2.8 Data analysis: effect of Mg^{2+} (in presence of O_2)

Case 7 and Case 8 analyze the electrochemical potentials in presence of Mg^{2+}.

2.2.8.1 Case 7: polydopamine with Mg^{2+} vs. Li^{+}

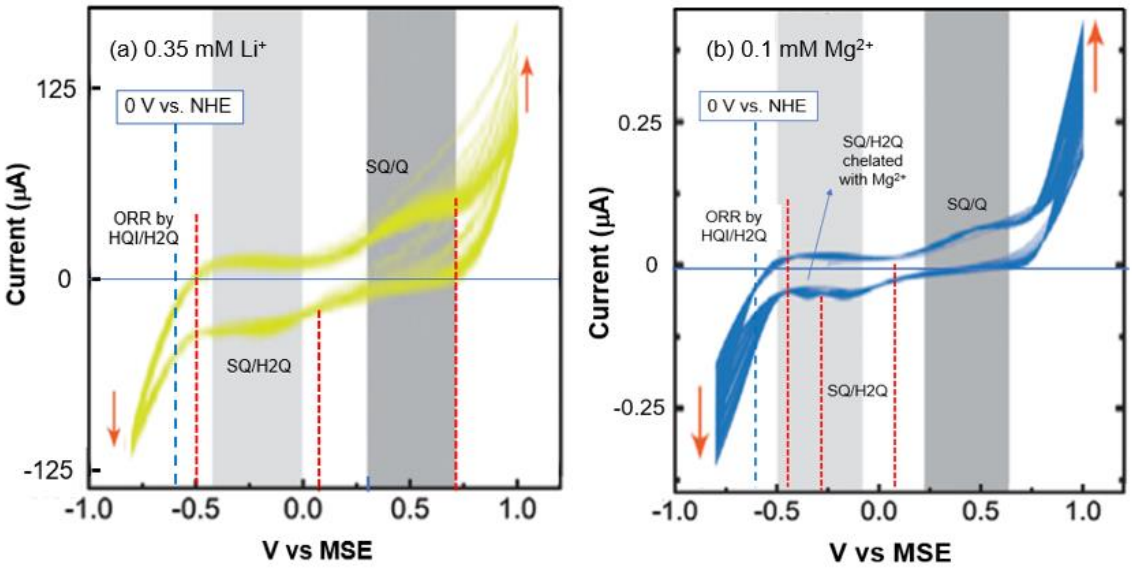

Figure 2.10 Case 7: Voltammogram of polydopamine on stainless steel at bulk pH 7 at 2 mV/s in (a) unbuffered LiCl (0.35 mM) (b) 0.1 mM $MgCl_2$. Adapted from [52].

In Case 7, mercury sulfate electrode (MSE) is used as the reference electrode, where

$$E \text{ (V vs. MSE, pH}_{bulk}) = E \text{ (V vs. Ag/AgCl, pH}_{bulk}) - 0.45 \qquad \text{Eq. 2.10}$$

or

$$E \text{ (V vs. MSE, pH}_{bulk}) = E \text{ (V vs. NHE, pH}_{bulk}) - 0.65 \qquad \text{Eq. 2.11}$$

In the voltammogram of Case 7 (Figure 2.10), the ORR occurs between ca -0.5 V/-0.8 V vs. MSE, assigned to the ORR catalytic activity of HQI/H2Q. The current related to ORR is higher than other contributions to the electrochemical current (Section 2.2.6.3). In the case of $MgCl_2$ electrolyte, an extra electrochemical feature with respect to LiCl is at ca -0.35 V vs. MSE, assigned as SQ/H2Q chelated with Mg^{2+} (Section 7.3.1.1 and Section 7.3.1.4). In a voltammogram involving Mg^{2+} at low concentration in this thesis, we also found a redox couple SQ/H2Q chelated with Mg^{2+} (Figure 7.10).

2.2.8.2 Case 8: natural eumelanin chelated with Mg^{2+} (high concentration)

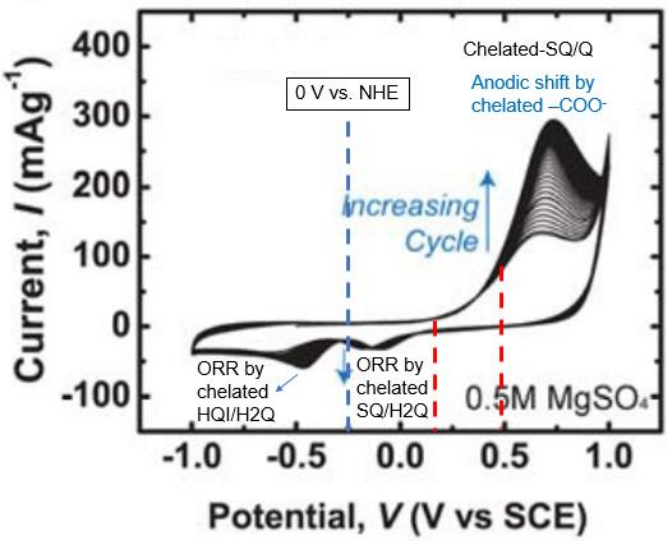

Figure 2.11 Case 8: Voltammogram of Sepia melanin in unbuffered $MgSO_4$ (0.5 M) at bulk pH 7 at 2 mV/s. Polytetrafluoroethylene (PTFE) is used as the binder for Sepia melanin on the current collector stainless steel. Adapted from [50].

In Case 8, we assigned the three peaks as indicated in Figure 2.11 [50]. The positions of the three peaks seem to show cathodic shifts of ca 0.3 V due to the chelation by Mg^{2+} at a high concentration (0.5 M) on each functional group (Section 7.3.1.1). For example, the end reduction potential of ORR by chelated HQI/H2Q is shifted from ca -0.30 V vs. SCE to ca -0.70 V vs. SCE; the end potential of ORR by chelated SQ/H2Q is shifted from ca 0.05 V vs. SCE to ca -0.25 V vs. SCE; the onset oxidation potential of a portion of the chelated SQ/Q is shifted from ca 0.5 V vs. SCE to ca 0.2 V vs. SCE. Meanwhile, the SQ/Q peak has another portion that has onset oxidation potential at ca 0.5 V, which can be a result of anodic shift by the chelation on $-COO^-$ (Section 7.3.1.2). Therefore, Case 9, with a high concentration of Mg^{2+}, shows the synergetic effect of both cathodic shift of all the redox potentials and anodic shift of the oxidation potential SQ/Q (Section 7.3.1.4).

CHAPTER 3 MATERIALS AND TECHNIQUES

3.1 Synthesis of chemically controlled eumelanin

3.1.1 Synthesis and storage of DHI- and DHICA-melanin

Both DHI- and DHICA-melanin are synthesized by oxidative polymerization from their monomers in ammonia vapor, i.e. buffered pH 12 (Section 3.1.3).

In Article 1, DHI-melanin is synthesized for 3 hours at pH 12. DHICA-melanin is synthesized for 16 hours. The resulting DHI-melanin and DHICA-melanin are both in semi-polymerized state (Section 7.5.1).

In Article 2, DHI-melanin is synthesized for ca 68 hours at pH 12. The resulting DHI-melanin is in fully-polymerized state (Section 7.5.1).

In Article 3, DHI-melanin and DHICA-melanin are synthesized for 3 hours and 16 hours, respectively, at pH 12, followed by storage in ambient condition (storage pH ca 7) for ca 1 year. The resulting DHI-melanin is in fully-polymerized state but the DHICA-melanin is in semi-polymerized state (Section 7.5.1).

The pH 12 makes the oxidative polymerization faster with respect to the pH 7 (Section 7.5.2.1).

3.1.2 Mechanism of synthesis of DHI- and DHICA-melanin

The mechanisms of chemically controlled eumelanin have been briefly reviewed in Section 2.1.1 and Section 2.1.2. In Chapter 7, we also discuss the possible further polymerization of DHI- and DHICA-melanin during cyclic voltammetry, sample storage (Section 7.5.2.1) and light irradiation (Section 7.5.3).

3.1.3 Estimation of synthetic pH

The synthetic pH, i.e. the pH value during the synthesis of the chemically controlled eumelanin, is estimated as follows. We used a simple glass cover (ca 12 dm^3) to build an ammonia chamber in ambient conditions. Inside the chamber, we have a vial containing ca 30 ml NH_3 aqueous solution (Sigma Aldrich, 28-30% w/v) and samples of eumelanin monomers on current collectors loaded

on sample holders. When the synthesis starts, the NH_3 and H_2O evaporate from the vial and fill the chamber. Eumelanin samples absorb H_2O and NH_3 and form NH_3H_2O on the sample, by

$$NH_3 + H_2O \rightleftharpoons NH_3H_2O \rightleftharpoons NH_4^+ + OH^- \qquad \text{Equilibrium 3.1}$$

with a dissociation constant of the base

$$K_b(NH_3H_2O) = \frac{[NH_4^+][OH^-]}{[NH_3]} = 1.8 \times 10^{-5} \qquad \text{Eq. 3.1}$$

Due to the dissociation constant, the pH value on the eumelanin sample is expected to remain almost the same throughout the synthesis. We hypothesize that, after a certain amount of time, the equilibria of the concentrations [H_2O] and [NH_3] are reached in each part of the chamber (eumelanin samples, the atmosphere, and the ammonia water in the vial). Therefore, the concentration of NH_3 in the eumelanin sample and the ammonia water in the (initial) vial are expected to be almost the same, and further the pH values.

Here we estimate the initial pH value of the ammonia water in the vial as follows. The NH_3 water with 28% w/v means 28 g NH_3 in 100 ml H_2O, i.e. ca 16 M. We set the concentration of generated [NH_4^+] and [OH^-] as x (M), then the [NH_3] after reaching Equilibrium 3.1 is $(16 - x)$ M. $K_b = x^2/(16 - x)$. Assuming this, because $K_b << 1$, $(16 - x)$ M ≈ 16 M, we obtain x = 0.01697 M and thus pH value is ca 12.2. Therefore, the synthetic pH is ca 12.

3.2 Cyclic Voltammetry

Cyclic voltammetry is an electrochemical technique commonly employed to investigate the oxidation and reduction processes undergone by the material as the working electrode interfaced with an electrolyte. By both cyclic voltammetry and galvanostatic charge-discharge techniques, we are able to obtain the capacity/capacitance, potential limit, as well as the cycling stability of the material electrode.

3.2.1 Three-electrode setup

A three-electrode setup is used for cyclic voltammetry measurements, including a working electrode, a counter electrode, and a reference electrode (Figure 3.1). The working electrode material is loaded on a current collector. Electrodes are immersed in an electrolyte, which can be

an aqueous or organic solution of salts. In this work and the related literature, aqueous electrolytes are used (Section 2.2). A potentiostat is used to control the applied potential of the working electrode with respect to the reference electrode potential. The potential at the working electrode is measured against the potential of the reference electrode and noted as "vs" the reference electrode [53].

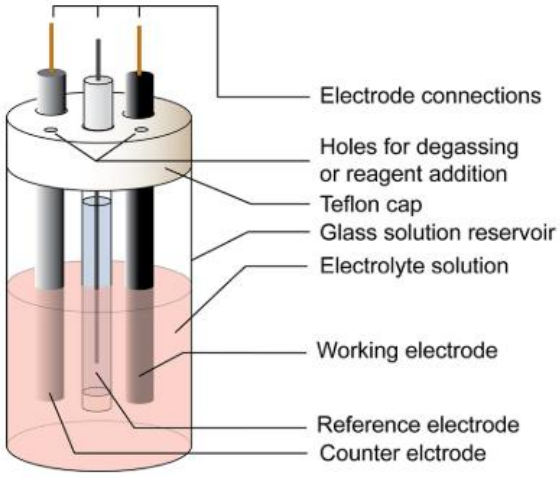

Figure 3.1 Electrochemical set-up for cyclic voltammetry [117].

3.2.2 Working principle of cyclic voltammetry

In cyclic voltammetry, the applied electrochemical potential *V* is linearly swept/scanned at a certain rate. Such rate is called sweeping rate (mV/s). During a voltammetric cycle, the potential is swept from the initial potential to a spositive potential, called the *switching potential*. It is then swept back to a negative potential, reaching another switching potential, and finally is swept back to the initial potential (Figure 3.2). The *i* vs. *V* plot is called a cyclic voltammogram [53][117]. The potential sweep towards a more positive potential is called an *anodic sweep/anodic scan*. The potential sweep towards a more negative potential is called a *cathodic sweep/cathodic scan* (Figure 3.2). The definition of anodic/cathodic current follows a different principle from the anodic/cathodic sweep in this work. *Anodic current* means positive current, whereas *cathodic current* refers to negative current. The anodic or cathodic current of eumelanin is mainly composed of oxidation or reduction current due to its redox activity.

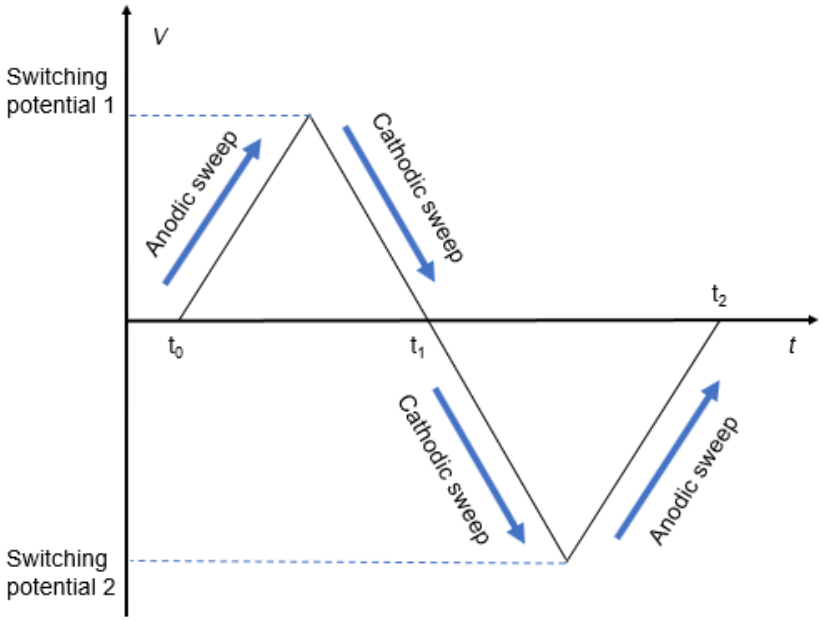

Figure 3.2 Scheme of cyclic voltammetry in the plot of potential *V* vs. time *t*.

In this thesis, we often conduct two cycles or more due to two reasons:

- To further observe the stability of the effects of interest. Such effects include the effect of light, transition metal ions, etc.
- The voltammograms of eumelanin can evolve cycle after cycle with the advancement of the polymerization reaction (Section 7.5.1).

3.2.3 Extraction of capacitance and capacity from cyclic voltammograms

3.2.3.1 Extraction of capacity

Capacity q (C) is the maximum ability of a material to store charge carriers. Capacitance C (F = C/V) describes how much charge carriers can be stored per potential unit, meaning the (maximum) efficiency of a material's charge storage.

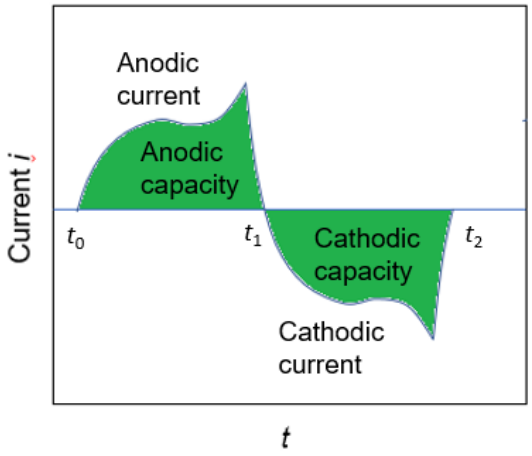

Figure 3.3 Extraction of capacity from cyclic voltammograms of redox-active materials.

The anodic/cathodic current is composed of oxidation/reduction current (peaking current), electrostatic current (box-shaped, Figure 3.4(a)) and ionic current. In this work, the anodic and cathodic capacities are extracted from the anodic (positive) current and cathodic (negative) current, respectively, noted as q_{an} and q_{ca}. The *anodic capacity* is the integration of the anodic current i_{an} vs. time t (Figure 3.3),

$$q_{an} = \int_{t0}^{t1} i_{an}\, dt \qquad \text{Eq. 3.2}$$

and the *cathodic capacity* is the integration of the cathodic current i_{ca} vs. time t,

$$q_{ca} = \int_{t1}^{t2} i_{ca}\, dt \qquad \text{Eq. 3.3}$$

In voltammograms at the same sweeping rate and potential range, higher current means higher capacity.

Oxidation/reduction capacity is defined as the capacity extracted from the oxidation/reduction (peaking) current, noted as q_{ox}/q_{red}.

3.2.3.2 Extraction of capacitance

For an electrical double-layer capacitive material, the capacitance C is defined as

$$C = \frac{q}{V} \qquad \text{Eq. 3.4}$$

which is the slope of the *q*-*V* plot (Figure 3.4(a)(b)). For a pseudocapacitor, the *q*-*V* plot has different slopes at different potential biases (Figure 3.4(d)). In this case, we find a part of the curve that is close to linear, here called the *quasi-linear curve*. We use the slope obtained from the linear regression of the quasi-linear curve as the capacitance *C*.

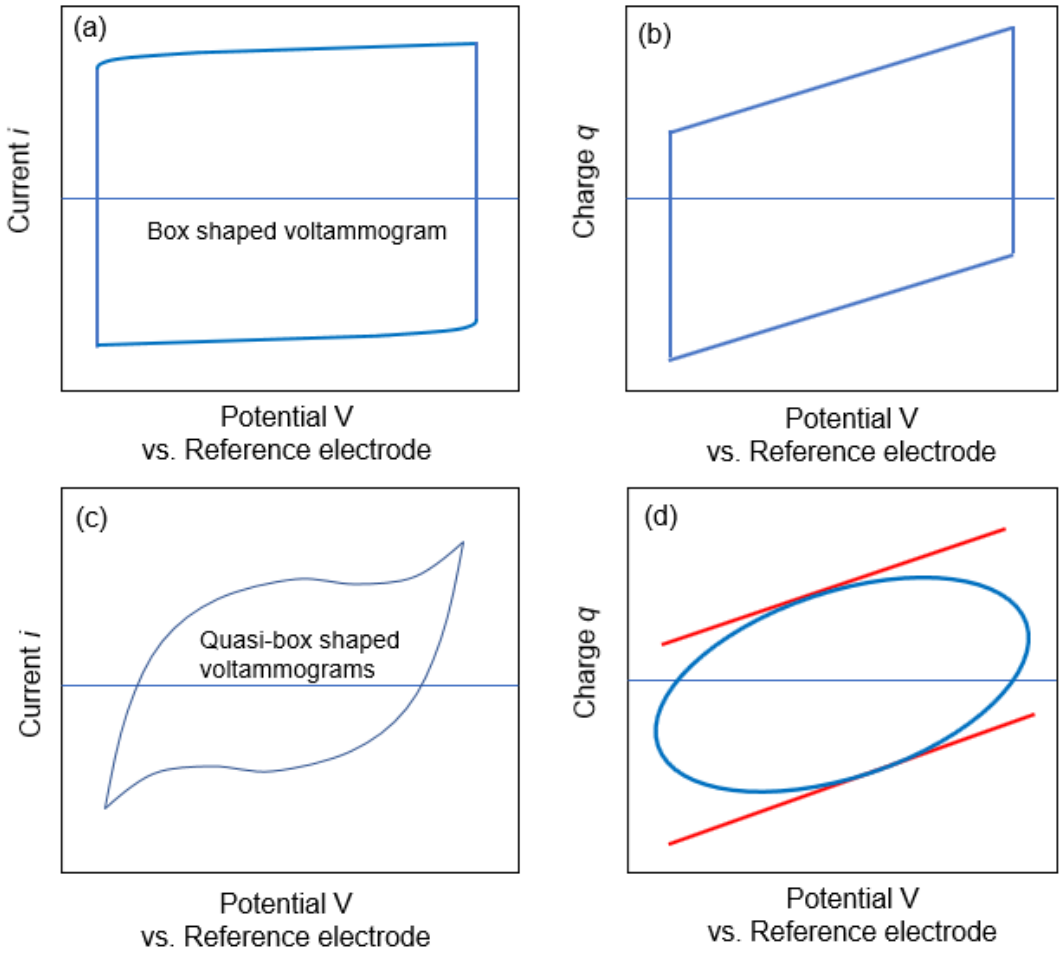

Figure 3.4 Extraction of capacitance in (a), (b) box-shaped cyclic voltammograms of electrostatic capacitive material and (c), (d) quasi-box shaped cyclic voltammograms of pseudocapacitive material. (d) includes linear regression on a quasi-linear curve to obtain capacitance.

Usually, capacity and capacitance have coherent trends of increase or decrease. The comparison of capacity and capacitance should be valid only when the parameters such as sweeping rate, potential range are the same.

3.2.4 Degassing procedure

A small amount of oxygen present in aqueous solutions could lead to ORR features in voltammograms (Section 2.2.6). Therefore, degassing should be conducted strictly throughout the experimental procedures. Pre-purging N_2 in the solution but conducting the cyclic voltammetry in ambient conditions can still result in ORR features in voltammograms of eumelanin.

The suggested degassing procedure is as follows.

1) Using electrolytes with small volumes will make it easier to degas. The larger the volume, the higher the pressure or longer the time required in Procedure 2).
2) Use a high pressure of N_2 gas to purge the aqueous solution. The time for this procedure depends on the quantity of electrolyte. The O_2 in the electrolyte is removed under a given pressure of N_2. For 10 ml aqueous solution, more than 4 min is suggested.
3) Lower the pressure of N_2 and withdraw the pipe above the liquid. This flow of N_2 prevents O_2 from getting into the electrolyte.

In Article 1, the pressure of N_2 does not seem to be high enough in Procedure 2) to exclude the impact of the ORR (Section 2.2.7.3). In Article 2 and Article 3, a higher pressure of N_2 is used in Procedure 2), therefore very little impact of ORR is observed.

3.2.5 Extraction of onset and end potentials

The onset potentials and end potentials are extracted as follows.

- In the case of asymmetric peaks, convoluted symmetric peaks with different onset/end potentials should be considered.
- For the first peak of a potential sweep, the onset potential is found where the slope of the curve initially changes (Figure 3.5). The same applies to the end potential of the last peak of a sweep.
- For the non-first peak of the sweep, its onset potential is usually the local minimum between this peak and the previous peak. If the non-first peak is at a given distance from the previous peak in potential, the extraction is like the first peak’s. The same applies to the end potential of the non-last peak.

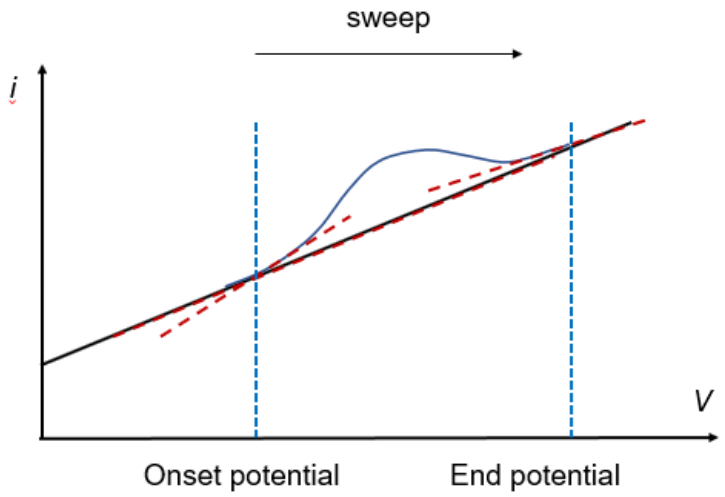

Figure 3.5 The onset and end potential of a peak during a potential sweep.

3.3 Galvanostatic charge-discharge

The galvanostatic charge-discharge electrochemical method is used to evaluate the electrochemical capacitance, resistance and cycling stability of the electrode material.

3.3.1 Working principle of galvanostatic charge-discharge

To evaluate a supercapacitor, two identical electrodes are set as working and counter electrode, respectively. A galvanostatic (constant) current is applied to the working electrode vs. the counter electrode as a function of time. The *cell potential* is therefore the potential difference between the working electrode and counter electrode. A *cut-off voltage* is set to be the potential limit of the cell potential. The resulting plot of galvanostatic charge-discharge is a *V*-*t* plot. The potential increases with time during the charging process, reaches the cut-off voltage, and then decreases with time during the discharging process. In an ideal double layer capacitor, the increase and decrease of the *V* vs. *t* is linear. In a pseudocapacitor, this plot is not strictly linear (Figure 3.6). In this work, a reference electrode is concurrently used to measure the actual potential at both the working electrode and counter electrode vs. the reference electrode (Figure S5 of [20]).

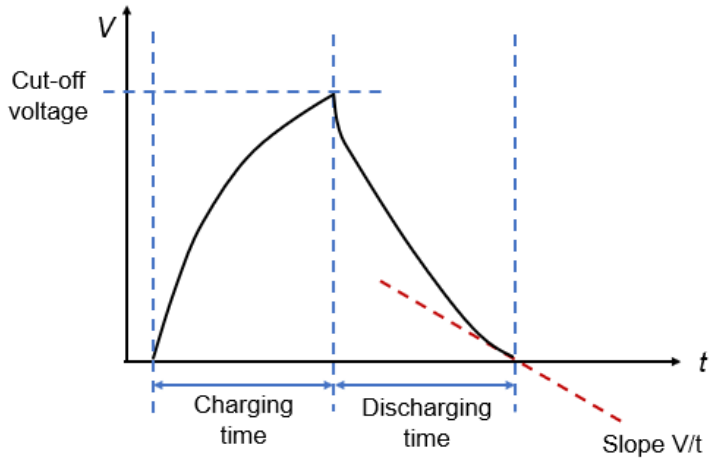

Figure 3.6 Scheme of galvanostatic charging-discharging *V-t* plot for a pseudocapacitor. The slope *V*/*t* is the linear regression for a quasi-linear part at the end of the discharging time.

Equations to calculate the Coulombic efficiency and equivalent resistance are described and calculated in this work in [20], [53], [54]. Extraction of capacitance and capacity are described in Section 3.3.2.

3.3.2 Extraction of capacity and capacitance from the data

The charging capacity and discharging capacity are the products of the constant current and the time for charging and discharging, respectively,

$$q = it \qquad \text{Eq. 3.5}$$

For an electrical double-layer capacitor, capacitance *C* is defined as

$$C = \frac{q}{V} = \frac{t}{V} \cdot i \qquad \text{Eq. 3.6}$$

which is the result of the constant current divided by the slope (*V*/*t*) of *V-t* plot. For a pseudocapacitor, where the *V-t* plot does not have the same slope at every point, we find a quasi-linear curve in the discharging *V-t* plot. In this work, the quasi-linear curve in the *V-t* plot is located at the end of discharging time (Figure 3.6). The slope of *V*/*t* for the calculation of the capacitance is obtained from the linear regression of the quasi-linear curve.

3.4 Electrochemical Impedance Spectroscopy (EIS)

During the EIS experiment, we register the response of an electrochemical cell to an applied potential experiencing a sinusoidal variation of the frequency. The potential is linked to the current through the impedance *Z*, expressed as

$$Z = \mathrm{Re}(Z) - j\ \mathrm{Im}(Z) \qquad \text{Eq. 3.7}$$

In this equation, Re(*Z*) is the real part of the impedance whereas Im(*Z*) is the imaginary part. The impedance is usually displayed in a Nyquist plot with x-axis as Re(*Z*) and y-axis as Im(*Z*) [118].

In this thesis, EIS was used to characterize the charge transfer properties of eumelanin samples [20].

3.5 Scanning Electron Microscopy (SEM)

SEM characterizes the structure of materials in nanometer scale [119]. The two major components of a SEM are the microscope column (also called electron column) and the control console. The electron column consists of an electron gun and electron lenses [120]. At the top of the column, the electron gun generates electrons and accelerates them to energy within the range 0.1-30 keV. The accelerated electrons travel down the column, passing through the lenses. The combination of lenses produces a focused electron beam that reaches the surface of the sample. The interaction between the electron beam and the sample generates signals that are detected and displayed on a computer screen. In particular, images can be taken either in backscattered electron (BSE) or in secondary electron (SE) mode [119].

3.5.1 Backscattered Electrons (BSEs)

BSEs are electrons that enter the surface, are “elastically” scattered back and eventually escape the surface of the specimen. Generally speaking, the higher the atomic number of a component of the specimen, the higher the amount of BSEs generated, therefore the brighter the component appears [119].

SEM in BSE mode in the present thesis has been used to observe the eumelanin-based samples deposited on carbon paper. During these experiments, the eumelanin-based samples were previously stained with heavy metal ions ($UO_2(CH_3COO)_2$ in Article 1 and [20]; $Fe_2(SO_4)_3$ and

$Cu(CH_3COO)_2$ in Article 3) [51], [121]. Eumelanin stained with heavy metal ions is distinguishable from the carbon paper in BSE mode due to the contrast in brightness in the image [119].

3.5.2 Secondary Electrons (SEs)

Secondary electrons (SEs) are loosely bound outer shell electrons ejected after inelastic scattering events undergone by the electrons of the electronic beam [122]. Compared to the behavior of BSE, the amount of SE generated is relatively insensitive to the atomic number [119].

In this thesis, SEM in SE mode was used to study the morphology of synthetic eumelanins loaded on ITO (Article 2).

3.6 X-ray Photoelectron Spectroscopy (XPS)

Surface analysis by XPS is carried out by irradiating a sample with monoenergetic X-rays and analyzing the energy of the detected electrons. Mg Kα (1253.6 eV) or Al Kα (1486.6 eV) X-rays are usually employed. The photoionization leads to two emitted electrons: a photoelectron and an Auger electron. The photoelectrons are generated by the photoelectric effect [123].

The binding energy (BE) of the photoelectron, i.e. the ionization energy, in its simplest form is given by

$$\mathrm{BE} = h\nu - \mathrm{KE} \qquad \text{Eq. 3.8}$$

where $h\nu$ is the energy of the incident photon and KE is the kinetic energy of the photo-emitted electron [124].

XPS can be used to determine the presence of chemical elements on the surface, based on the BE specific to each element [125]. Actually, since BE is affected by the chemical and physical environment, XPS can also be used to gain insight on the chemical state of the elements and functional groups present in the sample under study [126].

In the present thesis, XPS was used to determine elements in Fe/eumelanin samples and functional groups in eumelanin samples before/after exposure to H_2O_2 (Article 3).

3.7 Solar Simulator

A solar simulator is a source of light whose characteristics reproduce those of solar light. Air Mass (AM) filters are used to alter and refine the spectral distribution of the light source to simulate different solar spectral distributions on Earth [127].

The solar simulator used in the present thesis in Article 2 and [20] was a Xenon arc lamp.

3.8 UV-vis spectrophotometer

UV-vis (Ultraviolet-visible) spectrophotometer determines the UV-vis light absorption of a sample. The spectrophotometer is usually equipped with a highly reflective integrating sphere. In Article 1, the UV-vis spectrophotometer without an integrating sphere was used to obtain the spectra of eumelanin monomers in methanol (Figure S5 in Appendix A).

The detector can be placed on the wall of the integrating sphere. The integrating sphere collects all the light transmitted and diffused by the sample, limiting light losses due to diffusion. A spectrophotometer equipped with an integrating sphere produces high precision reflectance and scattered transmittance measurements [20][128]. In [20], the UV-vis spectrophotometer equipped with an integrating sphere in the present thesis was used to obtain optical absorption spectra of eumelanin samples.

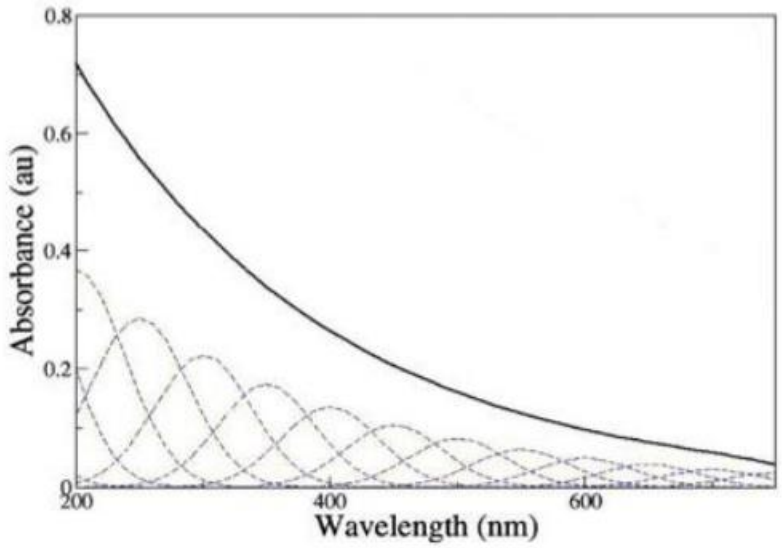

Figure 3.7 The broadband absorption of eumelanin and its convoluted absorption peaks. Adapted from [129].

The monomers of eumelanin have distinguished absorption peaks (Figure S5 in Appendix A). After a given time of polymerization, the optical absorption of eumelanin broadens due to the convolution of different absorption wavelengths, called *broadband absorption* of eumelanin (Figure 3.7 and Figure 1(a)(b) in [20]) [25]. Such broadband optical absorption is caused by the chemically and geometrically disordered structures formed during its polymerization (Section 1.1.2.3).

CHAPTER 4 ARTICLE 1: AN ELECTROCHEMICAL STUDY OF NATURAL AND CHEMICALLY CONTROLLED EUMELANIN

First, in Article 1, fundamental aspect of electrochemical properties of the eumelanins is to be studied with cyclic voltammetry. Article 1 has been published in the APL Materials on December 29th, 2017 [130]. *Its copyright belongs to the authors. The Supplementary Information is provided in Appendix A.*

4.1 Authors

Ri Xu[1], Carmela Tania Prontera[2], Eduardo Di Mauro[1], Alessandro Pezzella[2], Francesca Soavi[3] and Clara Santato[1]

[1] Department of Engineering Physics, Polytechnique Montreal, C.P. 6079, Succ. Centre-ville, Montreal, Quebec, H3C 3A7, Canada.

[2] Dipartimento di Scienze Chimiche, Università di Napoli Federico II, Cupa Nuova Cintia, 21, 80126, Napoli, Italy.

[3] Dipartimento di Chimica "Giacomo Ciamician", Alma Mater Studiorum – Università di Bologna, Via Selmi, 2, 40126, Bologna, Italy.

4.2 Abstract

Eumelanin is the most common form of the pigment melanin in the human body, with functions including antioxidant behavior, metal chelation, and free radical scavenging. This biopigment is of interest for biologically derived batteries and supercapacitors. In this work, we characterized the voltammetric properties of chemically controlled eumelanins produced from 5,6-dihydroxyindole (DHI) and 5,6-dihydroxyindole-2-carboxylic acid (DHICA) building blocks, namely, DHI-melanin, DHICA-melanin, and natural eumelanin, extracted from the ink sac of cuttlefish, Sepia melanin. Eumelanin electrodes were studied for their cyclic voltammetric properties in acidic buffers including Na^+, K^+, NH_4^+, and Cu^{2+} ions.

4.3 Introduction

Eumelanin is a black-brown biopigment found in the human body (e.g. in skin, hair and eyes), in other mammals, reptiles, amphibians and fishes as well as in invertebrates, such as cuttlefish and

insects [23], [131]. Eumelanin extracted from the ink sac of cuttlefish is commonly called Sepia melanin.

The biological functions of eumelanin include photoprotection, metal chelation, antioxidant activity and free radical scavenging [132]. Neuromelanin, a pigment made of eumelanin and pheomelanin (a yellow-red member of the melanin pigment family) present in the brain of humans and primates, is reported to be involved in neurotransmission in the *substantia nigra* of the brain [133].

Exciting technologies based on eumelanin have been recently demonstrated, such as biologically derived batteries and flexible micro-supercapacitors for edible electronics and electroceuticals [16], [50], [51].

The heterogeneous eumelanin macromolecules are constituted by the building blocks 5,6-dihydroxyindole (DHI) and 5,6-dihydroxyindole-2-carboxylic acid (DHICA). The building blocks can polymerize at different positions (indicated as 2, 3, 4, 7 in Scheme 4.1). Different redox states of the building blocks, namely hydroquinone, semiquinone and quinone, coexist in eumelanin (Scheme 4.1). Sepia melanin is made up of DHI and DHICA building blocks and includes a wide range of cations, e.g. Mg^{2+}, Ca^{2+}, Cu^{2+}, Fe^{3+} [23], [49], [134], [135].

Despite the tremendous interest of eumelanin and eumelanin derivatives, fundamental aspects of electron transfer processes in eumelanin are still largely undiscovered. Indeed, the limited solubility of eumelanin in most organic solvents has rendered challenging, through the years, the understanding of its physicochemical properties, including the electrochemical ones. Serpentini et al. studied the redox properties of DOPA–melanin by means of a carbon paste electrode at low potential scan rates [107]. In *thin-layer* conditions, the voltammogram of eumelanin at pH 5.6 revealed two main peaks in oxidation, at 460 and 525 mV versus SCE, one of the two attributable to the oxidation of an amino group of the indole unit of eumelanin, and two peaks in reduction, at 20 and 355 mV. The same authors did not observe any anodic peak attributable to 5,6-dihydroxyindole, located at 50 mV at pH 7.4, in contrast with Young et al [92], [114]. Gidanian et al. reported on the cyclic voltammetric polymerization of DHI building blocks, carried out between -0.35 V and 0.4 V vs Ag/AgCl, on gold disk electrodes, in phosphate buffers at pH 7.0 [136]. More recently, Kumar et al., reporting on eumelanin-based micro-supercapacitors, observed the absence

of distinguishable voltammetric signatures, attributed to the convolution of several redox processes taking place at redox sites featuring different molecular environments [51].

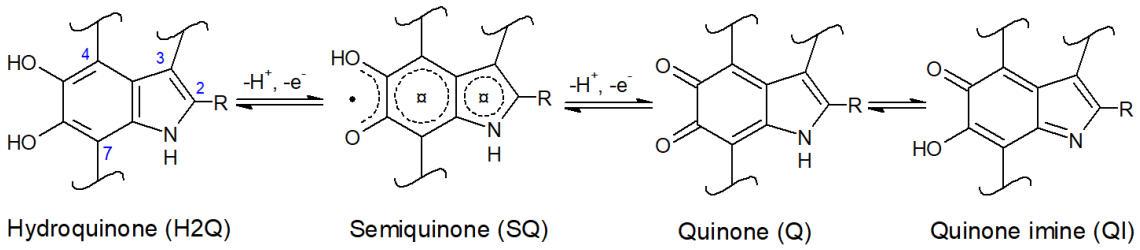

Scheme 4.1 Molecular structures of 5,6-dihydroxyindole (DHI) and 5,6-dihydroxyindole-2-carboxylic acid (DHICA): R is -H in DHI and -COOH in DHICA. The redox forms of DHI and DHICA are indicated: hydroquinone (H2Q), semiquinone (SQ) and quinone (Q). The quinone imine form (QI) is the tautomer of Q.

To assess the technological potential of eumelanin, it is imperative to systematically study electron transfer processes taking place at eumelanin-based electrodes. The scientific relevance of this type of study depends dramatically on the capability to control the molecular structure of the eumelanin and, considering the binding affinity of eumelanin for metal cations, on the choice of the electrolyte. Indeed, the molecular structure determines the nature of the redox sites where the transfer takes place. On the other hand, the electrolyte composition, and specifically the cation chemistry and its binding affinity to eumelanin, affects thermodynamic and kinetic aspects of the redox process.

In this work, we report on the cyclic voltammetric properties of chemically controlled eumelanins obtained from the solid-state polymerization of DHI and DHICA building blocks, namely DHI-melanin and DHICA-melanin. The study has been conducted in slightly acidic electrolytes, based on the well-established proton transport properties of eumelanin [21], [28], [51]. Different aqueous electrolytes were considered, including monovalent (NH_4^+, Na^+, K^+) and divalent cations (Cu^{2+}). Afterwards, the behavior of DHI-melanin and DHICA-melanin has been compared to that of Sepia natural eumelanin.

4.4 Experimental

Chemically controlled eumelanins, i.e. DHI-melanin and DHICA-melanin, were synthesized in situ on carbon paper electrodes by a solid-state polymerization method already reported in the literature [25]. Specifically, 10 mg/mL solutions of DHI and DHICA monomers in methanol were prepared

in ambient conditions. The monomer solution (5 μl) was dropcast on the carbon paper (Spectracarb^{TM} 2050A, 10 mils, geometric area 0.5 cm^2). The loading of DHI-melanin or DHICA-melanin on each carbon paper electrode was ca 0.1 mg cm^{-2}. After dropcasting, the samples were exposed to NH_3 vapors from $NH_{3(aq)}$ (Sigma Aldrich, 28-30% w/v) to catalyze the reaction. The polymerization takes about 3 hours for DHI and about 16 hours (overnight) for DHICA. For Sepia melanin, we drop cast on carbon paper solutions of filtered Sepia melanin (Sigma Aldrich) in DMSO (Sigma Aldrich, ⩾99.9%). Sepia was indeed dissolved in DMSO, sonicated and filtered (0.1 mm PTFE membrane with polypropylene housing, 25 mm diameter, PURADISC^{TM}), to yield suspensions of 10 mg mL^{-1}, approximately (as some eumelanin aggregates may have been trapped in the filter) [137], [138]. 0.25 M buffer solutions of NH_4CH_3COO, $NaCH_3COO$, KCH_3COO, pH ca 5, were prepared from NH_4CH_3COO (Caledon, ≥97.0%), $NaCH_3COO$ and KCH_3COO (Sigma Aldrich, ≥99.0%) dissolved in DI water (18.2 MΩ cm). 2.5 mM $Cu(CH_3COO)_2$ solution in 0.25 M NH_4CH_3COO buffer was prepared using $Cu(CH_3COO)_2$ from Sigma-Aldrich (98+%). Cyclic voltammetry was performed using a Biologic VSP 300 multichannel potentiostat in a three-electrode cell, where carbon paper electrodes loaded with eumelanin were the working electrodes, a Pt mesh was the counter electrode and $Ag/AgCl_{(aq)}$ was the reference electrode. Fresh electrodes were cycled in the potential range -0.2 V/0.2 V, -0.4 V/0.4 V and -0.6 V/ 0.6 V, for a total of 36 cycles (12 in each potential range), in NH_4CH_3COO, $NaCH_3COO$, KCH_3COO solutions and, for a total of 42 cycles (14 cycles in each potential range) in $Cu(CH_3COO)_2$-including NH_4CH_3COO electrolyte. The cyclic voltammograms (apart from those shown in Figures S1-S3) correspond to the 28th cycle for NH_4CH_3COO, $NaCH_3COO$, KCH_3COO solutions and the 33rd cycle for the $Cu(CH_3COO)_2$-including NH_4CH_3COO electrolyte. The first scan was performed towards positive values of the potential. The UV-vis spectra of the DHI and DHICA monomers in solution were obtained immediately after the monomers were dissolved in methanol (Sigma, anhydrous 99.8%) in ambient conditions, by a JASCO V-730 UV-visible spectrophotometer (Figure S4). Scanning Electron Microscopy (SEM) was performed at an acceleration voltage of 5 kV in backscattered electron (BSE) imaging mode using a Microscope JEOL JSM7600F. For staining, the samples were exposed to an aqueous solution of uranyl acetate (2%) for different times and then rinsed with deionized water for 5 min. The SEM images included in this work correspond to 60 min of staining for DHICA-melanin and bare carbon paper, 3 min for DHI-melanin and 10 min for Sepia melanin.

4.5 Results and Discussion

We characterized the morphological features of the eumelanins on carbon paper by SEM. To distinguish the eumelanin from the carbon paper substrate, we stained the biopigment with uranyl acetate [51], [139]. The bright regions observable in the SEM images after staining, mostly present at the junctions of the carbon fibers, indicate the presence of eumelanin (Figure 4.1 and Figure S5). Sepia melanin granules are expected to have lower interfacial area with the electrode and the electrolyte, compared to DHI-and DHICA-melanin.

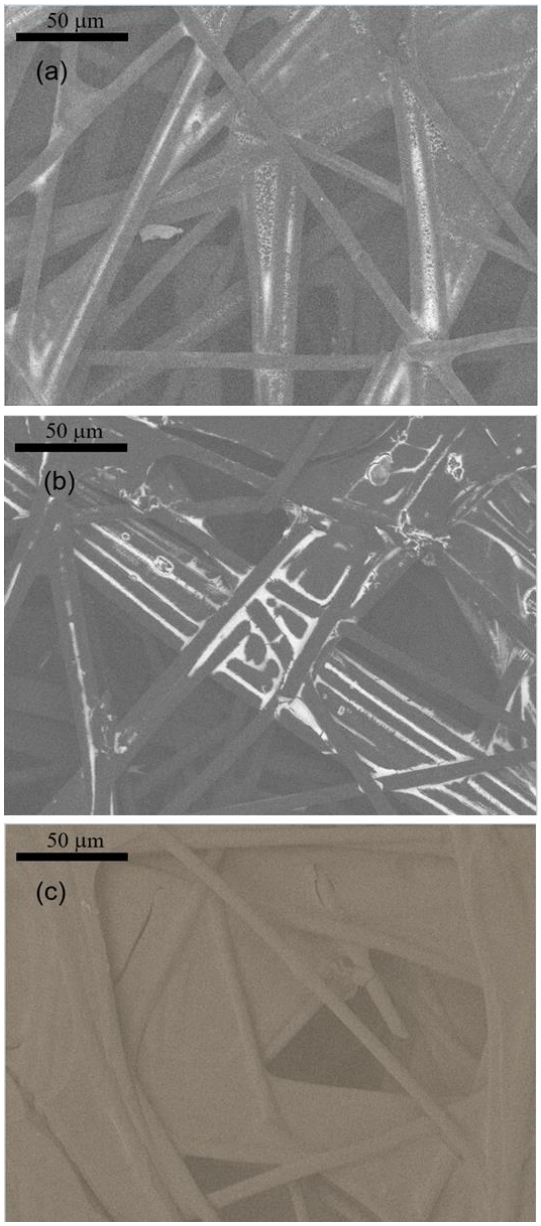

Figure 4.1 SEM images (backscattering mode, acceleration voltage 5 kV) of: Stained (a) DHICA-melanin (b) DHI-melanin, (c) bare carbon paper. Bar size: 50 µm.

We proceeded with the electrochemical characterization of DHI-melanin, DHICA-melanin and Sepia melanin in different aqueous electrolytes, slightly acidic, in agreement with the well-established proton conduction properties of eumelanin [21], [28], [51]. The mobility of the protons in eumelanin makes them effective to counterbalance the injected/extracted charge during electrochemical potential scans, thus promoting electroneutrality.

In presence of monovalent cations, a number of electrochemical signatures of DHI-melanin, DHICA-melanin and Sepia melanin, well distinguishable from those of the carbon paper (blank), were observable during the anodic and cathodic voltammetric scans. When explored within the potential interval -0.6/0.6V vs Ag/AgCl, the voltammograms of DHICA-melanin showed an oxidation shoulder located at ca 0.14 V and an oxidation peak at ca 0.31 V (Figure 4.2(a)). Reduction and oxidation peaks located at ca -0.06 V, could be also observed in the three electrolytes. The presence of different oxidation peaks is attributed to the heterogeneous structure of DHICA-melanin that features different quinone, hydroquinone and semiquinone redox functionalities, located in building blocks with different inter-unit conjugation [103]. A broad reduction wave, presumably resulting from the overlap of broad peaks, was observable within the range 0.3 V and -0.5 V vs. Ag/AgCl. The shape of the voltammograms of DHICA-melanin is the same for ammonium- and alkaline-based electrolytes whereas the intensities of the currents are different. The shoulder at 0.14 V has the same intensity in NH_4^+- and Na^+-based electrolytes whereas the peak at 0.31 V is weaker in NH_4^+- than in Na^+-based electrolytes. The situation is different for electrolytes containing K^+, where the voltammetric currents are lower than those in the other two electrolytes. In principle, the intensity of the voltammetric current is related to the kinetics of ion exchange at the eumelanin/electrolyte interface, strongly affected by the size of the ions. During the oxidation process, the acetate anions are expected to be inserted in the eumelanin network to balance the oxidation charge whereas the cations included in the eumelanin matrix are expected to be released in the electrolyte. The difference in the current intensities for the different electrolytes can be only in part explained by considerations on the ion size since the electrolytes feature a common acetate anion and the hydrated cation radii have similar values (e.g. the mean metal-oxygen bond distance for hydrated sodium and potassium cations have been determined to be 2.43 and 2.81 Å, considering respectively six and seven coordination) [140]. Specific interactions at different redox sites of DHICA-melanin immersed in the electrolytes are expected to contribute to determining the voltammetric currents. As an example, NH_4CH_3COO has acid-base properties expected to affect proton transfer processes associated to electron transfers and specific interactions between melanin and ammonium are well established in the literature [141].

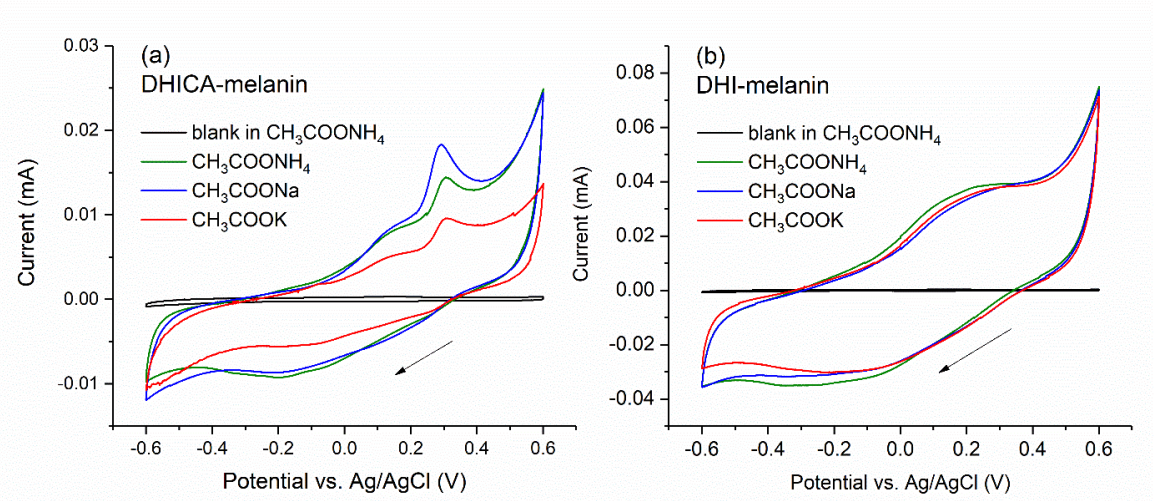

Figure 4.2 Cyclic voltammograms of DHICA-melanin (a) and DHI-melanin (b) run in three aqueous electrolytes as specified in the legend. Scan rate 5 mV/s. The electrochemical potential was cycled towards 0.6 V and then to -0.6 V vs Ag/AgCl.

DHI-melanin shows a voltammetric signature different from that of DHICA-melanin, in all the electrolytes. Specifically, a broad oxidation wave is included between -0.35 V and 0.4 V, which might result from the convolution of the peaks observed in DHICA-melanin. A broad reduction signature, similar to the anodic wave, is located between 0.4 V and -0.5 V, as for DHICA-melanin (Figure 4.2(b)). When compared to DHICA-melanin, DHI-melanin generally shows higher (~2 times) voltammetric currents, likely due to the more efficient π-π stacking in DHI-melanin with respect to DHICA-melanin [103]. The improved conjugation and corresponding electron delocalization might also explain the different shapes of the voltammograms: in DHICA-melanin, electron transfers and ion exchanges are likely more localized than in DHI-melanin thus leading to more resolved peaks.

For both melanins, we observe a broad and irreversible peak during the initial anodic scans, for all potential ranges investigated (Figure S1), analogously to our previous voltammetric studies conducted to advance the knowledge about mixed electronic-protonic transport in eumelanin and its exploitation for energy storage [28], [51], [108]. This broad anodic signature is attributed, at least in part, to the formation of oxidized species at the positive electrode, eventually coupling to give an increased intermolecular reticulation [137], [142].

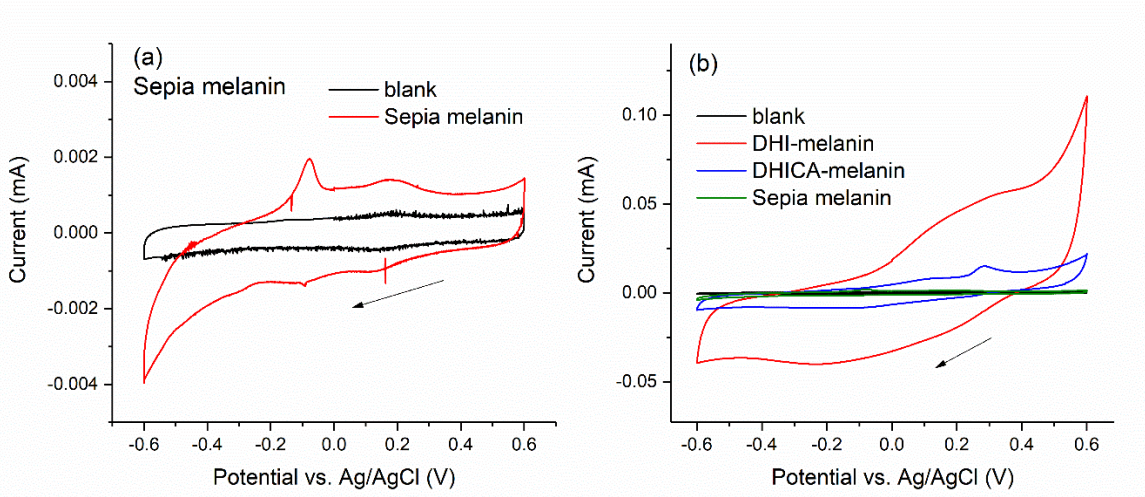

Figure 4.3 Cyclic voltammograms of (a) Sepia melanin and blank electrode, (b) DHI-melanin, DHICA-melanin, Sepia melanin and blank carbon paper electrodes in 0.25 M $NaCH_3COO_{(aq)}$. Scan rate 5 mV/s. The potential was scanned towards 0.6 V and then backward to -0.6 V vs Ag/AgCl.

With respect to DHI- and DHICA-melanin, Sepia melanin in NH_4^+, Na^+, and K^+-based electrolytes showed lower voltammetric currents (Figure 4.3), possibly due to the lower interfacial area of Sepia melanin with the carbon and the electrolyte, with respect to DHI-melanin and DHICA-melanin counterparts [143]. Eumelanin losses during the filtration process undergone by Sepia cannot be excluded as a potential cause of the decrease of the voltammetric current. Sepia melanin has oxidation and reduction signatures at ca 0.15 V as well as at ca -0.06 V, analogously to DHICA-melanin.

With respect to voltammograms carried out in electrolytes including NH_4^+, Na^+ and K^+, when Cu^{2+} is present in the electrolyte, in the form of $Cu(CH_3COO)_2$ added to our NH_4CH_3COO buffer, we observed dramatic changes in the voltammograms. Initially, with bare carbon paper electrodes (our blank), we observed an extremely broad reduction signature, attributable to the reduction of Cu^{2+} to Cu^+, located at ca -0.1 V, followed by an anodic peak at 0.1 V, attributable to the re-oxidation of Cu^+ to Cu^{2+} (Figure 4.4). The high symmetry of the triangle-shaped oxidation peak suggests a surface redox process, involving Cu^+ adsorbed on the carbon paper electrode [53]. With DHICA-melanin or DHI-melanin on carbon paper, the voltammograms change: the intensity of the reduction signature is significantly higher than for bare carbon paper (Figure 4.4(a) and (b)). This

might be explained with a higher surface electrode concentration of Cu^{2+}, with respect to bare carbon, caused by the binding affinity of melanin for Cu^{2+}.

Concerning the oxidation, the main peak attributed to the re-oxidation of Cu^{+} is anticipated at lower potentials when DHI- and DHICA melanin are present on the carbon paper electrodes. This is explained with a weaker adsorption of the reactant (Cu^{+}) at the surface of the melanin-on-carbon electrode with respect to bare carbon. Furthermore, a new broad peak (for DHICA-melanin) or shoulder (for DHI-melanin) appears at higher anodic potentials that could be assigned to the oxidation of Cu^{+} bound to eumelanin, formed during the cathodic scan.

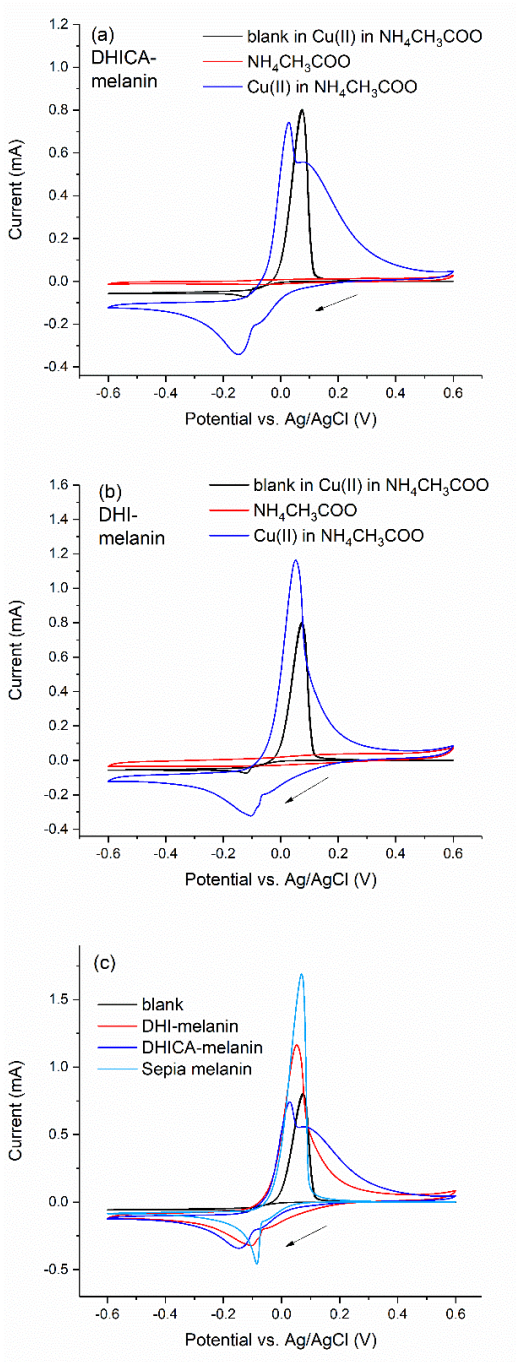

Figure 4.4 Cyclic voltammograms of (a) DHI-melanin, (b) DHICA-melanin and blank carbon paper electrodes in NH_4CH_3COO, $Cu(CH_3COO)_2$ (2.5 mM) in NH_4CH_3COO (0.25 M) buffer solutions, (c) DHI-melanin, DHICA-melanin, Sepia melanin and blank carbon paper electrodes in $Cu(CH_3COO)_2$ (2.5 mM) in NH_4CH_3COO (0.25 M) buffer solutions at pH 4.9 at scan rate of 5 mV/s.

Sepia melanin, known in the literature to bind Cu^{2+} at hydroxyl, carboxylic and amine groups [23], in solutions including Cu^{2+}, has sharper oxidation and reduction peaks with respect to DHI- and DHICA-melanin (Figure 4.4(c)). The reduction peak is also sharpened and anticipated with respect to the carbon paper, therefore further supporting the idea of the change of the Cu^{2+} reduction to Cu^{+} from a solution process to a surface one, as for DHI- and DHICA-melanin [53]. When comparing DHI-, DHICA-melanin and Sepia we observe that the oxidation peak current is more intense with DHI-melanin and Sepia melanin and that the anodic peak (shoulder) following the main peak at 0.1 V observed with DHICA (DHI)-melanin is not observed in the voltammograms of Sepia. This suggests the availability, in DHI-melanin and DHICA-melanin, of binding sites not present in Sepia melanin, pointing to the effect of the supramolecular structure on the electron transfer between eumelanin and copper.

4.6 Conclusions

In conclusion, in this work we reported on the cyclic voltammetric behavior, in acidic electrolyte buffers, of chemically controlled eumelanins obtained from the solid-state polymerization of the DHI and DHICA building blocks as well as of natural eumelanin, Sepia. Eumelanin samples were fabricated on carbon paper electrodes and studied in electrolytes including monovalent (NH_4^+, Na^+, K^+) and divalent (Cu^{2+}) cations. With respect to DHI, which shows in NH_4^+, Na^+ and K^+-including solutions broad oxidation and reduction signatures, DHICA-melanin shows a well distinguishable oxidation signature, observable at 0.31 V. Both the voltammograms of DHICA-melanin and Sepia melanin display redox features at -0.06 V and 0.15 V. All the eumelanin samples immersed in ammonium acetate buffers including Cu^{2+} have a strong oxidation peak at 0.1 V and reduction features included between -0.05 V and -0.09 V (shoulder) and -0.09V and -0.14 V (peak). DHI-melanin and DHICA-melanin have an additional oxidation feature at higher anodic potentials attributable to the oxidation of Cu^{+} bound to eumelanin, with respect to Sepia. Work is in progress to extend the present studies to other cations of biological interest, such as Fe^{2+}/Fe^{3+}, to better understand the biological function of eumelanin in living organism. Considering the optical properties of eumelanin, our work contributes to advance the development of biologically derived organic solar batteries, integrating the solar conversion and the energy storage functions.

4.7 Acknowledgments

The Authors are grateful to Y. Drolet (Polytechnique Montréal) and D. Gingras (Université de Montréal) for technical support. C.S. acknowledges financial support from NSERC (DG) and MESI. A. P. acknowledges financial support from MC-IRSES-612538 (POLYMED). F.S. and C.S. acknowledge the Executive Bilateral Program Italy-Quebec 2017-2019.

CHAPTER 5 ARTICLE 2: LIGHT-ENHANCED ELECTROCHEMICAL ENERGY STORAGE OF SYNTHETIC MELANIN ON CONDUCTIVE GLASS SUBSTRATES

Second, in Article 2 and [20]*, the energy storage application is to be explored with the idea of making use of the sustainable solar light. Article 2 has been published in MRS Advances on December 5th, 2019* [144]*, as a supplementary work after* [20]*. Article 2 is reproduced with the permission of Cambridge University Press.*

5.1 Authors

Authors: Ri Xu[1], Abdelaziz Gouda[1], Maria Federica Caso[2], Francesca Soavi[3] and Clara Santato[1]

[1]Department of Engineering Physics, Polytechnique Montréal, C.P. 6079, Succ. Centre-ville, Montréal, QC, H3C 3A7, Canada

[2]Nanofaber Spin-Off at ENEA, Casaccia Research Centre, Via Anguillarese 301, Roma, 00123, Italy

[3]Dipartimento di Chimica “Giacomo Ciamician”, Alma Mater Studiorum Università di Bologna, Via Selmi, 2, 40126 Bologna, Italy

5.2 Abstract

Eumelanin is a redox active, quinone-based biopigment, featuring a broadband absorption in the UV-Vis region. The combination of the redox and optical properties makes eumelanin an interesting candidate to explore light-assisted storage technologies. Electrodes of melanin on indium tin oxide (ITO) current collectors were investigated for their morphological and voltammetric characteristics in aqueous electrolytes. Under solar light, we observed that the capacity and the capacitance of the melanin electrodes significantly increase with respect to the dark conditions (by 63% and 73%, respectively).

5.3 Introduction

In order to face possible energy shortages caused by the increasing world population, it is relevant to develop sustainable and efficient solar energy storage technologies, combining the solar energy conversion and electrochemical energy storage functions [145]–[148].

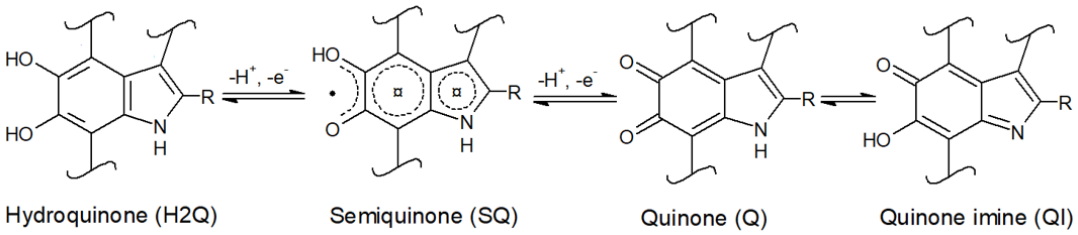

Scheme 5.1 Hydroquinone (H2Q), semiquinone (SQ) and quinone (Q) redox forms of the building blocks of eumelanin: 5,6-dihydroxyindole (DHI) and 5,6-dihydroxyindole-2-carboxylic acid (DHICA). R is –H in DHI whereas R is the –COOH group in DHICA. The quinone imine form (QI) is the tautomer of Q.

Nature is resourceful of environmentally benign and redox active materials, e.g. organic quinone-based species that can be assembled into energy storage devices [4], [7], [16], [17], [149], [8]–[15]. Eumelanin is a quinone-based biopigment ubiquitous in flora and fauna. It has interesting physicochemical features, such as UV-Vis absorption, photoconductivity, hydration-dependent electrical conductivity, metal binding affinity (chelation) [23], [150], [151]. In eumelanin, different redox states coexist in the two building blocks 5,6-dihydroxyindole (DHI) and 5,6-dihydroxyindole carboxylic acid (DHICA) making up the biopigment (Scheme 5.1). Eumelanin-based electrodes have been employed in energy storage devices, such as supercapacitors and batteries. Photovoltaic cells including eumelanin have been reported in the literature [16], [50], [51], [152], [153]. The broad band optical absorption of eumelanin can be explained by chemical disorder (co-existing chromophores) and geometric disorder models [35], [41].

In this work, we report on the capacity and capacitance of DHI-melanin and DHI/DHICA-melanin on ITO current collectors (indium tin oxide) in aqueous electrolytes, as enhanced by solar light illumination [154][25]. Synthetic, chemically controlled melanins, noted as DHI-melanin and DHICA-melanin, were obtained from the polymerization of the building blocks DHI or DHICA, respectively. DHI/DHICA-melanin (weight/weight 7/3), polymerized from both building blocks, was used to model the behaviour of natural melanin [137]. The transparent ITO current collector permitted rear illumination, expected to lead to higher solar light absorption, in turn leading to faster and higher electrochemical response, under solar light illumination, with respect to carbon paper current collectors. Scanning Electron Microscopy (SEM) images shed light onto the

morphology of the material. Cyclic voltammetry of eumelanin, under dark and light conditions, was used to gain insight on the improvement of capacity and capacitance.

5.4 Experimental

Chemically controlled melanins, i.e. DHI-melanin and (7/3 weight/weight) DHI/DHICA-melanin, were synthesized in situ on ITO surfaces by a solid-state polymerization method already reported in the literature [25]. 2 mg/mL solutions of DHI were prepared in ambient conditions and used as precursor. For DHI/DHICA-melanin, 10 mg of powder, including 7 mg of DHI monomer powder and 3 mg of DHICA monomer powder, were dissolved in 5 ml methanol, in ambient conditions, and the solution was used as precursor. Afterwards, the monomer solution (5 μl) was drop cast 3 times, sequentially, on the ITO surface (geometric area 1.56 cm^2). Between each drop casting step, the samples were exposed to NH_3 vapors from $NH_{3(aq)}$ (Sigma Aldrich, 28-30% w/v), a polymerization catalyst, for 1 hour. After the third drop cast step, samples were exposed to NH_3 vapors from $NH_{3(aq)}$ (Sigma Aldrich, 28-30% w/v) for more than 65 hours, to complete the polymerization reaction. The loading of eumelanin on ITO was ca 20 μg cm^{-2}. The morphology of the electrodes was examined by scanning electron microscopy (SEM, JEOL JSM7600F), with secondary electron mode, at an acceleration voltage of 5 kV. The morphology of the samples was examined by atomic force microscopy (AFM, D3100). 0.25 M buffer solutions of $NaCH_3COO$, pH ca 5, were prepared from $NaCH_3COO$ (Sigma-Aldrich >99%) and CH_3COOH (Sigma-Aldrich >99.7%), dissolved in DI water (18.2 MΩ cm). Electrochemical measurements were performed using a Biologic bipotentiostat (SP-300) in a three-electrode cell, with melanin loaded on ITO as the working electrode, a Pt mesh as the counter electrode and $Ag/AgCl_{(aq)}$ in 1 M KCl as the reference electrode. A solar simulator (SLB300A, Sciencetech) was used for electrochemical experiments under light conditions (1 sun, with air mass 1.5 G filter). The experimental configuration was realized by rear (back) illumination.

5.5 Results and Discussion

We used SEM to characterize the morphology of DHI-melanin and DHI/DHICA-melanin samples loaded on ITO. SEM images show dark and bright regions in both DHI-melanin and DHI/DHICA-melanin samples (Figure 5.1). DHI-melanin samples are quite homogeneous in terms of coverage (Figure 5.1(a) and (c)). DHI/DHICA-melanin samples are composed of continuous regions and

nanosized flakes, probably due to the aggregation of DHICA or DHI-DHICA components (Figure 5.1(b) and (d)) [103].

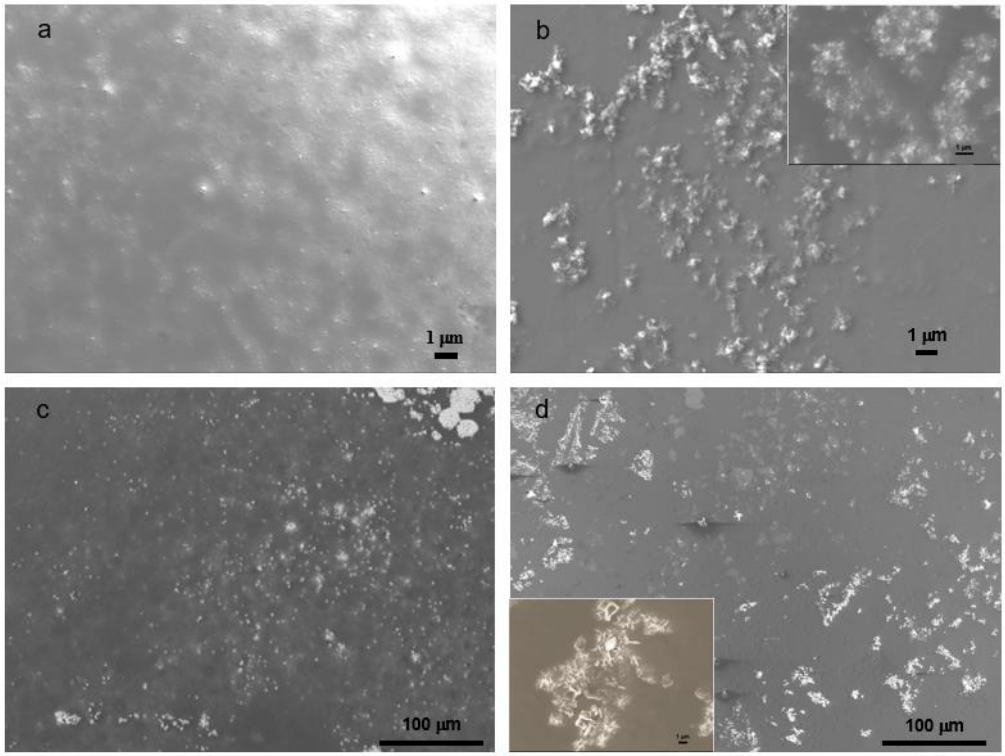

Figure 5.1 SEM images of (a, c) DHI-melanin and (b, d) DHI/DHICA-melanin on ITO (loading ca 20 μg cm^{-2}).

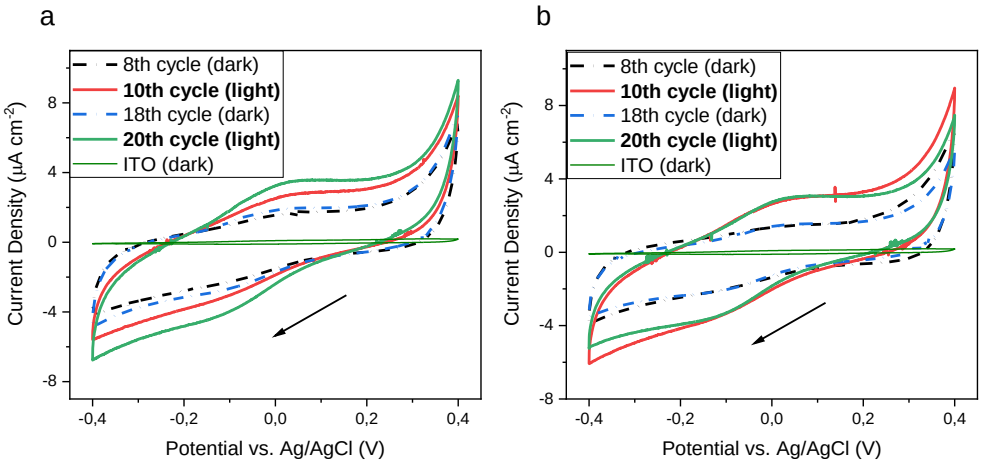

Figure 5.2 Cyclic voltammetries of (a) DHI-melanin and (b) DHI/DHICA-melanin on ITO at 5 mV/s in $NaCH_3COO$ aqueous buffer solution at pH 5. Protocol: dark (8 cycles) → light (5 cycles) → dark (5 cycles) → light (5 cycles). Only the cycle indicated in the legend is shown.

We performed cyclic voltammetry experiments following the protocol: dark (8 cycles) → light (5 cycles) → dark (5 cycles) → light (5 cycles) in a suitable aqueous electrolyte (Figure 5.2). The choice of the slightly acidic electrolyte was determined by considering the favourable proton transport properties of eumelanin [28]. Broad redox features, slightly more pronounced under light irradiation, are observable at 0.05 V and -0.1 V vs Ag/AgCl. Apart from such broad features, the voltammograms are characterized by a *quasi* box-shape behaviour, attributable to the pseudocapacitive nature of eumelanin, featuring Faradaic processes [20], [51], [54]. Light enhances the current in the quasi *box*-shaped voltammograms of eumelanin on ITO, suggesting the presence of a photo-enhanced pseudocapacitive behaviour (Table 5.1). For DHI-melanin, from dark (8^{th} cycle) to light (10^{th} cycle), the capacity (μC cm^{-2}, the total electric charge accumulated by melanin per unit of surface) and capacitance (μF cm^{-2}, the capability of melanin to accumulate electric charge per volt) both increase by about 50%.

Sample	Condition	Cycle number	Capacity ($\mu C\ cm^{-2}$)	Capacitance ($\mu F\ cm^{-2}$)
DHI-melanin	Dark	2	245	459
		4	216	409
		6	197	379
		8	188	361
	Light	10	252	495
		12	238	473
	Dark	14	235	432
		16	217	415
		18	211	409
	Light	20	312	617
		22	310	619
DHI/DHICA-melanin	Dark	2	419	554
		4	320	483
		6	215	359
		8	190	353
	Light	10	274	534
		12	267	532
	Dark	14	170	334
		16	156	308
		18	154	306

	Light	20	244	504
		22	237	497

Table 5.1 Capacity (extracted from integration of current vs. time plots within the cathodic current range, not shown) and capacitance (extracted from linear regression of charge vs. potential plots within the cathodic current range, not shown) of DHI- and DHI/DHICA-melanin on ITO extracted from the cathodic current measured during cyclic voltammetry (Figure 5.2).

Importantly, the improvement of the storage properties observed under light irradiation persists in the dark (e.g. cycle 15 vs cycle 8: capacity increases by 25% and capacitance by 30%). The second series of experiments under light irradiation (from 19^{th} to 24^{th}) gives even more encouraging results: ca 50% increase of capacity and capacitance, from dark to light conditions (18^{th} to 20^{th} cycle). In the case of DHI/DHICA-melanin, from dark to light (8^{th} to 10^{th} cycle), the capacity increases by 63% whereas the capacitance increases by ca 73%. From the 18^{th} cycle in the dark to the 20^{th} under light irradiation, the capacity increases by 58% and the capacitance increases by 64%. Bare ITO does not contribute to the overall current (Figure 5.2).

Condition	Cycle	DHI-melanin		DHI/DHICA-melanin	
		Capacity loss	Capacitance loss	Capacity loss	Capacitance loss
Dark	2 to 5	25%	27%	13%	12%
	5 to 8	8%	3%	8%	7%
Light	10 to 13	6%	2%	4%	-
Dark	15 to 18	5%	-	4%	2%
Light	20 to 23	4%	3%	3%	-

Table 5.2 Capacity and capacitance losses during cycling for DHI- and DHI/DHICA-melanin on ITO (extracted from Figure 5.1).

Interesting observations can be proposed with respect to the stability of the melanin samples on ITO. On the one hand, there are capacity and capacitance losses during cycling, possibly due to a limited compatibility of eumelanin on ITO surface (Table 5.2). From the 15th to the 18th cycle, for DHI-melanin, the capacity decreases by 5%, whereas the capacitance is maintained. For DHI/DHICA-melanin, the capacity decreases only by ca 4%, whereas the capacitance decreases only by 2%. On the other hand, our experiments suggest that the cycling stability of both melanins is acceptable after exposure to solar light. Surprisingly, the capacitance of DHI/DHICA-melanin is maintained during light irradiation.

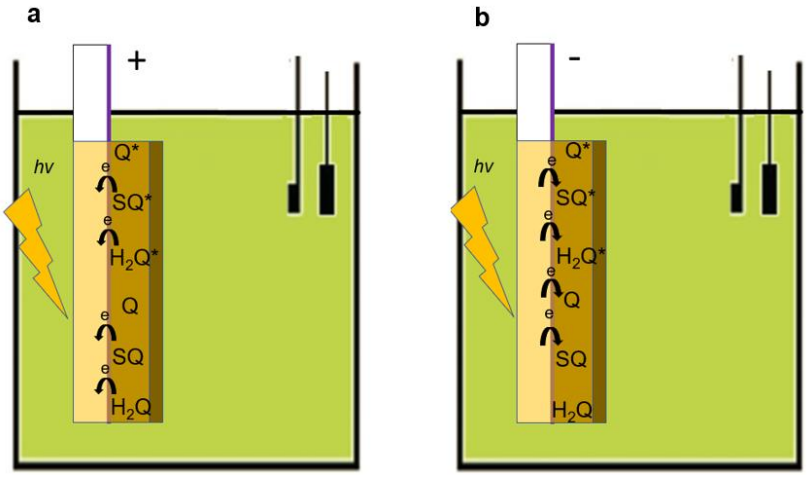

Scheme 5.2 Melanin photo-electrodes (a) positively biased and (b) negatively biased investigated in this work.

We explain the increased response of DHI- and DHI/DHICA-melanin under irradiation conditions by the action of the light that increases the number of charge carriers stored in the melanin (Scheme 5.2). In the dark, the positively biased melanin electrodes (with redox species largely present in the SQ and Q redox forms) experience electron transfers from SQ to ITO to produce Q. When the light is absorbed by the melanin, it excites electrons from the ground electronic state to the excited state, from where electrons are, in principle, easily transferred to ITO. Therefore, the total capacity of the melanin is enhanced under irradiation by the higher number of electron transfer events, due to photoinduced transfers from the excited states taking place in parallel to the transfers due to the applied electrochemical potential. On the other hand, the negatively biased melanin electrode (with redox species largely present in the H_2Q and SQ redox forms) in the dark, experiences electron transfers from ITO to SQ to produce H_2Q. When the light is absorbed by the melanin, the electrons are promoted to excited state and easily transferred from ITO, e.g., to SQ to produce H_2Q [53].

5.6 Conclusion

In conclusion, we reported on the use of chemically controlled melanins (DHI- and DHI/DHICA-melanins) deposited on transparent Indium Tin Oxide (ITO) electrode current collectors as sustainable organic redox materials where the electrode capacity and capacitance are improved under solar light. The broad band absorption and the redox properties offer the possibility to enhance the storage properties of melanin electrodes under solar light. We observed that the solar light improves the capacitance, capacity (by 63% and 73%, respectively, with DHI/DHICA-melanin) and stability of the melanin electrodes. Work is in progress to understand if there is an effect of the solar light on the structure of eumelanin on ITO to better explain the beneficial effects of the solar illumination on the storage performance and the good eumelanin stability on ITO.

CHAPTER 6 ARTICLE 3: AN ELECTROCHEMICAL STUDY ON THE EFFECT OF METAL CHELATION AND REACTIVE OXYGEN SPECIES ON A SYNTHETIC NEUROMELANIN MODEL

Third, in Article 3, the antioxidant/prooxidant dual properties of eumelanin are to be explored by electrochemical methods. Article 3 has been published by the Frontiers in Bioengineering and Biotechnology: Nanobiotechnology since October 18th, 2019 [155]. *The copyright of this article belongs to its authors. Supplementary Information is provided in Appendix B.*

6.1 Authors

Ri Xu[1], Francesca Soavi[2], Clara Santato[1]*

[1]Department of Engineering Physics, Polytechnique Montréal, C.P. 6079, Succ. Centre-ville, Montréal, QC, H3C 3A7, Canada

[2]Dipartimento di Chimica "Giacomo Ciamician", Alma Mater Studiorum Università di Bologna, Via Selmi, 2, 40126 Bologna, Italy

6.2 Abstract

Neuromelanin is present in the cathecolaminergic neuron cells of the *substantia nigra* and *locus coeruleus* of the midbrain of primates. Neuromelanin plays a role in Parkinson's disease (PD). Literature reports that neuromelanin features, among others, antioxidant properties by metal ion chelation and free radical scavenging. The pigment has been reported to have prooxidant properties too, in certain experimental conditions. We propose an explorative electrochemical study of the effect of the presence of metal ions and reactive oxygen species (ROS) on the cyclic voltammograms of a synthetic model of neuromelanin. Our work improves the current understanding on experimental conditions where neuromelanin plays an antioxidant or prooxidant behavior, thus possibly contributing to shed light on factors promoting the appearance of PD.

6.3 Introduction

Melanins are a family of biopigments ubiquitous in flora and fauna. The black-brown eumelanin, red-yellow pheomelanin and neuromelanin all belong to the melanin family [57]. Neuromelanin is mainly present in the cathecolaminergic neuron cells of the substantia nigra and locus coeruleus of

the midbrain of primates [22], [156]. Neuropathological studies report on the loss of pigmented neurons of the substantia nigra in patients affected by Parkinson's disease [90], [157], [158]. It has been proposed in the literature that neuromelanin could have a role in neurotransmission [151]. Electron microscopy studies revealed that neuromelanin has a core-shell pheomelanin-eumelanin structure [57]. Consequently, eumelanin can be proposed as a chemical model of neuromelanin to study interfacial processes between neuromelanin and its surroundings. Sepia melanin is the eumelanin extracted from the ink sac of cuttlefish [91].

Eumelanin is a biomacromolecule whose building blocks are 5,6-dihydroxyindole (DHI) and 5,6-dihydroxyindole-2 carboxylic acid (DHICA), co-existing in different redox states (Figure 6.1). Chemical synthesis permits to obtain chemically controlled DHI-melanin and DHICA-melanin, from exclusively one of the two building blocks (DHI or DHICA) [25]. By combining well-defined amounts of the two building blocks, it is also possible to obtain DHI-DHICA-melanin, a synthetic analogous of eumelanin of interest for fundamental studies [61]. Eumelanin binds metal ions, such as iron and copper cations, by electrostatic interactions and/or chelation (multidentate binding). When chelated by melanin, iron and copper ions share the same binding sites, including catechol, amine and, when available, carboxylic groups [23], [159].

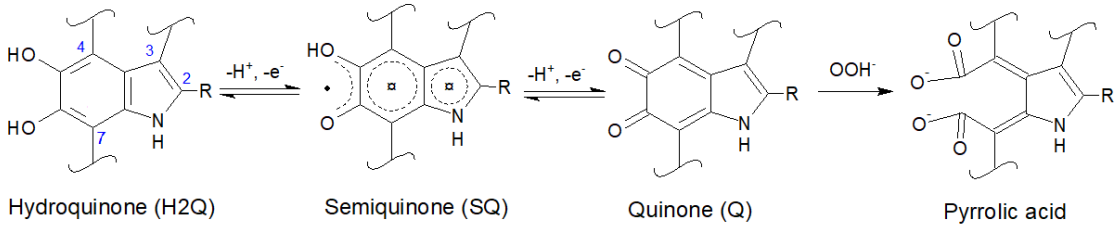

Figure 6.1 Molecular structures of 5,6-dihydroxyindole (DHI) and 5,6-dihydroxyindole-2-carboxylic acid (DHICA): R is -H in DHI and -COOH in DHICA. DHI and DHICA are building blocks of eumelanin. The redox forms of DHI and DHICA are indicated: hydroquinone (H2Q), semiquinone (SQ), and quinone (Q). OOH^- (the deprotonated form of H_2O_2, present in basic media) can oxidize quinone into pyrrolic acid [160]–[162].

The biorole of neuromelanin is object of debate in the scientific community [163]. On the one hand, neuromelanin could have an antioxidant behavior, *e.g.* by scavenging reactive oxygen species (ROS, *e.g.* $^{\bullet}OH$ and H_2O_2) and binding redox active transition metal ions [22], [121]. On the other

hand, neuromelanin could feature a prooxidant behavior, e.g. by generating ROS. Neuromelanin could indeed catalyze the oxygen reduction reaction to form H_2O_2 (and the catalysis is reported to be more effective if melanin is engaged in iron binding) [65], [66]. Redox reactions possibly happen between melanin and Fe^{3+} (Fe^{3+} + H2Q → Fe^{2+}/SQ + H^+ or Fe^{3+} + SQ → Fe^{2+}/Q + H^+) [78]. Fe^{2+}, free or chelated by melanin, can react with H_2O_2 to produce •OH by the Fenton reaction (Fe^{2+} + H_2O_2 → Fe^{3+} + •OH + OH^-) [76]–[78]. •OH can cause the degradation of neuromelanin and other molecular species in its proximity, including neurons and lipids [78], [84], [164], [165].

Electrochemical studies on neuromelanin samples in media including transition metal ions or ROS are expected to contribute to shed light on the nature of the experimental conditions where neuromelanin plays an antioxidant or a prooxidant behavior. Our groups reported on the electrochemical behavior of synthetic DHI- and DHICA-melanins in presence of NH_4^+, Na^+, K^+, and Cu^{2+}, at pH 5. We observed that DHICA-melanin voltammograms showed better resolved features than DHI-melanin, in $NaCH_3COO_{(aq)}$ whereas DHI-melanin voltammograms featured *quasi* box-shaped behavior. In presence of Cu^{2+}, both DHICA- and DHI-melanin featured adsorption peaks [130]. Zareba et al. reported that both precursors, DHI and DHICA, form melanin pigments in presence of •OH [101]. Cecchi et al. reported on the quantitative comparison between free radical scavenging and redox properties of eumelanin biopigments as measured by Briggs Rausher and Folin Ciocalteu assays, to study the antioxidant activity of Sepia and synthetic melanin [89]. Kim et al. used spectroelectrochemical reverse engineering to demonstrate that the free radical scavenging properties of Sepia and fungal melanin are affected by the redox state of the melanin [70]. The same research group, with a similar approach, demonstrated that pheomelanin has higher redox-based prooxidant activity than eumelanin [72]. They also reported that, with respect to bare polydopamine, the redox properties of polydopamine-Fe^{3+} complexes are strongly suppressed while those of polydopamine-Mg^{2+} complexes are maintained [71].

In this work, using the cyclic voltammetry technique, we studied the effect of metal chelation as well as presence of ROS moieties on the behavior of DHI-DHICA-melanin, considered as neuromelanin synthetic model, and of DHICA- and DHI-melanin. Specifically, we considered iron and copper ions (with corresponding metal-modified melanin samples named from now on as Fe/melanin, Cu/melanin, Cu/Fe/melanin) as well as H_2O_2 and •OH [91]. For our voltammetric studies, we used an electrolyte mimicking the intraneuronal cell solution. The morphology of the

Cu/Fe/melanin samples was studied by scanning electron microscopy (SEM) whereas the chemical effect on the surface of the melanin after exposure to metals and ROS was characterized by X-ray photoelectron spectroscopy (XPS).

6.4 Materials and Methods

6.4.1 Preparation of melanin samples on carbon paper

We synthesized DHI-melanin, DHICA-melanin, DHI-DHICA-melanin (1.3:1 mol:mol) *in situ* [137], on carbon paper current collectors (Spectracarb^{TM} 2050A, 10 mils) by solid-state polymerization from the corresponding building blocks [25]. DHI and DHICA building blocks were synthesized as described [25], [93]. 10 mg/mL solutions of DHI and/or DHICA monomers in methanol (99.8%, Sigma Aldrich) were prepared in ambient conditions. For DHI-DHICA-melanin, 10 mg of powder, including 5 mg of DHI monomer powder and 5 mg of DHICA monomer powder, were dissolved in methanol, in ambient conditions, and the solution was used as precursor. The monomer solutions (5 µl) were drop cast on carbon paper featuring a geometric area of 0.5 cm^2 (therefore the loading of the melanin samples was ca 0.1 mg cm^{-2}). After drop casting, the samples were exposed overnight to NH_3 vapors from $NH_{3(aq)}$ (Sigma Aldrich, 28-30% w/v) to catalyze the polymerization.

6.4.2 Preparation of Fe/melanin and Cu/Fe/melanin samples on carbon paper

Samples were prepared by two different routes: route i) and route ii). For both routes we prepared solutions as described in the following protocols. Fe_2SO_4 aqueous solutions (pH 7) were prepared from $FeSO_4 \cdot 7H_2O$ (≥ 99%, Fischer Scientific). $Cu(CH_3COO)_2$ aqueous solutions (pH 7) were prepared from $Cu(CH_3COO)_2 \cdot H_2O$ (≥ 98%, Sigma Aldrich). After 2 days in ambient conditions, the Fe_2SO_4 solutions showed yellow deposits of Fe_2O_3 [166]. 1 M H_2SO_4 aqueous solutions were prepared from H_2SO_4 95-98%, Sigma-Aldrich. In route i), $Fe_2(SO_4)_3$ aqueous solutions were adjusted at pH 3 using 1 M $H_2SO_{4\,(aq)}$ before pre-immersion [166]. The effect of metal ion chelation was studied on samples obtained by route i), based on pre-immersion of the melanin samples in solutions including copper and iron ions, and **route ii)** based on the exposure of melanin samples to copper and iron ions present in the electrolyte where the cyclic voltammetry experiments were carried out (see Table 6.1). In route i), Fe/melanin samples (0.04 mol:mol, 0.1 mol:mol and 0.2

mol:mol) were prepared by pre-immersing melanin electrodes in 10 ml $Fe_2(SO_4)_3$ solutions, with concentrations 1 μM, 3 μM, 6 μM, for 24 h (Table 6.1). Cu/Fe/melanin, with molar ratio of Cu:Fe:melanin 0.002:0.2:1, were prepared by pre-immersing fresh melanin electrodes in solutions (10 ml) including 6 μM $Fe_2(SO_4)_3$ and 0.05 μM $Cu(CH_3COO)_2$ at pH 3 (Table 6.1). Melanin samples obtained by the pre-immersion route were successively studied for their electrochemical properties in electrolytes free from copper and iron ions. In route ii), we studied the effect of Fe^{3+} and Cu^{2+} following two protocols: ii-a) 2 voltammetric cycles → addition of $Fe_2(SO_4)_3$ with Fe:DHICA-melanin 0.04 mol:mol → 2 voltammetric cycles → addition of $Fe_2(SO_4)_3$ with Fe:DHICA-melanin 0.14 mol:mol → 2 voltammetric cycles → addition of $Fe_2(SO_4)_3$ with Fe:DHICA-melanin 0.23 mol:mol → 2 voltammetric cycles → addition of $Cu(CH_3COO)_2$ to form Cu/Fe/DHICA-melanin with Cu:Fe:DHICA-melanin ratio 0.002:0.23:1 mol:mol:mol; ii-b): 2 voltammetric cycles → addition of $Cu(CH_3COO)_2$ with Cu:DHICA-melanin 0.002 mol:mol → 2 voltammetric cycles → addition of $Fe_2(SO_4)_3$ with Cu:Fe:DHICA-melanin 0.002:0.33:1 mol:mol:mol → 2 voltammetric cycles.

6.4.3 Preparation of Fe/melanin and Cu/Fe/melanin on fused silica

Fused silica (1 cm × 1 cm) was cleaned by sonication in acetone and water. Following a similar procedure as synthesis on carbon paper, we synthesized DHI-melanin, DHICA-melanin, DHI-DHICA-melanin (1:1 mol:mol) on fused silica by solid-state polymerization [25]. The monomer solution (40 μl) was drop cast on 1 cm^2 (therefore the loading of the melanin samples was ca 0.4 mg cm^{-2}, 4 times the amount of loading on carbon paper). Cu/Fe/melanin with molar ratio of Cu:Fe:melanin 0.002:0.2:1 were prepared on fused silica by pre-immersing fresh melanin on fused silica in solutions (10 ml) including 48 μM $Fe_2(SO_4)_3$ and 0.4 μM $Cu(CH_3COO)_2$ at pH 3 (Table 6.1).

6.4.4 Preparation of solutions containing H_2O_2 and $^{\bullet}OH$

H_2O_2 (3%, for microbiology) was purchased from Sigma Aldrich. $^{\bullet}OH$ was prepared by the Fenton reaction ($Fe^{2+} + H_2O_2 \rightarrow Fe^{3+} + {}^{\bullet}OH + OH^-$, see Table 6.1).

Table 6.1 Concentrations of the chemical species used in this work for the corresponding experiments (volume of the solutions: 10 ml).

Material	Conc. (μM)	Amount (nmol)	Material: melanin mol:mol	Experiment	Reference for the preparation of the material/ solution
Melanin	-	300	1	Melanin on carbon paper as working electrodes	[51], [130]
Fe^{3+}	1	10	0.04	Melanin on carbon paper by pre-immersion (route i)	[22], [77], [121], [167]
Fe^{3+}	3	30	0.1		
Fe^{3+}	6	60	0.2		
Cu^{2+}	0.05	0.5	0.002		[22]
Fe^{3+}	1	10	0.04	Melanin on carbon paper modified by metal ions in the electrolyte (route ii)	[22], [77], [121], [167]
Fe^{3+}	3	40	0.14		
Fe^{3+}	6	70	0.23		
Fe^{3+}	10	100	0.33		
Cu^{2+}	0.05	0.5	0.002		[22]
Fe^{3+}	48	480	0.2	Melanin on fused silica by pre-immersion (route i)	[22], [77], [121], [167]
Cu^{2+}	0.4	4	0.002		[22]
H_2O_2	1500	15000	50	Exposure to H_2O_2	[168]

Fe^{2+}	6	60	0.2	Preparation of Fenton's reagent	[22], [77], [121], [167]
$^{\bullet}OH$	6	60	0.2	Exposure to $^{\bullet}OH$	[84]

6.4.5 Electrochemical set-up

Cyclic voltammetry was performed using a Biologic VSP 300 multichannel potentiostat, with carbon paper current collectors loaded with melanin acting as the working electrode, Pt mesh as the counter electrode and $Ag/AgCl_{(aq)}$ (1 M KCl for Fe/melanin electrodes prepared by pre-immersion and 3 M NaCl for the rest of the work) as the reference electrode. The electrolyte (10 ml) was composed of 145 mM KCH_3SO_4 (99%, Acros Organics), 10 mM NaCl (≥99%, Sigma Aldrich), 2 mM $MgCl_2$ (≥99%, Sigma Aldrich), 10 mM $NaCH_3COO$ (≥99%, Sigma Aldrich), buffered with CH_3COOH at pH 7 [169], [170]. The electrolyte at pH 5 was composed of 0.25 M $NaCH_3COO$, buffered with CH_3COOH.

6.4.6 X-ray Photoelectron Spectroscopy (XPS)

The XPS survey scan and high-resolution XPS analysis was carried out with a VG ESCA- LAB 3 MKII instrument under Mg Ka radiation by applying 300 W (15 kV, 20 mA) power. The pressure in the chamber during the analysis was 3.0×10^{-9} Torr. The high-resolution spectra were acquired with a pass energy of 20 eV and electrons were collected at a 0 deg takeoff angle. Peak fitting was performed with symmetrical Gaussian–Lorentzian product functions after Shirley background subtraction. Wagner sensitivity factors were used to normalize the peak intensities for quantification.

6.4.7 Scanning Electron Microscopy (SEM)

SEM images were acquired at an acceleration voltage of 15 kV in the backscattered electron imaging mode using a FEI Quanta 450 Environmental Scanning Electron Microscope (FE-ESEM).

6.5 Results and Discussion

6.5.1 Cyclic voltammograms of melanins

We initially collected cyclic voltammograms of DHICA-melanin, DHI-melanin and DHI-DHICA-melanin, in electrolytes featuring different pH, namely pH 5 and 7 (Figure 6.2). At pH 5, the electrolyte was 0.25 M $NaCH_3COO$, selected on the basis of previous cyclic voltammetry studies carried out in our groups [28], [51], [130]. At pH 7, the electrolyte solution (described in Experimental) was selected to mimic the intraneuronal liquid [169], [170]. Surprisingly enough, two types of cyclic voltammograms are observable both for DHICA-melanin and DHI-DHICA-melanin (**Type 1** and **Type 2**, Figure 6.2), with all the experimental conditions fixed. Cyclic voltammograms of DHICA-melanin show oxidation peaks at ca 0.15 and 0.3 V vs. Ag/AgCl (3 M NaCl), at pH 5 (from now on named Type 1 DHICA-melanin, Figure 6.2 (A)) and broad cathodic peaks at ca. 0.25 V and -0.2 V vs. Ag/AgCl. At pH 7, only one anodic peak is detectable at ca 0.2 V vs. Ag/AgCl for Type 1 DHICA-melanin (Figure 6.2 (B)) whereas a cathodic peak is located at ca 0.2 V vs. Ag/AgCl. Type 2 DHICA melanin show additional anodic and cathodic peaks at both pHs. At pH 5, Type 2 DHICA-melanin features an additional sharp anodic peak at ca -0.05 V (Figure 6.2 (A)) and a broad wave at ca. -0.1 V. At pH 7, Type 2 DHICA-melanin features two additional anodic peaks at ca. at ca -0.05 V and 0.05 V and one additional cathodic peak at ca. 0.1 V (Figure 6.2 (B)), with respect to Type 1. We tentatively explain the possibility to observe different voltammograms, for formally identical DHICA-samples, with differences in the supramolecular structure of DHICA-melanin. Such differences are attributable to the heterogeneity of the carbon paper where melanin is overgrown; carbon paper is made up of fibers and flat regions at fibers' interconnections (see later, SEM images). Results also show that cycling causes the evolution of the redox features in Type 2 DHICA-melanin, at pH 7 (Figure 6.2(B)): the intensity of the oxidation feature at ca 0.2 V decreases whereas that one of the features at ca -0.05 V increases.

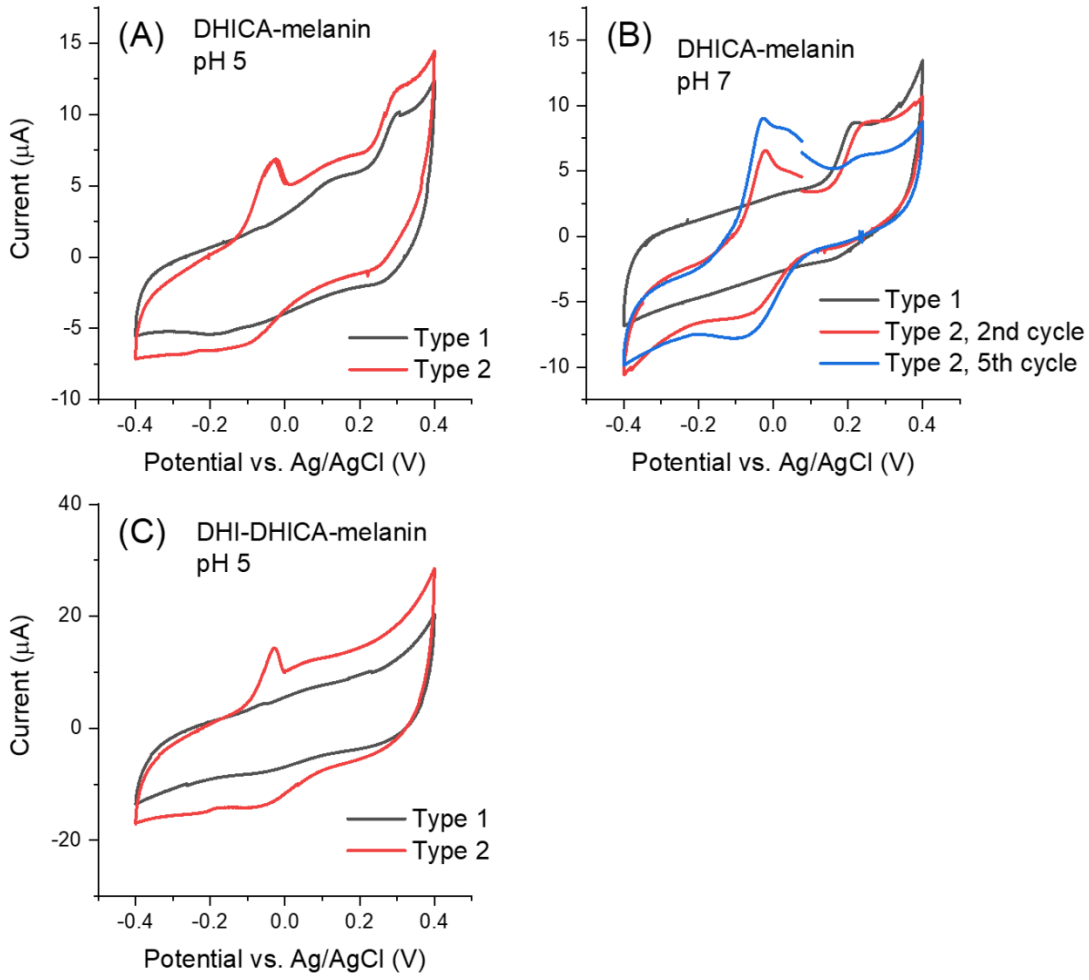

Figure 6.2 Cyclic voltammograms of **(A)** Type 1 and Type 2 DHICA-melanin in 0.25 M $NaCH_3COO$ pH 5, **(B)** Type 1 and Type 2 DHICA-melanin, at 5 mV/s, each for two cycles, in the simulated neurological fluid electrolyte pH 7, **(C)** Type 1 and Type 2 DHI-DHICA-melanin in 0.25 M $NaCH_3COO$ pH 5. DHI-mlanin only has one type of voltammogram. Only the second cycle is shown.

Voltammograms of DHI-DHICA-melanin can also feature two types of behavior, at pH 5 (from now on indicated as **Type 1** and **Type 2 DHI-DHICA-melanin**, Figure 6.2 (C)). The voltammogram of Type 1 DHI-DHICA-melanin is *quasi* box-shaped whereas Type 2 DHI-DHICA-melanin features an oxidation peak at ca -0.05 V and a broad reduction feature. DHI-melanin features a *quasi*-box-shaped behavior, in agreement with the literature, both at pH 5 and 7 (Figure 6.3(C) and Figure 6.3 (F)) [130].

After the study of bare melanins, we exposed the pigment to iron and copper metal ions and ROS. The concentrations of Fe^{3+} and Cu^{2+} were chosen based on the reported concentrations of Fe:melanin ratio in the *substantia nigra* and Cu:melanin ratio in the *locus coeruleus*. The concentration of H_2O_2 was chosen based on the concentration reported for endogeneous H_2O_2 in the neuron cells [22], [77], [84], [121], [167], [168].

6.5.2 Cyclic voltammograms of Fe/melanin prepared by pre-immersion (route i)

Fe^{3+} has considerably higher physiological concentrations with respect to Cu^{2+} in the brain (highest Fe:melanin ratio is ca 0.2 mol:mol in the *substantia nigra* whereas the highest Cu:melanin ratio is 0.002 mol:mol in the *locus coeruleus*). We therefore considered, initially, Fe^{3+} for the study of the effect of metal cations on the voltammetric properties of melanin. We initially adopted the pre-immersion route for the preparation of the samples (Fe/DHI-melanin, Fe/DHICA-melanin and Fe/DHI-DHICA-melanin, Figure 6.3).

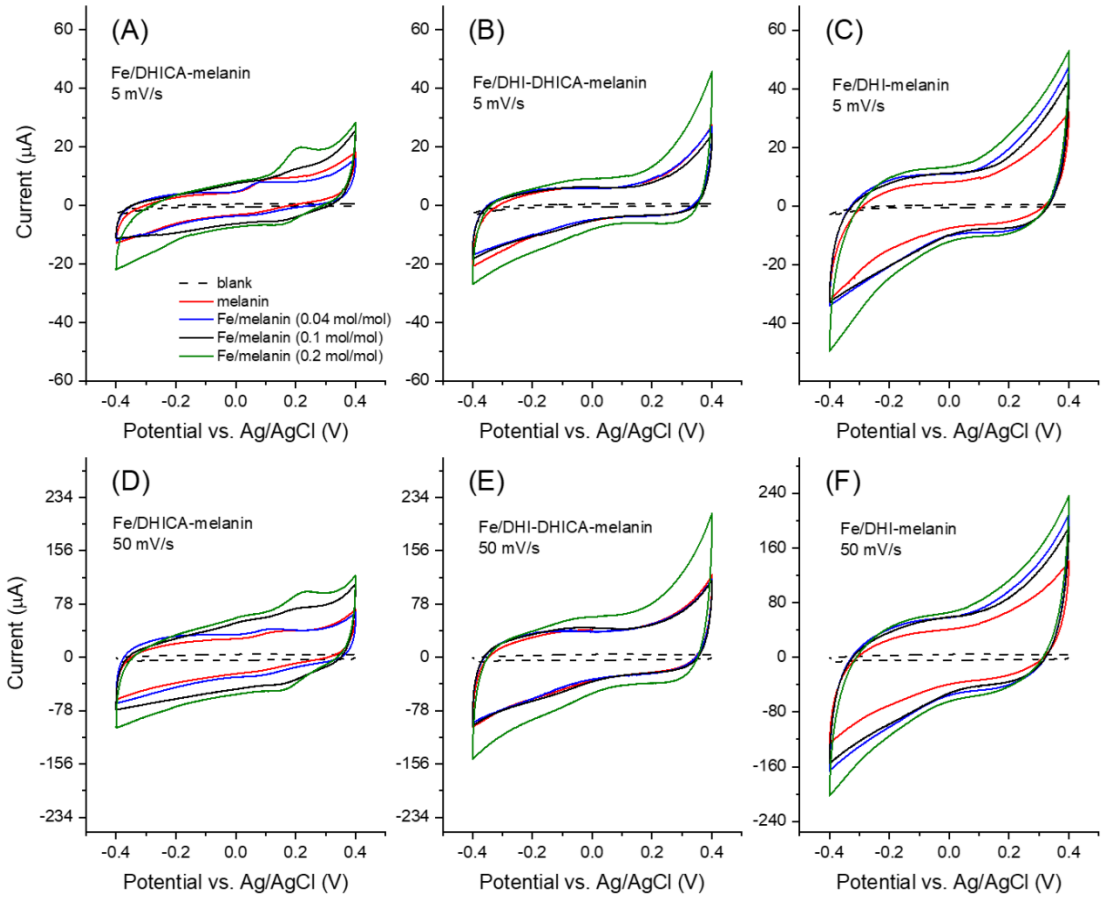

Figure 6.3 Cyclic voltammograms of Fe/melanin complexes prepared by pre-immersion at different Fe^{3+}:melanin ratios: **(A)**, **(D)** Fe/DHICA-melanin (Type 1 DHICA-melanin), **(B)**, **(E)** Fe/DHI-DHICA-melanin (Type 1 DHI-DHICA-melanin) and **(C)**, **(F)** Fe/DHI-melanin. Acquisition protocol: fresh electrodes were cycled in the potential range -0.1 V/0.1 V, -0.2 V/0.2 V, -0.3 V/0.3 V, -0.4 V/0.4 V at 5 mV/s and 50 mV/s, each for 2 cycles in the simulated neurological fluid (pH 7) (Table 6.1). Only the second cycle is shown.

The cyclic voltammograms were obtained in solutions at pH 7 at different iron concentrations and potential sweeping rates (Figure 6.3). Voltammograms obtained with Fe/DHICA-melanin (Type 1 DHICA-melanin, Fe:DHICA-melanin 0.04 mol:mol) are quite similar to those of bare melanin (Figure 6.3 (A), Figure 6.3 (D) and Figure 6.2). As the molar ratio of Fe:DHICA-melanin increases, the oxidation feature shifts anodically, to reach ca 0.2 V at 0.2 mol:mol (Figure 6.3 (A) and Figure 6.3 (D)) [53]. The anodic shift of the oxidation implies that melanin tends to have prooxidant

behavior after chelating Fe^{3+} [71]. We wish to remind here that an antioxidant is a substance that significantly delays or inhibits the oxidation of an oxidizable chemical substrate [61]. Oxidative stress is the imbalance between oxidants and antioxidants in favor of the oxidants, potentially leading to the damage of the substrate [58]. In this context, being prooxidant means to favor the oxidative stress [72]. In Fe/DHI-DHICA-melanin (Type 1 DHI-DHICA-melanin) and Fe/DHI-melanin voltammograms, no peaks are observable, unlike their bare counterparts (Figure 6.3 (B), Figure 6.3 (C), Figure 6.3 (E) and Figure 6.3 (F)).

The voltammograms of DHICA-melanin, Fe/DHI-DHICA-melanin and Fe/DHI-melanin are similar at 5 mV/s and 50 mV/s (Figure 6.3).

We did not conduct cyclic voltammetry of Cu/melanin or Cu/Fe/melanin samples prepared by pre-immersion.

The presence of Cu^{2+} in physiological concentration (Cu:melanin 0.002 mol:mol) was not expected to affect the shape of cyclic voltammetry of melanin or Fe/melanin significantly.

6.5.3 SEM images of Cu/Fe/melanin prepared by pre-immersion (route i)

Using SEM, we investigated samples prepared by the pre-immersion route, to gain insight on the morphology of the samples. DHI-melanin, DHICA-melanin and DHI-DHICA-melanin modified with copper and iron will be indicated from now on as Cu/Fe/DHI-melanin, Cu/Fe/DHICA-melanin and Cu/Fe/DHI-DHICA-melanin. Cu/Fe/DHICA-melanin on carbon paper feature rod-shaped aggregates, mainly located at the junctions of the carbon paper fibers (Figure 6.4(A)). SEM images of Cu/Fe/DHI-DHICA-melanin show granular aggregates (Figure 6.4 (B)). Rod-shaped and granular aggregates have sizes in the micrometric scale. Copper and/or iron chelation likely cause the morphological changes of DHICA- and DHI-DHICA-melanin with respect to bare melanins, where no such aggregates are observable (Figure 6.4 (A) and Figure 6.4 (B)) [51], [130]. No characteristic features are observable in the SEM images of Cu/Fe/DHI-melanin (Figure 6.4 (C)); this type of samples is not distinguishable from bare carbon paper, probably due to low amount of Cu and Fe chelation in DHI-melanin (Figure 4.1(c) in [130] (Article 1)).

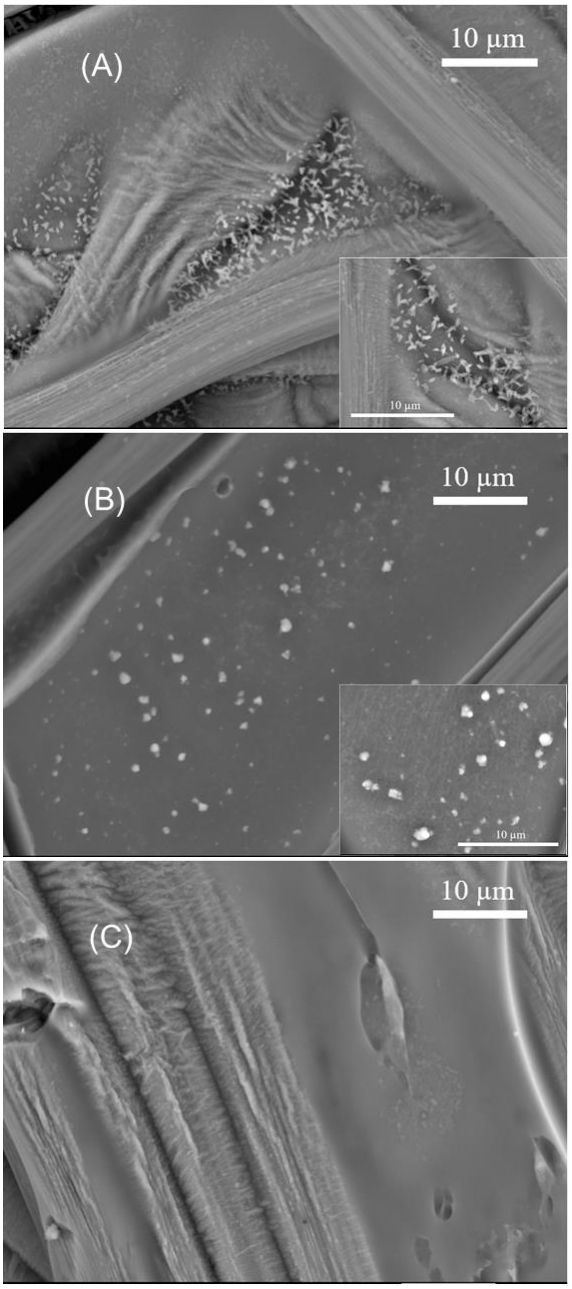

Figure 6.4 SEM images of **(A)** Cu/Fe/DHICA-melanin, **(B)** Cu/Fe/DHI-DHICA-melanin and **(C)** Cu/Fe/DHI-melanin on carbon paper. Molar ratio of Cu:Fe:melanin 0.002:0.2:1. Backscattering mode, acceleration voltage 15 kV.

6.5.4 XPS to study the presence of metals in Cu/Fe/melanin prepared by pre-immersion (route i)

After the characterization of their morphology, samples loaded on carbon paper and fused silica, prepared by pre-immersion, were studied by XPS, to shed light on the presence of iron and copper. Iron cations are detected on Cu/Fe/melanin samples loaded on fused silica (Figure S7 and Table S2). Copper cations are barely detected, here, probably due to the low concentration of Cu^{2+} used during samples' preparation (calculated to be ≤ ca. 0.018 atomic % for Cu/Fe/DHI-melanin, i.e. below the detection limit of XPS (0.1 atomic%)). Copper and iron are barely detected on samples loaded on carbon paper (Figure S6 and Table S1), likely due to the three-dimensional, open structure of the carbon paper, not ideal for XPS studies. Interestingly, literature reports that iron ion-binding capacity of neuromelanin is 10-fold greater than that of synthetic dopa melanin [90], [171].

6.5.5 Effect of the addition of Fe^{3+} to the electrolyte on cyclic voltammograms of DHICA-melanin (route ii)

Based on the more resolved voltammetric features observable with Fe/DHICA-melanin prepared by pre-immersion, with respect to Fe/DHI- and Fe/DHI-DHICA-melanins (Figure 6.3), we selected DHICA-melanin to study the effect of the presence of Fe^{3+} in the electrolyte solution where bare melanin samples are immersed (route ii). In this type of experiments, we added $Fe_2(SO_4)_3$ in the electrolyte to form Fe/DHICA-melanin (Type 1 DHICA-melanin, Figure S1(A), Figure S2). Similar results as for pre-immersed Fe/DHICA-melanin, i.e. an anodic shift of the oxidation potential upon increase of Fe^{3+} concentration is observed (Type 1 DHICA-melanin, Figure S1(A)).

6.5.6 Effect of Cu^{2+} addition in the electrolyte to cyclic voltammograms of DHICA-melanin (route ii)

We added $Cu(CH_3COO)_2$ in the electrolyte to form Cu/DHICA-melanin (route ii, Figure 6.5 (A)). The presence of Cu^{2+} in physiological concentration (Cu:melanin 0.002 mol:mol) does not seem to affect the shape of the cyclic voltammogram of DHICA-melanin but an oxidation peak at ca 0.1 V in the first voltammetric cycle, attributable to the adsorption process of Cu^{2+} cations on the Type 1 DHICA-melanin (Figure 6.5 (C)).

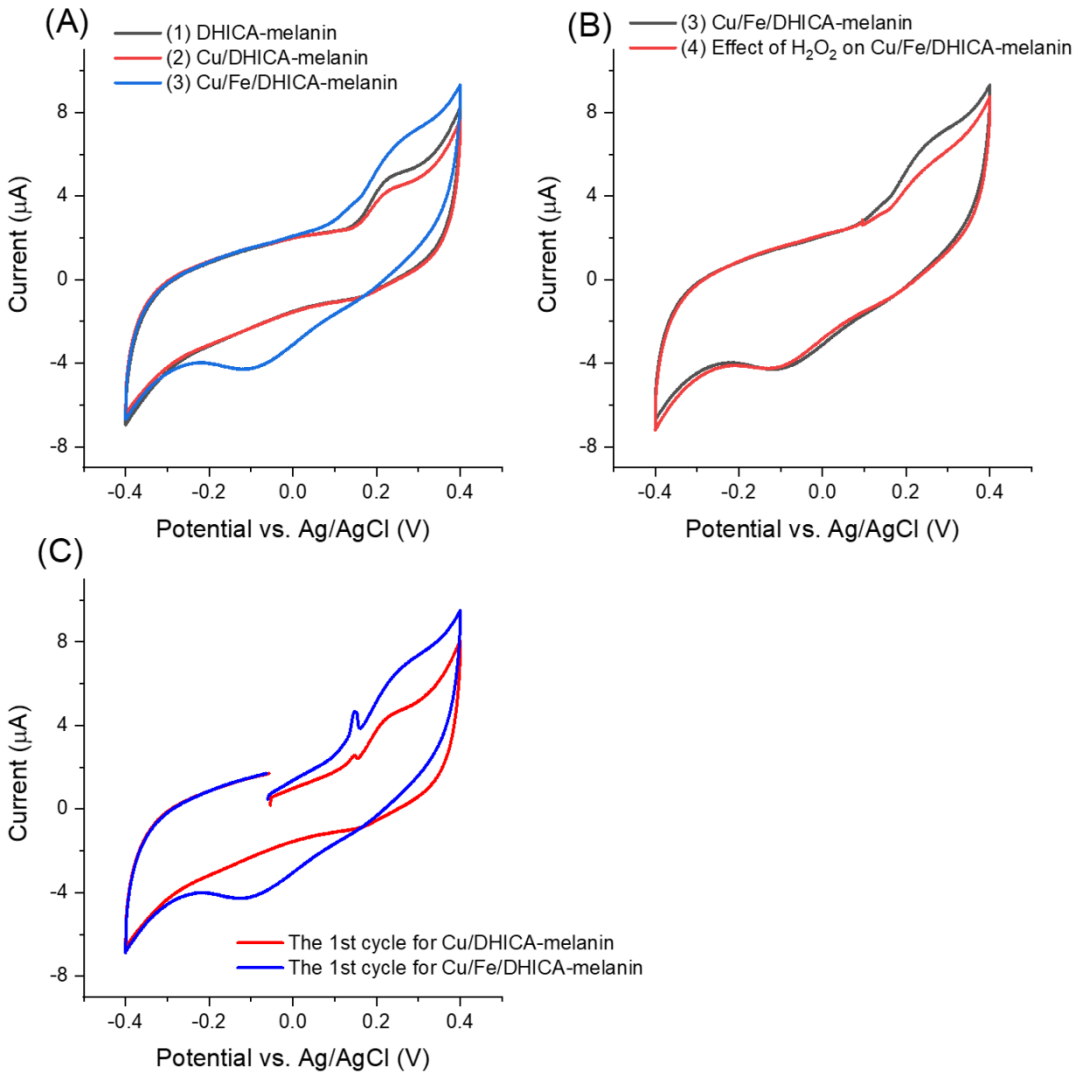

Figure 6.5 Effect of presence of **(A)**, **(C)** Cu^{2+}, Fe^{3+} and **(B)** H_2O_2 on cyclic voltammograms of Type 1 DHICA-melanin (route ii, see Table 6.1), at 5 mV/s, in the simulated neurological fluid electrolyte pH 7. Protocol: 2 voltammetric cycles → add $Cu(CH_3COO)_2$ with Cu:DHICA-melanin 0.002 mol:mol → 2 voltammetric cycles → add $Fe_2(SO_4)_3$ with Cu:Fe:DHICA-melanin 0.002:0.33:1 mol:mol:mol → 2 voltammetric cycles → expose the Cu/Fe/DHICA-melanin complex sample in H_2O_2 solution (0.15 mM) → 2 voltammetric cycles. Only the second cycle is shown apart from Figure 6.5 (C), where the cycle reported is the first one.

6.5.7 Effect of Cu^{2+} addition in the electrolyte to cyclic voltammograms of Fe/DHICA-melanin (route ii)

In the electrolyte, after adding $Fe_2(SO_4)_3$ solutions to form Fe/DHICA-melanin, we added $Cu(CH_3COO)_2$ (Table 6.1 and Figure S1(B)). The presence of Cu^{2+} in physiological concentration (Cu:melanin 0.002 mol:mol) does not seem to affect the shape of the cyclic voltammogram of Fe/DHICA melanin (Figure S1(B)), when copper ions are added after iron ions.

6.5.8 Effect of Fe^{3+} addition in the electrolyte to cyclic voltammograms of Cu/melanin (route ii)

In the electrolyte, after adding $Cu(CH_3COO)_2$ solutions to form Cu/DHICA-melanin, we added $Fe_2(SO_4)_3$ solution to form Cu/Fe/melanin (Figure 6.5(A) and Figure 6.5(C)). Interestingly, after adding Fe^{3+} in the electrolyte, an oxidation peak at ca 0.1 V appears in the first cycle, attributable to the adsorption process of the Fe^{3+} cations on the melanin (Figure 6.5). The presence of high concentration of Fe^{3+} (corresponding to Fe:melanin of 0.33 mol:mol), in simultaneous presence with Cu^{2+}, leads to a more pronounced oxidation between 0 V/0.4 V and an additional reduction wave between 0.2 V/-0.3 V for DHICA-melanin (Figure 6.5(A)).

6.5.9 Effect of H_2O_2 on melanin

Besides the effect of the presence of iron and copper ions, we studied the effect of ROS on the voltammetric behavior of bare melanin, to gain insight on a different aspect of the antioxidant behavior of melanin. Initially, we conducted experiments on the effect of exposure to H_2O_2 on melanin samples (Figure 6.6 and Figure S3).

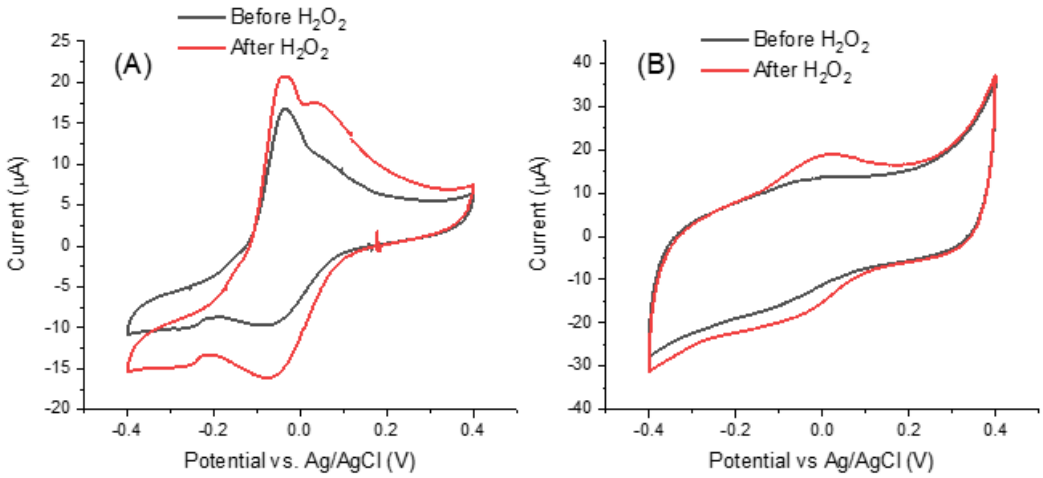

Figure 6.6 Effects of H_2O_2 on cyclic voltammograms of **(A)** Type 2 DHICA-melanin and **(B)** Type 1 DHI-DHICA-melanin, each for two cycles, at 5 mV/s, in a simulated neurological fluid electrolyte at pH 7 (Table 6.1, Fe^{3+} and Cu^{2+} are absent). Only the second cycle is shown.

Literature report that H_2O_2 can oxidize melanin into pyrrolic acids in neutral and alkaline media (Figure 6.1) [160]–[162]. After exposure to H_2O_2, Type 2 DHICA-melanin has more intense reduction and oxidation features (Figure 6.6 (A)). In the case of Type 1 DHI-DHICA-melanin, H_2O_2 brings about the appearance of broad oxidation and reduction features at ca 0 V (Figure 6.6 (B)). The cyclic voltammogram of DHI-melanin is not affected by H_2O_2 (Figure S3). Among other factors, the π-π stacking structure of DHI-melanin is expected to feature lower reactivity towards H_2O_2 with respect to DHICA-melanin, where H-bonding contributes to the formation of the supramolecular structure [103]. The effect of H_2O_2 on bare carbon paper is negligible (Figure S4).

6.5.10 XPS to study the effect of H_2O_2 on melanin

In order to explain the changes induced in melanin by exposure to H_2O_2, we used the XPS technique. For the XPS study we considered DHI-DHICA-melanin samples (Figure S8, Figure S9 and Table S3). Regarding changes on C 1s, ca 37% of the carbon atoms engaged in C=C disappear after exposure to H_2O_2 (from 26 at% to 16.3 at%). An increase of the presence of C-O (by 27%), C=O (by 43%) and O-C=O (by 17%) functional groups is observable. At the same time, the amount of C-C remains the same (Figure S9 and Table S3). These results point to the production of catechol, quinone and carboxyl group on the aromatic rings of melanin. Regarding changes involving O 1s,

the presence of aliphatic C-OH groups increases by 23% (from 7.8 to 10.3 at%) and the presence of aromatic C-OH groups increases by ca 33% (from 5.4 to 7.2 at%). The increased amount of redox active catechol and quinone can explain the more pronounced redox features observed in DHICA-melanin and DHI-DHICA-melanin, after exposure to H_2O_2 (Figure 6.6).

6.5.11 Effect of •OH on melanin

Based on the more pronounced effect of H_2O_2 on DHICA-melanin with respect to DHI-DHICA- and DHI-melanin, DHICA-melanin was selected to gain insight on possible effects of neuromelanin exposure to •OH (Figure S5). •OH was generated by the Fenton reaction (see Experimental part and Table 6.1). •OH moieties are expected to cause the oxidation or hydroxylation of melanin [84], [160]–[162] After exposure to •OH, the behavior of Type 1 DHICA-melanin is similar to that observed after exposure to H_2O_2, i.e. more pronounced reduction and oxidation features (Figure S5 and Figure 6.6), suggesting that H_2O_2 and •OH moieties play a similar effect on melanin. We did not observe the significant decrease of the current that we somehow expected due to melanin degradation by •OH moieties at acidic and neutral pH [77], [78], [164], [165].

6.5.12 Effect of H_2O_2 on Cu/Fe/melanin prepared by addition of the metals to the electrolyte (route ii)

Excessive amounts of transition metal ions bound by phenolics are reported to accelerate free-radical damage by ROS [62], which brought us to study the effect of H_2O_2 on Cu/Fe/neuromelanin. We selected Cu/Fe/DHICA-melanin (Type 1 DHICA-melanin, Figure S1(B) and Figure 6.5(B)) for this type of investigations. H_2O_2 was expected to generate •OH with Cu/Fe/melanin [76]–[78], due to the generation of Fe^{2+} by the redox reaction between melanin and Fe^{3+} (Fe^{3+} + H2Q or SQ $\rightarrow$ Fe^{2+}/SQ or Fe^{2+}/Q), in turn enabling the Fenton reaction [78]. The effect of H_2O_2 on the redox properties of Cu/Fe/DHICA-melanin (Type 1 DHICA-melanin) is not observable for molar ratios of 0.002:0.23:1 (Figure S1(B)). For higher concentrations of Fe^{3+}, i.e. Fe:DHICA-melanin 0.33:1 mol:mol, the oxidation feature of Cu/Fe/DHICA-melanin (Type 1 DHICA-melanin) at ca 0.25 V tends to disappear (Figure 6.5(B)). At this concentration, H_2O_2 may have caused a partial degradation of Cu/Fe/melanin, in agreement with literature [77], [78], [164], [165].

6.6 Conclusions and Perspectives

In this work, we studied the effect of metal ions and reactive oxygen species (ROS) on the redox (cyclic voltammetry) properties of a neuromelanin model, in order to shed light onto possible relationships between the voltammetric properties and the antioxidant versus prooxidant behavior of neuromelanin. Considering that literature proposes a core-shell pheomelanin-eumelanin structure for neuromelanin, we made the hypothesis that eumelanin, the shell wet by the electrolyte, is a good model to study the interfacial properties of neuromelanin and, among them, redox processes. SEM images showed the presence of changes in the morphology of DHI-DHICA-melanin and DHICA-melanin (obtained from a mix of the building blocks or exclusively from one of building block of eumelanin, DHI and DHICA) upon the simultaneous presence of iron and copper cations, with respect to bare melanin samples. Both Cu/Fe/DHI-DHICA- and Cu/Fe/DHICA-melanin, prepared by immersing melanin electrodes in solutions of the metals, form aggregates in the micrometric range. XPS showed the presence of iron in Cu/Fe/DHI-DHICA-, Cu/Fe/DHI- and Cu/Fe/DHICA-melanin whereas the detection of copper was more elusive.

We observed changes in the voltammetric properties of DHICA-melanin, in presence of iron ions: an anodic shift of the oxidation feature was observed in the voltammograms (Fe:melanin 0.2 mol:mol), implying that the antioxidant properties of DHICA-melanin tend to be weaker when it chelates iron ions.

We also observed the evolution of the voltammetric properties of DHI-DHICA- and DHICA-melanins upon exposure to H_2O_2. The presence of H_2O_2 renders more pronounced the voltammetric features for DHICA-melanin and DHI-DHICA-melanin with respect to non-exposed melanin, likely due to the increase of the density of catechol and quinone groups after exposure to H_2O_2, in agreement with XPS results.

More challenging has been to detect the effect of metal ions and ROS on DHI-melanin. Among other factors, the π-π stacked structure of DHI-melanin could bring lower reactivity with respect to DHICA-melanin. Indeed, literature reports that the redox properties of DHICA-melanin are attributable to the destabilizing effects of hindered intermolecular conjugation, which lead to non-planar structures with monomer-like behavior [103].

Our results seem to suggest that DHICA is the more reactive component in eumelanin. We propose to consider the reactivity of the DHICA component, with respect to the DHI component, during studies on the loss of pigmented neurons of the *substantia nigra* in patients affected by Parkinson's disease.

In perspective, we plan to improve our neuromelanin model including a pheomelanin component in the structure and we wish to follow by time-resolved Electron Paramagnetic Resonance the effect of ROS on the charge transfer properties of neuromelanin.

6.7 Conflict of Interest

The authors declare that the research was conducted in the absence of any commercial or financial relationships that could be construed as a potential conflict of interest.

6.8 Author Contributions

R. Xu designed the experiments and drafted the manuscript. Prof Soavi helped in the interpretation of the electrochemical measurements. Prof. Santato proposed the idea, supervised the work and helped drafting the manuscript. All the Authors gave their critical contribution on the whole manuscript.

6.9 Funding

See Acknowledgements.

6.10 Acknowledgments

E. Di Mauro is acknowledged for careful proof-reading. Y. Drolet is acknowledged for technical support. C.S. and F.S. acknowledge the Italy-Quebec Mobility program (MRIF) for financial support. C.S. is grateful to NSERC (Discovery).

CHAPTER 7 GENERAL DISCUSSION

7.1 Hypothesis of proton-assisted electron transfer (PAET) process of eumelanin

This section builds the basic hypothesis on factors determining the values of the electrochemical potentials of eumelanin before critically discussing the literature (Section 2.2) and experimental data of this work (Section 7.2 to Section 7.6). First of all, *local pH* is induced by the electrical bias (Section 7.1.1). Proton-assisted electron transfer (PAET) processes of eumelanin are proposed based on its deprotonation/protonation of the functional groups (Section 7.1.3). Equations for such PAET processes corresponding to electrochemical potentials are deduced based on the Nernst equation (Section 7.1.4.1). Indeed, due to the control of PAET processes by local pH, the dependence of electrochemical potentials on sweeping rates can be explained (Section 7.1.4.5). Following this section, the effect of unbuffered electrolytes are included in Section 2.2.3 to critically discuss the literature data.

7.1.1 Local pH induced by electrochemical potential

Literature data of electrochemical polymerization by the constant potential technique are listed in Table 2.3. In basic pH (pH 13), a very negative potential (-0.96 V) is required, whereas a positive potential (0.5 V) is required for pH 7 [36][105]. There seems to be a correlation between the bulk pH and the electrochemical potential.

To our knowledge, an electrolyte of pH 13 does not favor synthesis (Section 7.5.6.3). Instead, decompositions are reported at pH 13 [172]. Does it mean that the negative potential brings a local pH close to the synthetic pH range ($6.5 \leq pH < 13$)? Here, *local pH*, also noted as pH_{local}, is defined as the pH value in a small space surrounding the interface of electrode/electrolyte. The pH of the solution is named the *bulk pH* or pH_{bulk}.

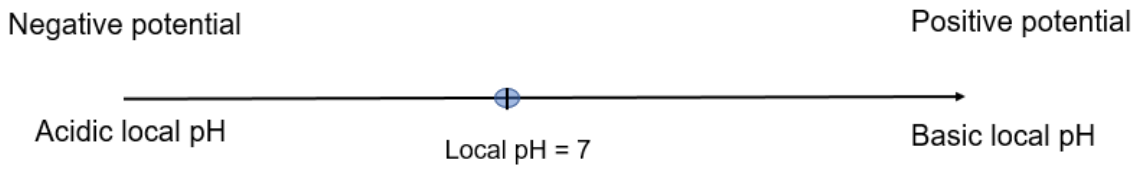

Figure 7.1 The relation between the local pH and the electrochemical potential. The *local pH* is defined as the pH value in a small space around the interface of electrode/electrolyte.

Therefore, based on the electrostatic considerations, we propose a simple hypothesis as follows. There is a potential that we set as E^*, where $pH_{local} = 7$. When the electrode is negatively biased vs. E^*, H^+ in the solution are attracted to the electrode and the local pH becomes acidic. At a positively biased potential vs. E^*, OH^- or the anions of buffering salt A^- for the deprotonation of eumelanin are attracted to the electrode and the local pH becomes basic (Figure 7.1).

7.1.2 Notations of pK_a and electrochemical potentials

In this work, a pK_a value corresponding to a protonation/deprotonation is noted as *pK_a(deprotonated form/protonated form)*. Oxidation peaks/features are noted as *protonated form/deprotonated form* and reduction peaks/features as *deprotonated form/protonated form*. The oxidation and reduction features are paired according to the reversible proton-assisted electron transfer (PAET) process. Here we name them *redox couples* and note them as *redox couple deprotonated form/protonated form* (Section 7.1.4.4).

7.1.3 PAET processes of eumelanin

Possible redox routes of eumelanin corresponding to local/bulk pH = pK_a are described in Figure 7.2. Different from other quinone-based materials, eumelanin has amine groups that can be deprotonated/protonated that also leads to redox activities of quinone groups (pK_a(HQI/H2Q) ca 6.3). Here we name HQI as *protonated quinone imine* that has amine group deprotonated but with quinone groups protonated. At local/bulk pH ca 6.3, the H2Q deprotonates to form HQI that can tautomerize and lose an electron to form SQ. Tautomerization means that proton of an organic compound moves from one functional group to another functional group. Here the proton moves between one hydroquinone group and the amine group (Figure 7.2).

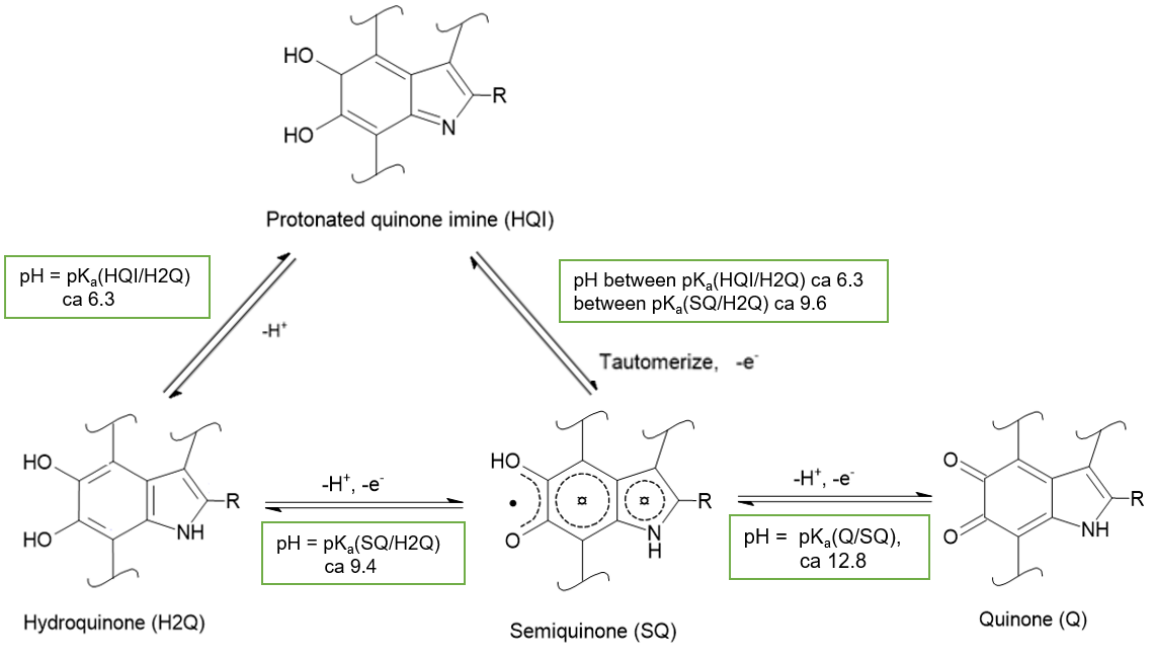

Figure 7.2 Redox processes of eumelanin corresponding to local/bulk pH = pK_a. -R is -H in DHI and -COOH in DHICA.

Throughout this work, we have noticed from literature data and experimental evidence that pH seems to be a key to control the oxidation processes of eumelanin (Section 7.5.2.1 and Section 7.4.4). Therefore, for *proton-assisted electron transfer (PAET) processes*, we hypothesize that during anodic potential sweeps of cyclic voltammetry, the oxidation processes of eumelanin happen after deprotonation, i.e. $pH_{local} \geq pK_a$. The potential corresponding to $pH_{local} = pK_a$ is hypothesized as the onset potential for oxidation (Figure 7.3).

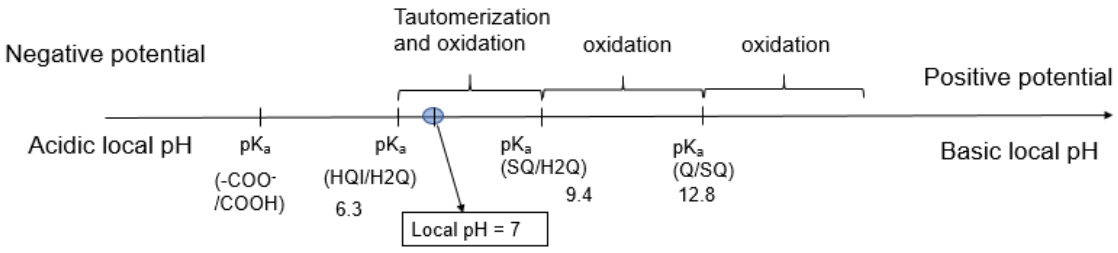

Figure 7.3 The local pH ranges for the oxidation processes of eumelanin.

7.1.4 Calculations of potentials from pH/pK_a values in the buffered electrolytes

7.1.4.1 Calculation of onset oxidation potentials from pK_a

We can tentatively calculate the corresponding potentials as follows.

We start with the Nernst equation regarding bulk pH

$$E_{redox}\,(pH_{bulk}) = E_{redox}\,(pH_{bulk} = 0) - 0.059\ pH_{bulk} \qquad \text{Eq. 7.1a (V vs. NHE)}$$

where E_{redox} (vs. NHE, pH_{bulk}) is a redox potential as a function of the bulk pH. NHE (normal hydrogen electrode) is a reference electrode. Eq. 7.1a means that changing the bulk pH shifts the redox potentials E_{redox} by a factor of 0.059. Eq. 7.1a also applies to an onset oxidation potential $E_{ox(onset)}$, by

$$E_{ox(onset)}\,(pH_{bulk}) = E_{ox(onset)}\,(pH_{bulk} = 0) - 0.059\ pH_{bulk} \qquad \text{Eq. 7.1b (V vs. NHE)}$$

From Section 7.1.3, we understand that an oxidation process happens at $pH_{bulk} \geq pK_a$. Therefore, we here hypothesize that the oxidation process happens at $pH_{bulk} \geq pK_a$ without the applied bias, that is,

$$E_{ox(onset)}\,(pH_{bulk} = pK_a) = 0\ V\ (vs.\ NHE) \qquad \text{Eq. 7.2}$$

therefore

$$E_{ox(onset)}\ (V\ vs.\ NHE,\ pH_{bulk} = 0) = 0.059\ pK_a \qquad \text{Eq. 7.3a}$$

Using another reference electrode Ag/AgCl, where

$$E\ (V\ vs.\ Ag/AgCl,\ pH_{bulk}) = E\ (V\ vs.\ NHE,\ pH_{bulk}) - 0.2 \qquad \text{Eq. 7.4}$$

therefore

$$E_{ox(onset)}\ (V\ vs.\ Ag/AgCl,\ pH_{bulk} = 0) = 0.059\ pK_a - 0.2 \qquad \text{Eq. 7.3b}$$

E (vs. Ag/AgCl, pH_{bulk}) at different bulk pHs can again be calculated with the Nernst equation

$$E_{ox(onset)}\ (pH_{bulk}) = E_{ox(onset)}\ (pH_{bulk} = 0) - 0.059\ pH_{bulk}$$ Eq. 7.1c (V vs. any reference electrode)

Therefore, the onset oxidation potential is expressed as

$$E_{ox(onset)}\ (pH_{bulk}, pK_a) = 0.059\ (pK_a - pH_{bulk})$$ Eq. 7.5a (V vs. NHE)

which reveals the relation between the onset oxidation potentials and the pK_a values (Figure 7.3). Based on discussions later in Section 7.1.4.4, Eq. 7.5a will be assigned later as both *onset oxidation potentials* and *end reduction potentials* in the buffered electrolytes. From pK_a(Q/SQ) ca 13 and pK_a(SQ/H2Q) ca 9.3, we can calculate from Eq. 7.5a that the expected potential difference between these two electron transfer processes is ca 0.38 V, as estimated by Kim et al. [50]. The onset potentials predicted by Eq. 7.5a are found to fit the results in this work (Section 7.2.2). However, the predicted data by Eq. 7.5a do not fit the literature data. The major reason can be the use of unbuffered electrolytes (Section 2.2.3).

7.1.4.2 Relation between local pH and applied potential

We tentatively expand the calculating method of Eq. 7.5a for obtaining the local pHs in electrolytes of any bulk pHs. From Eq. 7.1b, we set $pH_{bulk} = pH_{local}$ and $E(pH_{bulk} = pH_{local}) = 0$ V vs. NHE. Then we obtain

$$E_{app}\ (pH_{bulk} = 0, pH_{local}) = 0.059\ pH_{local}$$ Eq. 7.3c (V vs. NHE)

$$E_{app}\ (pH_{bulk} = 0, pH_{local}) = 0.059\ pH_{local} - 0.2$$ Eq. 7.3d (V vs. Ag/AgCl)

Eq. 7.3c and Eq. 7.3d reveal the linear relationship between pH_{local} and the potential (Figure 7.1). Combining with the effect of the bulk pH (Eq. 7.3c), we obtain

$$E_{app}\ (pH_{bulk}, pH_{local}) = 0.059\ (pH_{local} - pH_{bulk})$$ Eq. 7.5b (V vs. NHE)

Eq. 7.5b indicates that at local pH = bulk pH, the potential is 0 V vs. NHE, no matter at which bulk pH. Eq. 7.5b also implies how the change of the local pH is driven by the applied potential. Eq. 7.5b is used in this work to further discuss the effect of unbuffered electrolyte (Section 2.2.3).

7.1.4.3 Reversible PAET process

We here hypothesize that each *reversible PAET process* has capacity equality of reduction and oxidation at each redox potential, that is

$$q_{red} = q_{ox} \qquad \text{Eq. 7.6}$$

which means that, as long as the peak currents of peak capacities of a redox couple are not equal, this redox reaction is not reversible. For example, in Article 1, all the three oxidation peaks of DHICA-melanin at pH 5 are irreversible (Figure 7.6).

As to the relative position of oxidation potential vs reduction potential, first of all, we would like to define an ideal reversible PAET process (Section 7.1.4.4). After that, we derive such situation for the effect of sweeping rates (Section 7.1.4.5).

7.1.4.4 Ideal reversible PAET process

In an ideal PAET process, we expect the same position of the reduction peak as the oxidation peak. To express them in terms of onset potentials ($E_{ox(end)}$ and $E_{red(end)}$) and end potentials ($E_{red(end)}$ and $E_{ox(end)}$), it is $E_{red(end)} = E_{ox(onset)}$ and $E_{ox(end)} = E_{red(onset)}$ (Figure 7.4). In this work, most of the voltammograms are obtained at 5 mV/s. Some redox couples have electrochemical potentials close to the ideal PAET processes as described in this Section, such as Sepia melanin and DHI-DHICA-melanin (Figure 7.11).

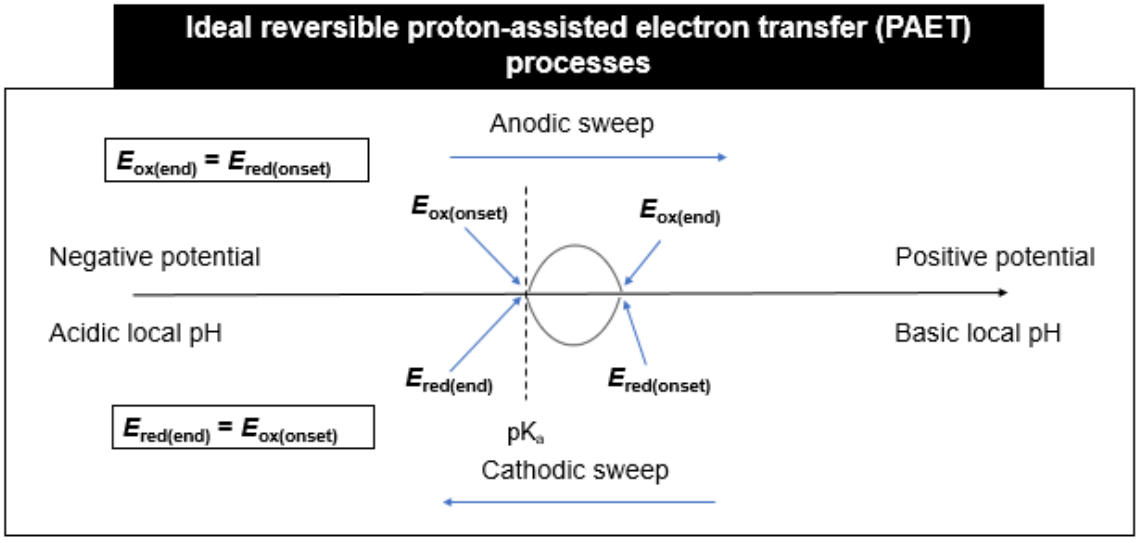

Figure 7.4 Ideal reversible proton-assisted electron transfer (PAET) processes.

7.1.4.5 Effect of sweeping rates

During the anodic sweep, eumelanin is deprotonated by the anions A^- generated by a buffered electrolyte or OH^- by H_2O in an unbuffered electrolyte (Section 2.2.3.1) The sweeping rate means how fast the increase/decrease of potential is. When the sweeping rate is higher than the rate that H^+ or OH^- (or A^-) can accumulate at the interface of electrode/electrolyte, there is a lag between the change of the local pH with respect to the change of the applied potential. From the ideal reversible PAET where $E_{red(end)} = E_{ox(onset)}$ (b), the $E_{red(end)}$ at higher sweeping rate shifts cathodically and $E_{ox(onset)}$ shifts anodically (Figure 7.5). The degree of potential shift is dependent on the sweeping rate. Such phenomenon is shown in the voltammograms in the buffered electrolytes (Figure 6.3, Figure S3 and Figure S4 in Appendix A). For example, in presence of monovalent metal ions, the onset potential of oxidation peak SQ/Q of DHICA-melanin shifts anodically from 0.24 V vs. Ag/AgCl at 5 mV/s to 0.29 V at 100 mV/s (Figure S3(b) in Appendix A).

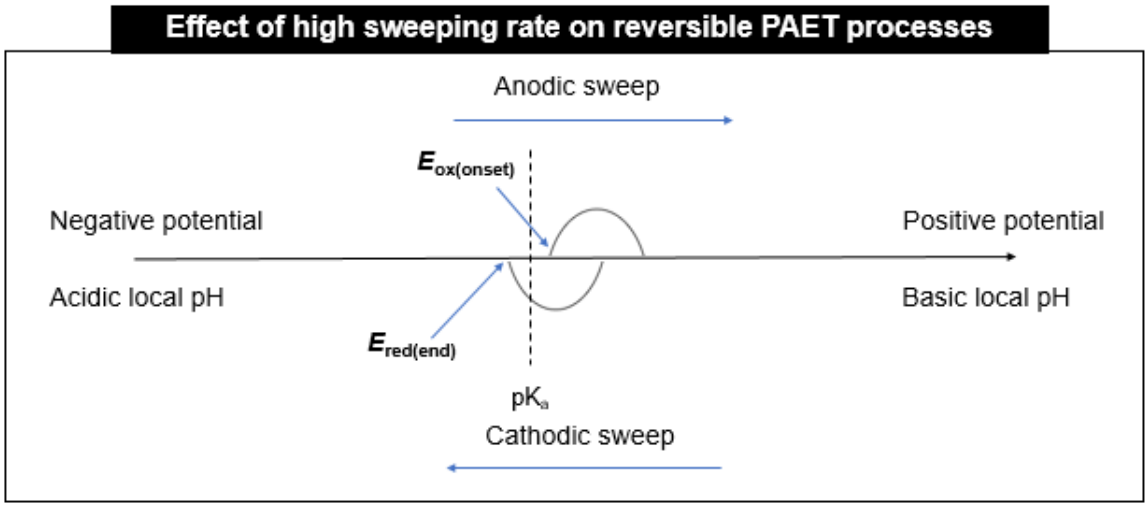

Figure 7.5 The effect of high sweeping rate on the reversible proton-assisted electron transfer (PAET) process.

7.2 Electrochemical potentials and supramolecular structures of DHICA-melanin in presence of monovalent metal ions

7.2.1 Environmental pH vs. pK_a of eumelanin

7.2.1.1 Concept of environmental pH

Before starting the comparison of experimental data and expected data, we would like to define the environmental pH. The *environmental pH* means the pH surrounding the eumelanin sample. It can be synthetic pH (pH 12), storage pH (pH 7), bulk pH of the electrolyte, local pH when electrical biases are applied, etc.

7.2.1.2 Hypothesis: pK_a values of eumelanin shift towards environmental pH during polymerization

Various experimental evidence points that, when the eumelanin is in a new environment, it begins to (further) polymerize or depolymerize depending on the pH. The main evidence is as follows:

- Yang et al. reported that the adhesion properties of polydopamine vary with pH changes, noted by the detachment ratio [172]. The detachment ratio varies at the change of every pH unit except for pH 4-7.
- Analyzing the experimental data of this work, it seems that pK_a values of DHICA-melanin are more close to the environmental pH that it experienced (Section 7.2.2).

Therefore, we hypothesize that, during the (further) polymerization of eumelanin in a new environment, the pK_a value that is close to the environmental pH shifts towards the environmental pH, so that the polymerization rate decreases until it reaches a given level.

Indeed, eumelanin is prone to be (further) polymerized in hydrated conditions due to the coexisting redox forms H2Q and Q (Section 2.1.1). Even during immersion of the working electrode without electrical bias, when the electrolyte is being degassed, eumelanin can also undergo further polymerization.

7.2.2 Data analysis of DHICA-melanin

In this section, we review the important voltammograms in this work and discuss the pK_a values of the eumelanin and their relation to environmental pH that it experienced.

At bulk pH 5, the oxidation peak H2Q/HQI seems convoluted (Figure 7.6 (a)). The convoluted peaks have onset potentials ranging between -0.14 V and -0.07 V vs. Ag/AgCl, corresponding to ca 6.0 and ca 7.2. The original pK_a(HQI/H2Q) ca 6.3 has shifted towards the storage pH (ca pH 7). The onset potential of H2Q/SQ is ca 0.02 V vs. Ag/AgCl, corresponding to a pK_a value ca 8.7. This probably results from the shift of the original pK_a(SQ/H2Q) ca 9.4 towards the storage pH 7. The onset potential of SQ/Q is ca 0.22 V vs. Ag/AgCl, with pK_a(Q/SQ) ca 12.1 equaling the synthetic pH (Section 3.1.3).

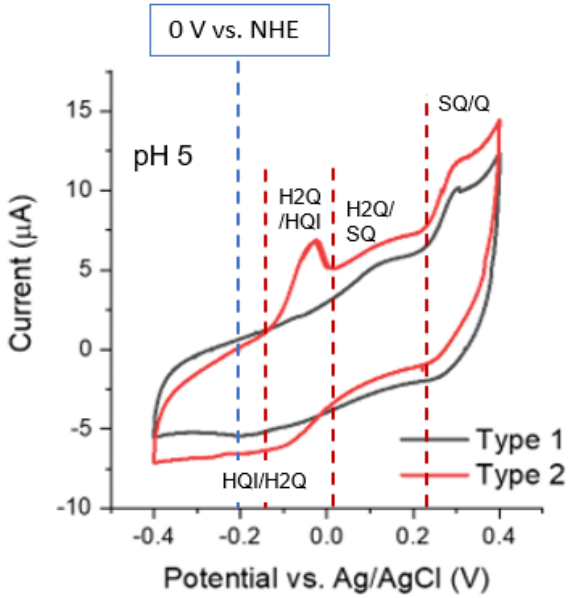

Figure 7.6 Type 1 and Type 2 DHICA-melanin in 0.25 M buffered $NaCH_3COO$ bulk pH 5. Adapted from Figure 6.2.

7.2.3 Supramolecular structures of DHICA-melanin

7.2.3.1 Supramolecular structures of two types of DHICA-melanin

In this work, the oxidation peak H2Q/HQI differentiates Type 1 from Type 2 DHICA-melanin (Figure 7.6). We tentatively explain such a difference as follows.

On a single DHICA monomer, one side has quinone groups and the other side has amine and $-COO^-$. DHICA oligomers form rod-shaped assemblies by hydrogen bonding between these functional groups (Figure 2.2). The cause of the oxidation peak H2Q/HQI is the deprotonation of the amine groups. Therefore, we deduce that, in Type 1 DHICA-melanin, the side with $-COO^-$ and amine groups may form hydrogen bonds inside the rod-shaped structure. In such a situation, the

amine groups have a low chance of being approached and deprotonated by the anion CH_3COO^-. In Type 2 DHICA-melanin, the side with amine groups and $-COO^-$ is exposed outside of the rod-shaped structure for deprotonation of amine groups.

7.2.3.2 The altering supramolecular structure from Type 1 to Type 2 DHICA-melanin during cycling

The tendency of DHICA-melanin to change from Type 1 to Type 2 can be explained as follows (Figure 7.6(b)). The buffering anion CH_3COO^- has a $-COO^-$ group whose polarity is similar to that of $-COO^-$ groups of eumelanin building blocks. Therefore, the buffering anion CH_3COO^- attracts $-COO^-$ and causes the oligomer of DHICA to change the side of amine groups and $-COO^-$ from inward (Type 1 DHICA-melanin) to outward (Type 2 DHICA-melanin). The diminishing oxidation peak SQ/Q is due to further oxidative polymerization by cyclic voltammetry (Section 7.5.1).

7.2.3.3 Possible mechanism of forming supramolecular structure of Type 1 DHICA-melanin

In the literature, most voltammograms with distinguished potentials include the redox potential(HQI/H2Q). In this work, we observe more Type 1 DHICA-melanin than Type 2 DHICA-melanin (20 samples vs. 5 samples in the presence of monovalent metal ions at pH 5). We tentatively attribute this tendency to the synthetic route and storage environment used. Due to similar polarity, the oxidants O_2 and H_2O_2 tend to attach to the quinone groups. Therefore, the quinone groups face outward from the rod-shaped structure of DHICA-melanin.

During the deprotonation of the quinone groups or amine groups, the OH^- generated by Equilibrium 3.1 forms H_2O with H^+ provided by these functional groups (Section 3.1.3). Due to this reaction, NH_4^+ is largely generated (Equilibrium 3.1). NH_4^+, due to its similar polarity to amine groups, attaches to and gives a proton to the amine group. It then evaporates after donating the proton:

$$NH_4^+ \rightarrow NH_3 + H^+ \qquad \text{Reaction 7.1}$$

Therefore, the amine groups of DHICA-melanin preferentially acquire the protons needed to form hydrogen bonds for their rod-shaped structure.

7.2.3.4 Supramolecular structure of Fe/DHICA-melanin formed by pre-immersion

In Article 3, all the voltammograms of Fe/DHICA-melanin formed by pre-immersion show Type 1 DHICA-melanin. We deduce that Fe^{3+} probably chelates $-COO^-$ at pH 4 (the solution for pre-

immersion), as pH 4 is much lower than the pK_a values of other functional groups (Section 7.3.2.2). Each Fe^{3+} probably chelates on more than one $-COO^-$ i.e. each Fe^{3+} probably chelates with several DHICA building blocks with $-COO^-$ inside the rod-shaped structure (Figure 6.4(A)). Therefore, the Fe/DHICA-melanin formed by pre-immersion is in the supramolecular structure of Type 1 DHICA-melanin (Section 7.2.3.1).

7.3 Effect of multivalent metal ions on DHICA-melanin

7.3.1 Hypothesis of effect of multivalent metal ions on eumelanin

The effect of multivalent metal ions seems an overlapped effect of the following.

7.3.1.1 Cathodic shifts of redox potentials due to lower pK_a values

A decrease of pK_a is shown in the titration results for a DHI-melanin sample in the presence of Fe^{3+} and Cu^{2+} [49][171]. The chelation energy of multivalent metal ions likely promotes the deprotonation of the functional groups, resulting in lower pK_a values. Therefore, the cathodic shifts of the redox potentials occur with respect to the non-multivalent metal ions counterpart (Figure 7.7).

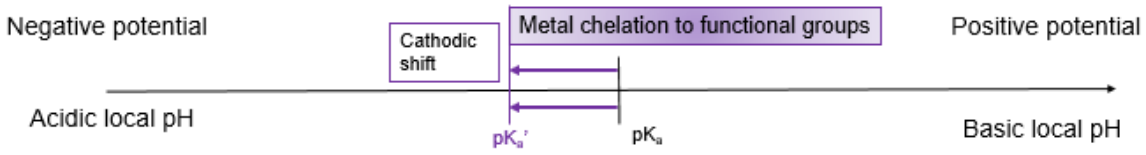

Figure 7.7 Possible cathodic shift of an onset oxidation potential due to lower pK_a value caused by the chelation of multivalent metal ions.

Examples of such cathodic shifts are observed in cases of Cu^{2+} at high and low concentrations (Section 7.3.2.1 and Section 7.3.2.3) as well as in cases of Mg^{2+} at high and low concentrations in the literature (Section 2.2.8.1, Section 2.2.8.2 and Section 7.3.2.4).

7.3.1.2 Anodic shifts of potentials due to chelation on $-COO^-$

The $-COO^-$ group of DHICA-melanin is an electron-withdrawing group. Functionalizing $-COO^-$ on quinone-based materials usually results in increases of redox potentials [173]. The chelation of multivalent metal ions on $-COO^-$ can make the degree of electron-withdrawing from the eumelanin molecules to $-COO^-$ higher than the non-chelated counterparts. The resulting redox potentials of eumelanin are expected to shift anodically with respect to non-chelated counterparts. Examples of

such anodic shifts are observed in Mg^{2+} and Cu^{2+} at high concentrations (Section 2.2.8.2 and Section 7.3.2.1) and Fe^{3+} at low concentrations (Section 7.3.2.2 and Section 7.3.2.3).

7.3.1.3 Oxidative polymerization by transition metal ions

Transition metal ions, such as Cu^{2+} and Fe^{3+} have certain redox potentials that are oxidative for eumelanin (Equilibrium 7.1 and Equilibrium 7.2). Eumelanin may undergo further polymerization in the presence of the oxidative transition metal ions.

$$Cu^{2+} \rightleftharpoons Cu^{+} + e^{-} \quad (0.16 \text{ V vs. NHE}) \qquad \text{Equilibrium 7.1}$$

and

$$Fe^{3+} \rightleftharpoons Fe^{2+} + e^{-} \quad (0.77 \text{ V vs. NHE}) \qquad \text{Equilibrium 7.2}$$

Examples are mainly found in cases of Cu^{2+} (Section 7.3.2.1 and Section 7.3.2.3).

In the voltammograms of this work, Fe^{3+} does not seem to promote the oxidative polymerization of eumelanin. There may be a decreased potential of Fe^{3+} due to its forming oxide Fe_2O_3 at much lower environmental pH than Cu^{2+} (ca pH 4 vs. ca pH 7 at the applied concentration) [174][175].

7.3.1.4 Effect of concentrations of multivalent metal ions

From low to high concentration of multivalent metal ions, the impacts on above aspects of electrochemical potentials increase differently. When the concentration is relatively low, only part of the eumelanin sample has its functional groups chelated with the multivalent metal ions. In addition to the intrinsic redox features, the voltammogram shows corresponding extra redox features with a small degree of cathodic potential shift, here called *extra chelation potential* (Section 7.3.1.1). When the concentration is high, the metal ions seem to chelate on all the functional groups and create both high cathodic and anodic potential shifts of redox potentials (Section 7.3.1.1 and Section 7.3.1.2) [23].

In case studies, for Mg^{2+}, at Mg^{2+}:eumelanin 67:1 mol:mol (2 mM), there is an extra chelation potential with cathodic shift of H2Q/SQ is ca 0.1 V (Section 7.3.2.4). At high concentration 0.5 M (ca 100 times higher) with Sepia melanin, ca 0.3 V cathodic shift as well as ca 0.3 V anodic shift of SQ/Q is observed (Section 2.2.8.2). At low concentration 0.1 mM with polydopamine, extra chelation potential exists but no significant cathodic shift is observed (Section 2.2.8.1).

For Cu^{2+}, at Cu^{2+}:eumelanin 0.002:1 mol:mol, an extra chelation potential is present and cathodic shift is only ca 0.06 V. At 83:1 mol:mol, the cathodic shift is up to ca 0.3 V and the anodic shift ca 0.2 V.

7.3.2 Data analysis: effect of multivalent metal ions

7.3.2.1 Effect of Cu^{2+} (Cu^{2+}: eumelanin 83:1 mol:mol)

In Figure 7.8, the effect of Cu^{2+} on DHICA-melanin is compared with its counterpart in the presence of monovalent metal ions. The data analysis for this is provided in Section 7.2.2. The analysis is tentatively given as:

1) In the presence of Cu^{2+}, eumelanin comparing with the bare current collector, the sharp peak at ca 0 V represents the oxidation reaction of the mobile Cu^{2+} (that are not chelated on eumelanin) in the electrolyte (Equilibrium 7.1). Therefore, when we analyze the effect of Cu^{2+} on eumelanin, we do not analyze the sharp oxidation peak at ca 0 V.

2) Cu^{2+} makes the oxidation current higher than the reduction current, probably because Cu^{2+} causes the further oxidative polymerization of the eumelanin (Section 7.3.1.3). The portion of the current that is not due to oxidative polymerization is probably the chelated redox current of Cu^{2+}.

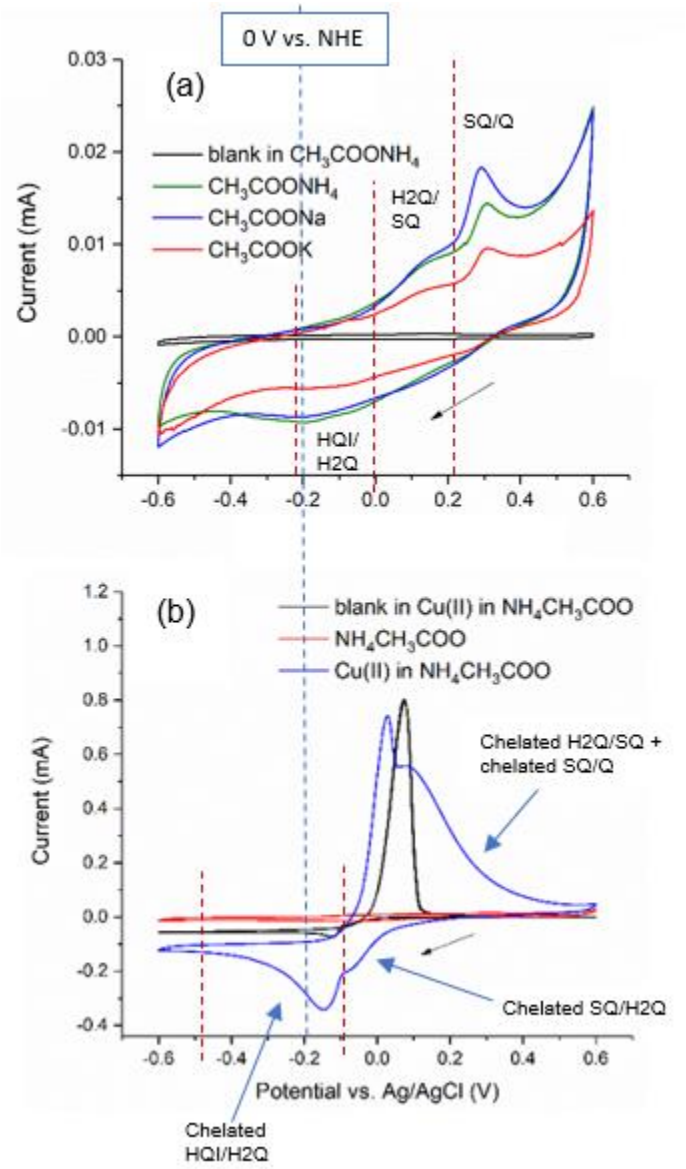

Figure 7.8 DHICA-melanin in the presence of (a) monovalent metal ions and (b) Cu^{2+}. Adapted from Figure 4.2 and Figure 4.4.

3) The redox features are broad and are convolutions of chelated functional groups with different pK_a values. For example, the broad oxidation peak in potential range -0.1 V/0.6 V seems to be a convolution of a few different peaks of chelated SQ/Q and chelated H2Q/SQ (Figure 7.8). The broad reduction peak chelated HQI/H2Q ranges from ca -0.1 V/-0.5 V. Such broad ranges can be explained by point 3) and point 4) as follows.

4) The onset oxidation potentials or end reduction potentials of all the broad features seem to have cathodic shifts of ca 0.3 V (Section 7.3.1.1). For example, the broad end reduction potential of

chelated SQ/H2Q has a cathodic shift from ca 0.2 V to ca -0.1 V. The broad end reduction potential of chelated HQI/H2Q has a cathodic shift from ca -0.2 V to ca -0.5 V (Figure 7.8). The high cathodic shift is also found during the analysis of the effect of Mg^{2+} at high concentrations (Section 2.2.8.2).

5) Anodic shift ca 0.2 V of part of the SQ/Q peak. Part of the oxidation peak SQ/Q becomes convoluted peaks in the potential range of ca 0.3 V/0.6 V (Section 7.3.1.2) (Figure 7.8).

6) The capacity and capacitance of all the three eumelanins (DHI-, DHICA- and Sepia melanin) enhanced dramatically after adding Cu^{2+} (Figure 4.4). For example, Sepia melanin has enhancements of two orders of magnitude in both capacity (3.2 C/g vs. 280 C/g) and capacitance (4 F/g vs. 440 F/g).

7.3.2.2 Pre-immersed Fe/DHICA-melanin (Fe^{3+}: eumelanin 0.2 mol:mol)

The solutions for pre-immersion are at bulk pH 4, which only enables chelation of Fe^{3+} on $-COO^-$, because pK_a($-COO^-$/-COOH) of eumelanin is ca 3 [176]. Therefore, due to the higher degree of electron-withdrawing given by the chelation of Fe^{3+} on $-COO^-$ with respect to non-chelated eumelanin, the anodic shift of the oxidation peak SQ/Q is observed (Figure 6.3) (Section 7.3.1.2).

7.3.2.3 Effect of Cu^{2+} and Fe^{3+} during voltammetry in electrolyte (Cu^{2+}:Fe^{3+}:eumelanin 0.002:0.2:1 mol:mol:mol)

After adding Fe^{3+} and Cu^{2+} to the electrolyte at bulk pH 7, the metal ions were expected to be chelated to both $-COO^-$ and amine groups. When Cu^{2+} (Cu^{2+}: eumelanin 0.002 mol:mol) was added, the oxidation peak SQ/Q seemed to diminish slightly (Figure 7.9 (b)). In Article 3, we explained that the concentration of Cu^{2+} may be too low to have an impact. Another possibility is that the slightly decreased intensity of oxidation peak SQ/Q can signify further polymerization of DHICA-melanin by Cu^{2+} (Section 7.3.1.3 and Section 7.5.1).

After Cu^{2+}, Fe^{3+} was added (Fe^{3+}: eumelanin 0.2 mol:mol). The chelation of Fe^{3+} on $-COO^-$ caused an anodic shift ca 0.05 V in the SQ/Q peak from ca 0.13 V to ca 0.18 V (Section 7.3.1.2) (Figure 7.9 (b)). The impact of chelating on amine is not shown, because the DHICA-melanin is Type 1 DHICA-melanin that does not show the oxidation peak H2Q/HQI (Section 7.2.2).

When voltammetry is conducted, the potential induces higher local pH that permits chelation on SQ/Q, therefore, the addition of Cu^{2+} and Fe^{3+} both induce small oxidation peaks of chelated SQ/Q at 0.1 V vs. Ag/AgCl in their first cycles (Figure 7.9 (a)). Such potential has lower onset oxidation

potential than oxidation peak SQ/Q for ca 0.06 V, which represents cathodic shift due to lower pK_a values (Section 7.3.1.1).

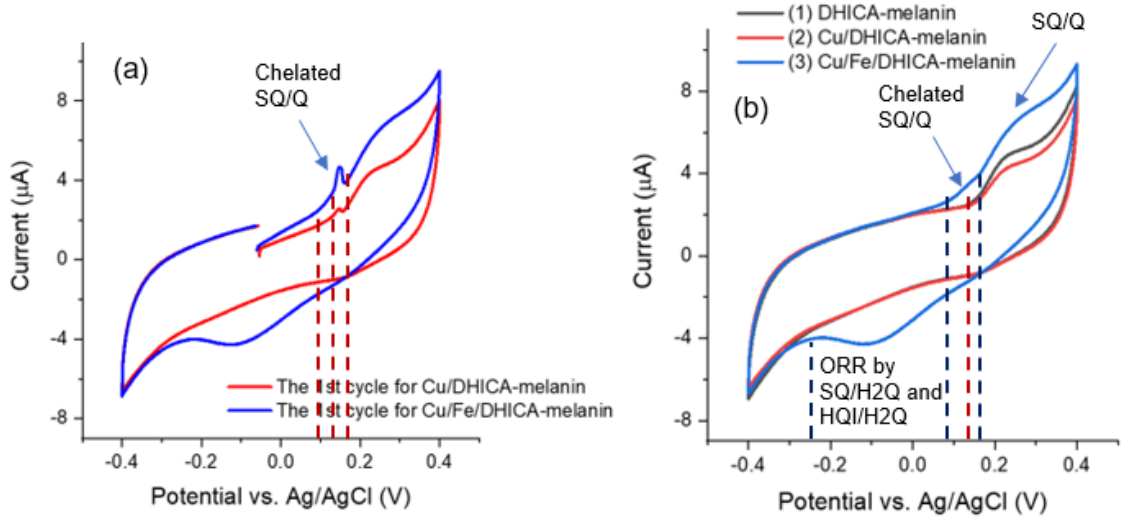

Figure 7.9 Effect of Cu^{2+}, Fe^{3+} on voltammograms of Type 1 DHICA-melanin in buffered $NaCH_3COO$ with 145 mM KCH_3SO_4, 10 mM NaCl and 2 mM $MgCl_2$, at 5 mV/s. The first cycles under effect of Cu^{2+}, Fe^{3+} are in (a). Adapted from Figure 6.5.

The broad reduction feature after addition of Fe^{3+} is assigned as ORR feature by SQ/H2Q and HQI/H2Q. The presence of the O_2 is probably due to the addition of Fe^{3+} solution, which is not degassed before being added to the electrolyte (Section 2.2.7.3).

7.3.2.4 Effect of Mg^{2+} (Mg^{2+}: eumelanin 67:1)

Due to the high concentration of Mg^{2+} used in the electrolyte, we need to discuss the electrochemical potentials of DHICA-melanin in the presence of Mg^{2+} separately from in the presence of monovalent metal ions (Section 7.2.2).

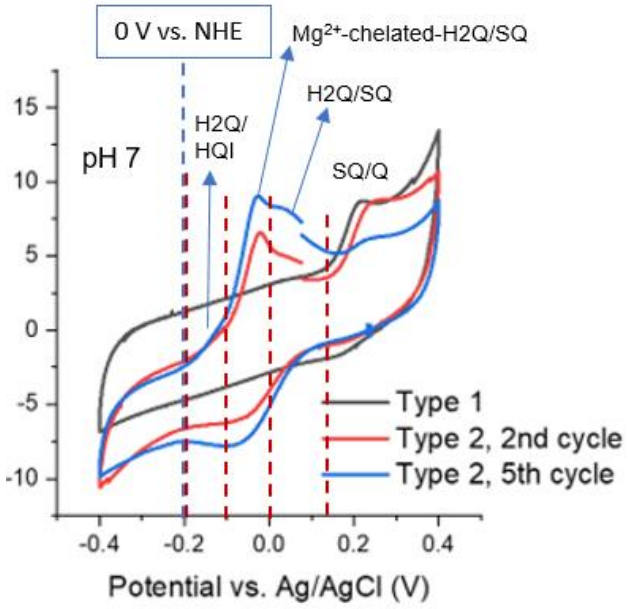

Figure 7.10 DHICA-melanin in 10 mM buffered $NaCH_3COO$ with 145 mM KCH_3SO_4, 10 mM NaCl and 2 mM $MgCl_2$ at bulk pH 7. Adapted from Figure 6.2.

The oxidation peak H2Q/HQI seems convoluted with oxidation peak Mg^{2+}-chelated-H2Q/SQ and oxidation peak H2Q/SQ (Figure 7.10). The onset potential of oxidation peak H2Q/HQI is -0.2 V vs. Ag/AgCl, corresponding to a pK_a value 7, shifted from 6.3 towards the storage pH and the electrolyte pH (both pH 7) (Section 7.2.1.2). Oxidation peak Mg^{2+}-chelated-H2Q/SQ has onset potential ca -0.1 V vs. Ag/AgCl, corresponding to a pK_a value 8.7. It means a cathodic shift from the original pK_a(SQ/H2Q) ca 9.4 due to the Mg^{2+} chelation on quinone groups (Section 7.3.1.1). This extra chelation potential is similar to Case 7 in the literature review, where Mg^{2+} affects the electron transfer of H2Q/SQ in a similar way (Section 2.2.8.1) [52]. The onset potentials of oxidation feature H2Q/SQ and SQ/Q are at ca 0 V and 0.13 V, corresponding to pK_a values 10.4 and 12.6, respectively. They both seem to have an anodic shift ca 0.05 V due to chelation of Mg^{2+} on $-COO^-$, from potentials -0.06 V and 0.10 V, corresponding to ca pK_a values 9.4 and 12 (Section 7.3.1.2). From the above data analysis, Mg^{2+} may not have chelated on amine groups, but probably on $-COO^-$ and quinone groups [50]. This has also been reported in the literature [23] (Section 1.1.2.4).

7.4 Broad (DHI-dominant-melanin) vs. distinguishable electrochemical features (DHICA-dominant-melanin)

7.4.1 pK_a values of DHI-melanin

DHI-melanin is featured with broad redox peaks that result from convoluted redox peaks (Figure 4.2b, Figure 5.2a and Figure 6.3). The redox peaks are convoluted in DHI-melanin, which has disordered chemical structure as well as disordered supramolecular structure (Section 1.1.2.3). The convoluted redox peaks mean that DHI-melanin has various pK_a values, some of which may be lower than 6.3 (pK_a(HQI/H2Q)) (Section 7.1.4). The change of pK_a in DHI-melanin during its polymerization may not have a direction, due to its multiple polymerization sites and high reactivity under the large amount of H_2O_2 generated (Section 7.6.1.2).

7.4.2 Broad features due to the disordered structure of DHI component

The difference between broad voltammetric features and distinguishable features can be caused by the different ratios of DHI:DHICA. The DHI component is reactive and has various polymerization sites, therefore DHI-melanin is disordered and has a convolution of features (broad) in voltammograms (Section 2.1.2 and Section 4.5) [52][136]. Such eumelanin is called here *DHI-dominant-melanin.* The chemically and geometrically disordered structure of eumelanin was initially proposed to explain its broadband optical absorption (Section 2.1.1). Here we found the disordered model also useful to explain the convoluted electrochemical features or quasi-box-shaped voltammogram of DHI-dominant-melanin. Conversely, the DHICA component likely has ordered structures and distinguishable voltammetric features (Section 2.1.2 and Section 4.5). Therefore, when the ratio of DHI:DHICA of eumelanin is below a certain level, distinguishable features are shown in voltammograms. Such eumelanin is called here *DHICA-dominant-melanin*. The controlling factors for the ratio of DHI:DHICA depend on the conditions for DOPA to synthesize into DHI or DHICA monomers (Section 7.4.4).

7.4.3 Interaction between DHI and DHICA components in DHI-DHICA-melanin

DHI-melanin is easy to further polymerize (Section 2.1.1 and Section 7.4.1). The irreversible feature SQ/Q of both Type 1 and Type 2 DHICA-melanin disappears due to its oxidative or reductive polymerization with DHI component. The redox couples H2Q/HQI and H2Q/SQ of Type 2 DHICA-melanin remains in Type 2 DHI-DHICA-melanin, because they are reversible electron-transfer processes for fully-polymerized Type 2 DHICA-melanin (Figure 7.11(b)) (Section 7.5.1). Such phenomenon is consistent with Sepia melanin, with DHI:DHICA ratio 1:3 (Figure 7.11) [137].

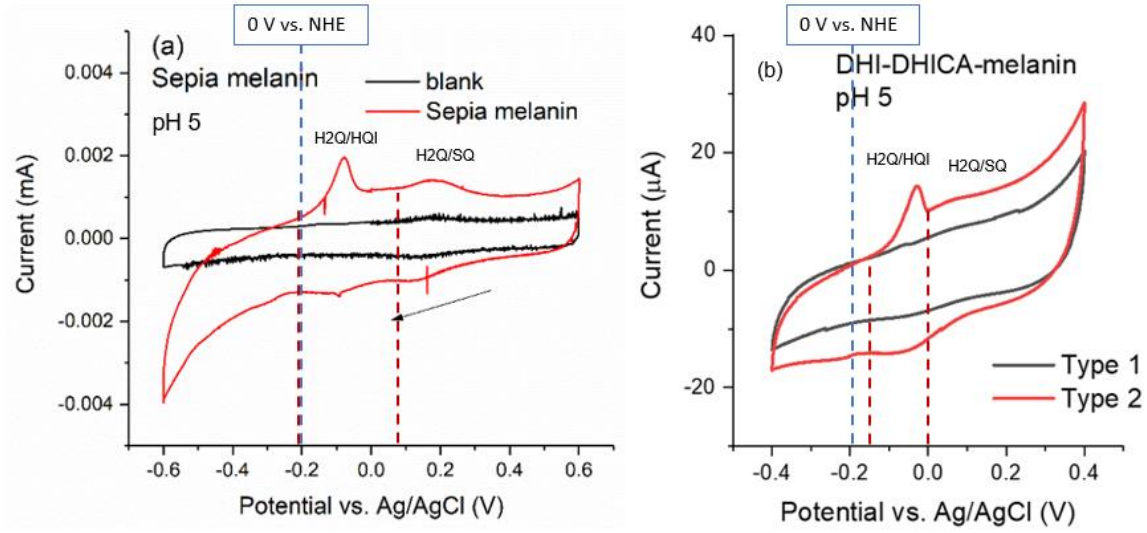

Figure 7.11 Cyclic voltammograms of (a) Sepia melanin and blank electrode, and (b) Type 1 and Type 2 DHI-DHICA-melanin, at 5 mV/s in 0.25 M $NaCH_3COO$ pH 5. Adapted from Figure 4.3(a) and Figure 6.2(c).

7.4.4 Controlling factors for DHI:DHICA ratio

In this section, we tentatively discuss the controlling factors for this ratio during synthesis of DHI and DHICA (Part 1 Synthesis).

In Part 1 Synthesis (Figure 7.12), tyrosine or DOPA is first oxidized to form dopaquinone (Procedure (1)). Dopaquinone spontaneously cyclizes into dopachrome (Procedure (2)).

Dopachrome has an oxidized form (noted as dopachrome in Figure 7.12) and a reduced form (noted as leucodopachrome in Figure 7.12). The oxidized dopachrome gets further oxidized into DHI and/or DHICA in their quinone forms.

The oxidation processes involved seem to be also controlled by the synthetic pH. Indeed, [113] reported low pH (pH 8.3) to produce DHI and high pH (pH 13) to produce DHICA using $K_3Fe(CN)_6$ as the oxidant, in the absence of O_2. We tentatively explain the synthetic pH values as follows. In procedure (4) and (5), the aliphatic five-membered-ring functionalized with $-COO^-$ is not stable being connected beside the aromatic benzene ring, therefore tends to stabilize by forming an aromatic (pyrrolic) ring. It can form it by being further oxidized, i.e. losing one proton and one electron, to have one more double bond in the molecule. Losing the $-COO^-$ functional group, here called *decarboxylation*, is a competitive reaction with such oxidation. Therefore, by using a low pH between pK_a(HQI/H2Q(DOPA)) ca 6.3 and pK_a(SQ/H2Q(DOPA)) ca 8.7, we can slow down the oxidation and let decarboxylation occur [114][115]. Indeed, the production of DHI takes longer time (40 min -1 h) than for DHICA (10 -15 min) [113][93].

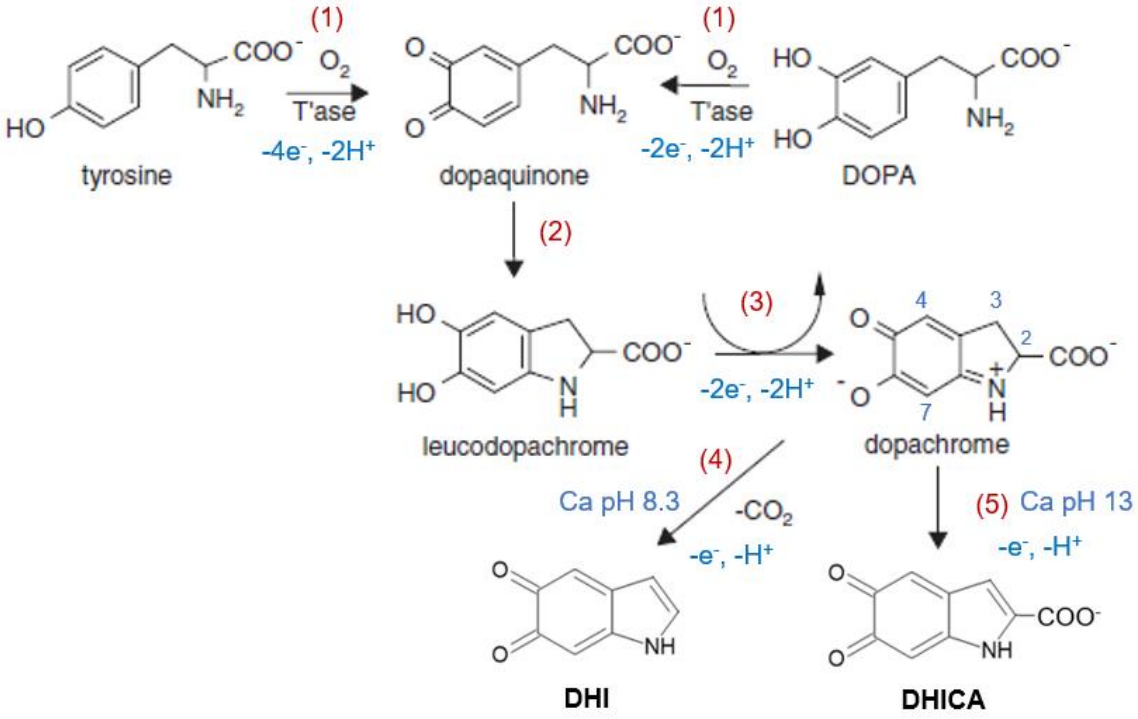

Figure 7.12 Pathways for the production of DHI and DHICA in quinone forms (Part 1 Synthesis of eumelanin). Adapted from [93].

There are other factors, such as the presence of transition metal ions, probably related to how high their redox potentials are, that can oxidize DOPA [94][95]. Another important factor is the mechanism of enzymes catalyzing this reaction, such as tyrosinase, should be further investigated.

7.5 Energy storage of eumelanin: capacity and cycling stability

For energy storage devices based on eumelanin, the capacity/capacitance and the cycling stability are connected. They all depend on the polymerization states (Section 7.5.1), potential limits (Section 7.5.2), adhesion between the eumelanin and the current collector (Section 7.5.4). In most cases, there is a trade-off between the capacity/capacitance and the cycling stability [51]. However, the light irradiation seems to offer the possibility of improving both the capacity/capacitance and the cycling stability of DHI-melanin. Furthermore, part of the improvement of capacity in DHI-melanin seems to be persistent. In Section 7.5.3, we discuss a possible mechanism to induce persistent improvement in DHI-melanin. In Section 7.5.4.2, a possible explanation on improvement of the adhesion property of DHI-melanin is suggested.

7.5.1 Capacity vs. polymerization states of eumelanin

In the literature and in this work, there are relations, q_{an} vs. q_{ca}, and i_{an} vs. i_{ca}, in voltammograms of eumelanin (Section 3.2.3 for extraction of *q)*. In this section, we tentatively sort these relations and associate them with different polymerization states of eumelanin in Table 7.1.

Table 7.1 Polymerization states of eumelanin sorted by q_{an} vs q_{ca} or i_{an} vs i_{ca}. Monovalent metal ions are employed in the electrolytes except where noted.

State of eumelanin	q_{an} vs q_{ca} or i_{an} vs i_{ca} (except for current of OER or HER)	Example of voltammograms
Monomeric/Oligomeric eumelanin	$q_{an} > q_{ca}$ or $i_{an} > i_{ca}$	DHI-melanin [136] DOPA-melanin [51] Natural eumelanin preloaded with Na^+ [16] DOPA-melanin [107] (Figure 2.6)

		DHI- and DHICA-melanin, Sepia melanin with Cu^{2+}(2.5 mM) in electrolyte (Figure 4.4)
Semi-polymerized DHI-melanin and [1]DHI-dominant-melanin	$q_{an} \approx q_{ca}$, but q is high or $i_{an} \approx i_{ca}$, but i is high [2] q_{ca} of semi-polymerized DHI-melanin is ca 140 C g^{-1}	DHI-melanin (Figure 4.2b in Article 1) DOPA-melanin [108]
Semi-polymerized DHICA-melanin and DHICA-dominant-melanin	$q_{an} \approx q_{ca}$ or $i_{an} \approx i_{ca}$ [2] q_{ca} of semi-polymerized DHICA-melanin is ca 13 C g^{-1} Feature SQ/Q is present in both types of DHICA-melanin.	DHICA-melanin (Figure 4.2a in Article 1) DOPA-melanin [36] (Figure 2.5)
Fully-polymerized DHI-melanin	$q_{an} \approx q_{ca}$, but q is low or $i_{an} \approx i_{ca}$, but i is low [2] q_{ca} is ca 23 C g^{-1}	Sepia melanin (Figure 4.3a in Article 1) DHI-melanin (Figure 5.2 in Article 2 and Figure 6.3 in Article 3)
Fully-polymerized DHICA-melanin	Feature SQ/Q is not present in both types of DHICA-melanin. [2] q_{ca} of fully-polymerized Type 1 DHICA-melanin is ca 13 C g^{-1}	5^{th} cycle of Type 2 DHICA-melanin (Figure 6.2(B)) Cu/Fe/DHICA-melanin under the effect of H_2O_2 (Figure 6.5(B))

	Redox features H2Q/HQI and H2Q/SQ are pronounced in Type 2 DHICA-melanin.	Type 2 DHICA-melanin (Figure 6.6a)
Any of the above but in the presence of a certain amount of O_2	$q_{an} < q_{ca}$ or $i_{an} < i_{ca}$ ORR* current is high	Polydopamine [52] (Figure 2.10) Natural eumelanin and DOPA melanin [106] (Figure 2.9)

[1] DHI-dominant-melanin and DHICA-dominant-melanin are defined in Section 7.4.2
[2] the capacity is provided based on voltammetric data extracted from cathodic currents in potential range -0.4 V/0.4 V at 5 mV/s.
[3] ORR: oxygen reduction reaction
OER: oxygen evolution reaction
HER: hydrogen evolution reaction

The monomers of eumelanin are oxidatively polymerized automatically in aqueous electrolytes at bulk pH ≥ 6.3 (pK_a(HQI/H2Q)), which is the bulk pH of electrolytes used in most of the literature. Therefore, we assume *monomeric/oligomeric eumelanin* as the initial polymerization state of eumelanin in voltammograms.

Oligomeric eumelanin has the tendency to undergo oxidative polymerization, i.e. formation of covalent bonds. This process is irreversible during cycling, shown by the higher oxidation current than the reduction current (Section 2.2.5.2). From oligomeric eumelanin to *semi-polymerized eumelanin*, such oxidative current is reduced from cycle to cycle (Figure 2.6). For *semi-polymerized* eumelanin, oxidation current is almost equal to reduction current, i.e. $i_{an} \approx i_{ca}$.

After semi-polymerized eumelanin, we consider a polymerization state called *fully-polymerized eumelanin.* Semi-polymerized and fully-polymerized eumelanin are categorized by DHI and DHICA components. From semi-polymerized to *fully-polymerized* DHI-(dominant)-melanin, the redox current/capacity undergoes a big decrease. Fully-polymerized DHI-(dominant)-melanin shows quasi-box shape in voltammograms and its capacity does not decrease under high oxidative potential. For example, semi-polymerized DHI-melanin has a capacity (140 C g^{-1}) ca 6 times higher with respect to fully-polymerized DHI-melanin (23 C g^{-1}). Again, the high current of semi-polymerized state with respect to the low current of fully-polymerized state of DHI-(dominant)-

melanin is due to the irreversible oxidative polymerization (Section 7.5.2.2). Semi-polymerized DHICA-(dominant)-melanin is represented by the irreversible oxidation feature SQ/Q in voltammograms. Type 1 and Type 2 DHICA-(dominant)-melanin both exist for semi-polymerized or fully-polymerized DHICA-(dominant)-melanin. Fully-polymerized DHICA-(dominant)-melanin does not have the oxidation feature SQ/Q in voltammograms. Type 2 fully-polymerized DHICA-(dominant)-melanin has increased redox features HQI/H2Q and SQ/H2Q with respect to semi-polymerized DHICA-(dominant)-melanin.

Considering that the amounts of transferred electrons are close due to the same loading, the higher capacity of fully-polymerized DHI-melanin (23 C g^{-1}) than fully-polymerized DHICA-melanin (13 C g^{-1}) should be due to the better electron transport of DHI-melanin favored by its π-π stacked structures.

There are also cases where $i_{an} < i_{ca}$. In such cases, O_2 is present and the cathodic current is high due to ORR (Section 2.2.6 and Section 2.2.7).

7.5.2 Capacity vs. potential limit for eumelanin

Readers are urged to read Section 7.6.1.1 before reading this section, as the prooxidant properties of eumelanin are essential for the discussion of oxidative polymerization of eumelanin.

7.5.2.1 Effect of environmental pH on the polymerization states

In Article 1, the eumelanin used is semi-polymerized. In Article 2, [20] and Article 3, the DHI-melanin samples are fully-polymerized. We showed two paths of chemical polymerization of DHI-melanin from semi-polymerized state to fully-polymerized state on carbon paper, influenced by environmental pH (Section 3.1.1):

- Prolonged polymerization at environmental pH 12 for ca 65 hours (Samples for [20]).
- Prolonged polymerization at environmental pH 7 for ca 1 year (Samples for Article 3).

According to Section 7.6.1.1, the synthetic polymerization processes of eumelanin in this work are driven by the potential difference between H_2O_2 or O_2 and eumelanin. From Eq. 7.1a, we assume that the change of environmental pH does not change such potential differences. Therefore, the control of environmental pH seems a key factor to control the redox properties of eumelanin (Section 7.1.3).

7.5.2.2 Definition of potential limit

In this work, semi-polymerized DHI-dominant-melanin $i_{an} \approx i_{ca}$ but the currents can decrease very slowly within a given potential range. Such potential range is called here the *high-current potential range*. It is estimated and discussed in Section 7.5.2.3 and Section 7.5.2.4. Outside such a potential range, we call it the *low-current potential range*. In this range, the currents of DHI-dominant-melanin decrease very fast, i.e. DHI-dominant-melanin reaches its fully-polymerized state quickly. The boundary potential between the high-current and low-current potential range is here called the *potential limit*.

7.5.2.3 Estimation of potential limit from local pH

Electrochemical measurements in this work do not seem to provide the possibility of separating environmental pH (here local pH) and the oxidative/reductive force.

When a high electrochemical potential (in low current potential range) is applied to eumelanin, it has two roles:

- to provide high oxidative or reductive force for eumelanin
- to induce a local pH that is very basic or very acidic. Such a pH is related to the pH that can depolymerize eumelanin.

From Section 7.5.2.1, we hypothesize that the local pH can play an important role in determining the potential limits. We here tentatively calculate the potential limits based on local pH 4 and ca 13, which are the pHs for the decomposition of eumelanin. The high-current potential range calculated for pH 5 buffered by $NaCH_3COO$ are -0.32 V/0.27 V vs. Ag/AgCl. The adopted potential ranges for applications are close to these values.

For example, the semi-polymerized DHI-dominant-melanin shows ca 40% capacitance retention after 20,000 cycles in galvanostatic charge-discharge measurement, with cut-off potential 0.75 V. The resulting potential ranges are -0.6 V/0 V and 0 V/0.2 V vs. Ag/AgCl for negatively biased electrode and positively biased electrode, respectively [51].

Such high-current potential range seems to apply to fully-polymerized eumelanins too. In [20], fully-polymerized DHI-DHICA-melanin is applied with cut-off potential 0.4 V. The resulting ranges are -0.25 V/0 V and 0 V/0.20 V vs. Ag/AgCl for negatively biased electrode and positively

biased electrode, respectively (Figure S5 in [20]). The capacitance retention is ca 89% after 2000 cycles.

Such potential range can be extended by adopting unbuffered aqueous electrolytes, which can make the potential limit higher for ca 0.53 V (Section 2.2.3). For unbuffered bulk pH 7, the calculated high-current potential range is -0.97 V/0.68 V vs. Ag/AgCl. The applied potential range for the Sepia melanin-based electrode during the galvanostatic charge-discharge measurement is close, ca -0.75 V/0.85 V vs. Ag/AgCl. The capacity retention is close to 100% after 500 cycles [50].

7.5.2.4 Possible high potential limit of DHI-melanin

DHI-melanin may have pK_a values both higher than pK_a(SQ/Q) ca 12 and lower than pK_a(HQI/H2Q) ca 6.3 (Section 7.4.1). Therefore, fully-polymerized DHI-melanin may buffer the local pH during potential scan/potential changes at higher potentials than DHICA-melanin. Therefore, higher potential limits of DHI-melanin with respect to calculated limits in Section 7.5.2.3 are expected.

7.5.3 Mechanism of persistent light-enhanced energy storage

Results of Article 2 and [20] show the possibility of realizing persistent light-enhanced energy storage properties of DHI-melanin. DHICA component seems to resist such persistent enhancement. This section explains the possible mechanisms behind these phenomena.

7.5.3.1 Hypothesis: light-induced polymerization of DHI-melanin

DHI-melanin seems easy to polymerize in every polymerization state except for the fully-polymerized state. However, in Article 2, the fully-polymerized DHI-melanin seems to undergo further polymerization induced by the light irradiation.

For positively biased DHI-melanin, after excitation by photons, a higher amount of oxidized form Q is generated in eumelanin (Scheme 5.2). The generated Q form eumelanin combines with eumelanin of reduced form H2Q that is present. Therefore, further oxidative polymerization of eumelanin is initiated by light irradiation (Section 2.2.4). For the same reason, in negatively biased DHI-melanin, the excitation of light can induce reductive polymerization of eumelanin by generating a higher amount of the H2Q form of eumelanin (Section 2.2.4).

After oxidative/reductive polymerization, DHI-melanin may have formed oligomers composed of higher numbers of building blocks, that is, a larger area of each π-π stacked oligomer for electrons to delocalize.

7.5.3.2 Possible blockage of light-induced polymerization by DHICA

The light-induced polymerization of DHI-melanin seems to be blocked by a small portion of DHICA component (DHI:DHICA 7:3). Possible reasons include:

- steric hindrance by the -COOH group of DHICA (Section 2.1.1)
- limited polymerization sites of DHICA (Section 2.1.1).

Because of these two factors, DHICA component may have blocked a part of the light-induced polymerization of fully-polymerized DHI-melanin.

7.5.4 Adhesion properties

Adhesion is important to maintain good cycling stability. For example, eumelanin does not have good adhesion on ITO, as shown by its faster drop of capacity/capacitance than on carbon paper (Table 5.2) [154].

7.5.4.1 Choice of current collectors

Using a 3D carbon paper current collector may provide good adhesion properties for the following reasons:

- π-π interacts with aromatic rings of eumelanin
- The carbon fibers have very small spaces between themselves. After being drop-cast, monomers in methanol stay in the small space due to the capillary action. Capillary action is the ability of a liquid to flow in narrow spaces without the assistance of external forces like gravity. During cycling, eumelanin is in a (soft) hydrated solid-state. It is adhesive to the carbon fibers in the small spaces due to its surface tension [177]. Surface tension tends to minimize the surface area. Surface tension exists because the molecules on the surface are attracted to the molecules in the bulk. In SEM images, eumelanin is located in the space between fibers (Figure 4.1 and Figure 1 in [20]).

7.5.4.2 Light irradiation improves adhesion of DHI-melanin

Adhesion can be improved by further polymerization, by oxidative potentials or light irradiation of DHI-melanin. Indeed, polydopamine, with the same molecular structure as DHI-melanin, has been utilized as binders for electrode materials (Section 1.1.2.1) [178]. We tentatively explain the effect of further polymerization of DHI-melanin on adhesion as follows. The multiple polymerization sites of DHI-melanin enable each two DHI building blocks to bond with each other at more than two polymerization sites, here called *quasi-cross-linking* of DHI-melanin (Figure 1.2 (b)(c)). *Cross-linking* in polymer chemistry describes the formation of covalent bonds between polymer chains. Such bonding is similar to that of *networked polymers* caused by *cross-linking*, here called *networking of DHI-melanin*. Polymers are found to be more adhesive with increased molecular weight or the degree of cross-linking [179]–[182]. Therefore, by further polymerization, DHI-melanin can increase its molecular weight as well as the degree of networking, and therefore its adhesion. Light irradiation, in particular, could induce further oxidative/reductive polymerization of DHI-melanin that improves its adhesion properties. Indeed, slightly higher cycling stability of DHI-melanin and DHI-DHICA-melanin are shown under light irradiation (Table 5.2).

7.5.5 Comparison of energy storage properties of eumelanin and other quinone-based materials

7.5.5.1 Comparison of capacity/capacitance and cycling stability

Capacity/capacitance and cycling stability are related to polymerization states of eumelanin (Section 7.5.1), potential range applied during measurements (Section 7.5.2) and adhesion properties between the eumelanin and current collectors (Section 7.5.4). Therefore, we do not think these properties of eumelanin and different quinone-based materials can be compared.

7.5.5.2 Comparison of electrochemical potentials

For the following reasons, the electrochemical potentials of eumelanin and other quinone-based materials may not be comparable:

- The oxidation potentials of materials with quinone-based materials seem highly dependent on the composition of the electrolyte (Section 2.2.3 and Section 2.2) and the sweeping rates (Section 7.1.4.5). Therefore, the electrochemical potentials may only be comparable if all the materials of interest are tested under the same conditions by cyclic voltammetry.

- The applicability of the theory proposed for PAET process (Section 7.1) to other types of quinone-based materials is not yet proved. Therefore, it is not reasonable to simply compare pK_a values of eumelanin to other types of quinone-based materials.

7.5.6 Processing of natural eumelanin

7.5.6.1 Interfacial area of Sepia melanin and current collector

In this work, Sepia melanin (q_{ca} 3.2 C g^{-1}) has a capacity ca 7 times lower than that of DHI-DHICA-melanin (q_{ca} ca 22 C g^{-1}). We tentatively explain such difference as follows. The Sepia melanin has very little interfacial area with the current collector due to its shape composed of big granules with diameters ranging from ca 5 μm to ca 10 μm (Figure S1 in Appendix A and [183]). Such a shape can be due to metal ion chelation.

In reference [183], Ethylenediaminetetraacetic acid (EDTA)-treated Sepia melanin, i.e. deionized Sepia melanin, shows smaller granular sizes, close to Fe/Cu/DHI-DHICA-melanin (Figure 6.4(B)). Therefore, the key to process natural eumelanin to increase its interfacial area with current collectors can be deionizing by a strong ion chelator such as EDTA.

7.5.6.2 Possible methodology to separate DHI and DHICA components

This work points out the importance of separating DHI and DHICA components during the fabrication of energy storage devices based on eumelanin. A possible way to separate them may be extraction by solvents. Natural sourced eumelanin usually has fully-polymerized DHI and DHICA components (Section 7.5.6.1). Cross-linked or networked polymers are usually insoluble [184]. Therefore, the DHI component in natural eumelanin is probably in networked structure that is insoluble in many kinds of solvents (Section 7.5.4.2) [40]. Conversely, DHICA component is probably soluble due to its limited polymerization sites (Section 2.1.1). Indeed, in this work, we observe insoluble DHI-melanin in methanol, whereas DHICA-melanin still seems soluble in methanol after storage in the freezer for 1 year (results not shown). Therefore, a possible way to separate DHI and DHICA is to use some type of solvent similar to methanol followed by filtration.

7.5.6.3 Depolymerization by basic solutions

Using basic solutions such as NaOH (ca pH 13) in the presence of O_2 can fully depolymerize eumelanin depending on the pH [36][116]. Therefore, the networked DHI component can be

depolymerized by *oxidative depolymerization* and later polymerized into films with possibly higher interfacial area with current collectors (Section 7.5.6.1).

7.6 Antioxidant/prooxidant properties of eumelanin

This section aims to explain the effect of ROS on the redox properties of DHI- and DHICA-melanin (Section 7.6.2) and proposes possible methods to suppress the prooxidant properties (Section 7.6.3). Before giving such explanations, we need to clarify the relation between reductive properties of eumelanin and its antioxidant/prooxidant properties in the presence of O_2 (Section 7.6.1). Indeed, the prooxidant properties of eumelanin are paramount for discussion of the effect of ROS on DHICA-melanin (Section 7.6.1.2). Because O_2 is ubiquitous in the human body, discussions of conditions in the absence of O_2, i.e. without prooxidant properties, may not be practical (Section 7.6.1). Lastly, comparisons of antioxidant properties are offered (Section 7.6.4).

7.6.1 Reductive properties vs. antioxidant and prooxidant properties

Both antioxidant (scavenging H_2O_2) and prooxidant processes (generating H_2O_2) are both based on the reductive properties of eumelanin (Section 7.6.1.1). DHI-melanin is found to generate more H_2O_2 than DHICA-melanin [101]. Section 7.6.1.2 gives a tentative explanation of the differences inf prooxidant behavior of DHI-melanin and DHICA-melanin. Such differences can be the reason for the different effects of ROS on DHI-melanin and DHICA-melanin (Section 7.6.2).

7.6.1.1 Antioxidant and prooxidant processes coexist in the presence of O_2

During the prooxidant process, O_2 oxidizes eumelanin and becomes H_2O_2, namely ORR (Section 2.2.6).

$$O_2 + 2H^+ + 2e^- \rightarrow H_2O_2 \quad (0.7 \text{ V vs. NHE}) \qquad \text{Reaction 7.2}$$

Here we also call Reaction 2.2 the *generation of H_2O_2 by eumelanin* in the presence of O_2.

After the prooxidant process occurs, the antioxidant process begins, where H_2O_2 oxidizes eumelanin and becomes H_2O.

$$H_2O_2 + 2H^+ + 2e^- \rightarrow H_2O \quad (1.76 \text{ V vs. NHE}) \qquad \text{Reaction 7.5}$$

Reaction 7. is here called *H_2O_2 reduction*. Due to the reductive properties of eumelanin, there are both antioxidant and prooxidant processes in the presence of O_2. The oxidative polymerization of eumelanins in the presence of O_2 is probably driven by the potential differences between H_2O_2 or O_2 and eumelanin (Reaction 2.2 and Reaction 7.).

7.6.1.2 Antioxidant and prooxidant properties: DHI-melanin vs. DHICA-melanin

In this section, we tentatively further discuss the mechanisms of antioxidant and prooxidant properties of DHI- and DHICA-melanin based on their various polymerization states (Section 7.5.1). This section may explain the phenomenon where there are different results of ROS scavenging when comparing DHI- and DHICA-melanin [89][101].

Table 7.2 Antioxidant and prooxidant properties of DHI- and DHICA-melanin at different polymerization states

Material	Polymerization states	Antioxidant (scavenging H_2O_2) and prooxidant properties (generating H_2O_2)
DHI-melanin	Oligomeric to semi-polymerized state	Antioxidant properties are high due to fast oxidative polymerization [101] (Section 7.6.1.1)
		Prooxidant properties are high due to fast oxidative polymerization [101]
	Semi-polymerized state	Lower antioxidant properties than oligomeric state
		Lower prooxidant properties than oligomeric state
	Fully-polymerized state	Very low antioxidant properties
		Very low prooxidant properties
DHICA-melanin	Oligomeric to semi-polymerized state	Antioxidant properties are low due to blockage of oxidative polymerization [101]
		Prooxidant properties are low due to blockage of oxidative polymerization [101]

	Semi- to fully-polymerized state	Antioxidant through “trapping mechanism” by rod-shaped supramolecular structure
		Prooxidant properties are negligible

In reference [101], a ROS scavenging experiment is conducted, where 2-deoxy-D-ribose (Dxrb), a component of DNA, is degraded using Fenton reagent. The results regarding how much ROS is scavenged are indicated using a relative extent of degradation of Dxrb (A/A_0) by the ROS in presence (A) or absence (A_0) of the radical scavenger. A is the amount of product of degradation of Dxrb detected by thiobarbituric acid assay. Results in a buffered environmental pH 7.4 point out that 0.8 mM DHI monomers/oligomers generate a significantly higher amount of H_2O_2 than its scavenged H_2O_2 (ca 1.7 vs. ca 0.2 A/A_0, ca 9 times higher). Conversely, 0.8 mM monomeric/oligomeric DHICA does not seem to generate a noticeable amount of H_2O_2 compared to the H_2O_2 that it scavenges (ca 0.22 vs. 0.09 A/A_0, ca two times higher). Notably, the ROS scavenging properties of DHI are higher than those of DHICA (ca 0.2 vs. 0.09 A/A_0) [101].

Combining the data analysis in this work, we tentatively explain the different prooxidant properties of monomeric/oligomeric DHI and DHICA as follows (Table 7.2). The pK_a(HQI/H2Q) 6.3 of DHICA shifts towards the environmental pH 7.4 during polymerization. At the same time, the environmental pH 7.4 shifts towards 6.3 due to acidification by $-COO^-$/-COOH (pK_a ca 4) and HQI/H2Q (pK_a ca 6.3) (Section 7.2) [111][49]. After a given time of oxidative polymerization of DHICA-melanin, the pK_a(HQI/H2Q) of DHICA-melanin is close to the environmental pH. In such a state, the reductive properties of DHICA-melanin may be suppressed. Therefore, monomeric/oligomeric DHICA may be reductive by its oxidative polymerization and cease being reductive after a given time of polymerization. The antioxidant behavior of semi-polymerized and fully-polymerized DHICA-melanin may be simply due to its rod-shaped supramolecular structure that traps the ROS between the oligomers, here called *trapping mechanism* (Section 2.1.2) [103].

Monomeric/oligomeric DHI-melanin has high reductive properties due to its continuous oxidative polymerization, thus both high antioxidant and high prooxidant properties (Section 2.1.1). When going from semi-polymerized to fully-polymerized, DHI-melanin’s antioxidant and prooxidant properties both decrease because the rate of oxidative polymerization decreases (Table 7.2). The

layer-by-layer π-π stacked supramolecular structure of DHI-melanin is not expected to play a role in ROS scavenging [103].

7.6.2 Effect of ROS on redox properties of eumelanin

Except for the increased amount of quinone groups or carbonyl groups demonstrated by the XPS results (Section 6.5.10), ROS promotes the oxidative polymerization of eumelanin (Section 7.6.1). DHI-melanin generates a significant amount of H_2O_2 that promotes its oxidative polymerization during its synthetic process and storage in ambient conditions. DHICA-melanin does not generate enough H_2O_2 to favor its oxidative polymerization (Section 7.6.1.2). Therefore, in Article 3, the DHI-melanin is fully-polymerized and DHICA-melanin is semi-polymerized. The additional ROS during the experiments in Article 3 promotes the oxidative polymerization of DHICA-melanin into fully-polymerized DHICA-melanin (Section 7.5.1). For both Type 1 and Type 2 DHICA-melanin, the oxidation feature SQ/Q tends to disappear under the oxidative stress of ROS (Figure 6.5(B)). The redox peaks H2Q/HQI and H2Q/SQ have increasing currents in Type 2 DHICA-melanin (Figure 6.6(A)). Sometimes such an effect is overlapped with the effect of generated quinone groups in eumelanin and carbon paper current collector by ROS (Figure S5 in Appendix B and Section 6.5.10).

7.6.3 Possible methods to suppress prooxidant processes

Based on above discussions, possible methods to suppress prooxidant processes while maintaining antioxidant processes may include:

- Controlling the amount of O_2 in the media.
- Increasing the DHICA:DHI ratio of eumelanin. By having more DHICA component, the reductive properties are expected to be suppressed at a given level and the trapping mechanism of radical scavenging is expected (Section 7.6.1.2). DHICA component also has $-COO^-$ as additional chelation sites than DHI component without reducing the oxidative transition metal ions (Section 7.1.3).

7.6.4 Comparison of antioxidant properties of eumelanin to other hydroquinone-based materials

7.6.4.1 Comparison by antioxidant capacity

The antioxidant capacity, i.e. oxidation capacity of the first cycle during cyclic voltammetry, mainly depends on the polymerization of the quinone-based materials (Section 7.5.1), which evaluates the *antioxidant status* of each sample [185]. Therefore, the different antioxidant compounds may not be comparable, as comparison depends on the antioxidant status of the antioxidant compounds.

7.6.4.2 Comparison by antioxidant power

The comparison of antioxidant powers, i.e. the electrochemical potentials in cyclic voltammograms, is presented in Section 7.5.5.2. For such comparisons, we need to consider the environmental pH required for the antioxidant process to take place, as it can determine whether the redox process can occur (Section 7.5.2.1), or potentially change the pK_a values of the material (Section 7.2.2).

CHAPTER 8 CONCLUSIONS AND PERSPECTIVES

In this work, we investigate in depth the redox properties of eumelanin. We conducted electrochemical measurements on eumelanin and draw insights on ways to improve its energy storage properties and its antioxidant properties. Eumelanin is composed of building blocks 6-dihydroxyindole (DHI) and 5,6-dihydroxyindole-2-carboxylic acid (DHICA). Chemically controlled eumelanins are synthesized from building blocks DHI and/or DHICA, namely *DHI-melanin*, *DHICA-melanin* and *DHI-DHICA-melanin*. Specifically, in this work, chemically controlled eumelanins were synthesized from DHI and/or DHICA monomers by solid-state polymerization [25], [93]. We explored the effects of various metal ions in the electrolyte, solar irradiation, and reactive oxygen species (ROS) on the charge transfer properties of chemically controlled eumelanins. The principal technique employed was cyclic voltammetry. Exploiting the metal chelation properties of eumelanin, we observed the morphology of the samples by SEM on carbon paper current collectors, after staining them with $UO_2(CH_3COO)_2$, $Fe_2(SO_4)_3$ and $Cu_2(COOCH_3)_2$ [23], [186]. XPS was used to characterize the chemical properties of the samples. UV-Vis spectrophotometry was used to characterize their optical absorption.

8.1 Conclusions and recommendations

8.1.1 Electrochemical potentials of DHI- and DHICA-melanin

Eumelanin permits proton-assisted electron transfer (PAET) processes. Experimental data in the literature and this work point that each deprotonation initiates an oxidation process and protonation for a reduction process (Section 7.1.3). *H2Q*, *SQ* and *Q* stand for hydroquinone, semiquinone and quinone forms, respectively. *HQI* stands for protonated quinone imine, which tautomerizes and loses an electron to form SQ (Section 7.1.3). According to the pK_a values of its functional groups, eumelanin has six electron transfer processes, noted as oxidation H2Q/HQI, H2Q/SQ, SQ/Q and reduction Q/SQ, HQI/H2Q, SQ/H2Q.

In cyclic voltammetry, the electrically biased working electrode material induces *local pH* by electrostatic force (Section 7.1.4). From the Nernst equation, by assuming that the onset potentials equal zero at pH equaling pK_a values, we obtained a linear relationship between the redox potentials of eumelanin and its pK_a values (Eq. 7.5a). Voltammograms of DHICA-melanin have distinguishable redox potentials that fit the expected data in Eq. 7.5a. DHI-melanin has broad

electrochemical features which are convolutions of its redox peaks at different potentials corresponding to different pK_a values. DHI has multiple polymerization sites, so DHI-melanin has disordered chemical structures that have various pK_a values (Figure 1.2 and Section 7.4.1). DHICA has a limited number of polymerization sites due to the steric hindrance provided by the carboxyl group. Therefore, DHICA-melanin has ordered chemical structures that show distinguishable electrochemical potentials.

This hypothesis explains why eumelanin has 3 distinguishable voltammetric potentials in aqueous solutions in most cases. The literature reports 2-electron and 2-proton redox process on quinone-based materials in aqueous electrolytes instead, resulting in only one voltammetric potential [34][7][15].

For the concept local pH, we suggest efforts be made on how we can define the *effective volume* for local pH and benefit the research in other fields. pH = -log $[H^+]$, which is related to the concentration of proton in a certain volume of the solution.

8.1.2 Polymerization states vs. electrochemical properties

Redox activities initiate polymerization. The polymerization mechanism can be *oxidative polymerization*, i.e. induction of a higher amount of Q, or *reductive polymerization*, i.e. induction of a higher amount of H2Q. The most common mechanism of polymerization of eumelanin is oxidative polymerization. Cyclic voltammetry in most cases promotes the oxidative polymerization of eumelanin. Storing eumelanin in ambient conditions (in the presence of O_2) also initiates its oxidative polymerization.

Several polymerization states are observed in the voltammograms: *monomeric/oligomeric state, semi-polymerized state* and *fully-polymerized state*. From monomeric/oligomeric state to semi-polymerized state, the anodic current is higher than the cathodic current, due to the irreversible oxidation current for oxidative polymerization. From semi-polymerized to fully-polymerized DHI-melanin, within a certain *potential limit*, the current decreases very slowly during cycling (Section 7.5.1). This explains the phenomenon where there seems to be a trade-off between cycling stability and capacity/capacitance [51] (Section 7.5.2.3). At potentials higher than the potential limit, the current decreases fast due to the fast oxidative polymerization. From semi-polymerized to fully-polymerized DHICA-melanin, the irreversible feature SQ/Q disappears in its voltammograms.

8.1.3 Antioxidant/prooxidant properties of DHI-melanin and DHICA-melanin

DHI-melanin can continuously undergo oxidative polymerization due to its multiple polymerization sites, therefore it is highly reductive. Such high *reductive properties* enable both high prooxidant and antioxidant properties. During the prooxidant process, O_2 is reduced to H_2O_2 by DHI-melanin, called *H_2O_2 generation* [101]. During the antioxidant process, H_2O_2 is reduced by DHI-melanin to H_2O. Therefore, there are two oxidants for the oxidative polymerization of DHI-melanin: H_2O_2 and O_2.

DHICA-melanin undergoes less oxidatively polymerization than DHI-melanin, therefore it is less reductive. DHICA-melanin does generate much H_2O_2, i.e. DHICA-melanin shows very low prooxidant properties [101]. DHICA-melanin is antioxidant by trapping radicals in its rod-shaped supramolecular structures [103].

To improve the antioxidant properties of eumelanin, we need to suppress its prooxidant properties. Increasing the ratio of DHICA:DHI may maintain high antioxidant properties of eumelanin while suppressing its prooxidant properties (Section 7.6.3 and 7.6.1.2)..

8.1.4 pH vs. electrochemical properties of DHICA-melanin

In this work, the *environmental pH* is the pH surrounding the sample, which includes *synthetic pH*, *storage pH* (ambient conditions), *bulk pH* of the electrolyte, *local pH* induced by electrical bias, etc. Below we simplify the term “environmental pH” as “pH”. When we mention change of pH, it also means an option of local pH by applied potentials.

In this work, we observe fast oxidative polymerization at higher pH (pH 12) vs. slow oxidative polymerization at moderate pH (pH 7) (Section 7.5.2.1). This evidence, among others, proves that the redox properties of eumelanin are controlled by pH (Section 7.4.4) [116][187].

In the meanwhile, the pH affects the pK_a values of eumelanin. When eumelanin is in a new pH that favors the oxidative polymerization of eumelanin, the pK_a values of eumelanin shift towards the pH during the polymerization (Section 7.2.2). By shifting its pK_a values towards pH values, eumelanin lowers the reaction rate at which it is further oxidized (polymerized) (Section 7.2.1). We expect structural changes to be involved.

We suggest effort be made to control the pK_a values of DHICA-melanin with pH during synthesis, therefore controlling its redox potentials. The synthesis experiment can also be conducted using electrochemical polymerization, by various local pH induced by applied potentials.

8.1.5 Ratio of DHI:DHICA vs. electrochemical properties

The ratio of DHI:DHICA affects whether the voltammograms are quasi-box shaped or distinguishable. The more DHICA, the more distinguishable the voltammetric potentials.

The ratio of DHI:DHICA depends on the synthetic conditions for DOPA to become DHI and DHICA (Section 7.4.4). Such a chemical synthesis process is also a pH-controlled oxidation process. The factors such as transition metal ions and the enzyme tyrosinase and the synthetic pH should be studied from such a point of view.

We suggest effort be made to investigate how to separate DHI and DHICA components from natural eumelanins (Section 7.5.6). In this work, DHI-melanin is suggested for fabricating light-enhanced energy storage devices (Section 7.5.3), whereas DHICA-melanin is suggested for antioxidant purposes (Section 7.6.3 and 7.6.1.2).

8.1.6 Multivalent metal ions vs. electrochemical properties

We studied the effect of Cu^{2+}, Fe^{3+} and Mg^{2+} (Section 7.3). The following were found:

- Transition metal ions can induce the further oxidative polymerization of eumelanin. This is observed with Cu^{2+}.
- Cathodic shift of redox potentials because chelation of multivalent metal ions lowers the pK_a values of eumelanin. At relatively low concentrations, a small peak appears at a potential slightly lower than the potential of H2Q/SQ or SQ/Q, here called *extra chelation potential* (Section 7.3.1.4).
- Anodic shift of the oxidation potential SQ/Q occurs by chelating to the electron-withdrawing functional group $-COO^-$ of eumelanin (Section 7.3.1.2).

Therefore, multivalent metal ions can be used to fine-tune the electrochemical properties of eumelanin. We suggest studying the effects of different concentrations of each type of metal ions on the supramolecular structure and electrochemical properties of eumelanin.

8.1.7 Supramolecular structure vs. electrochemical properties of DHICA-melanin

DHICA-melanin has a rod-shaped supramolecular structure with oligomers assembled by hydrogen bonds (Section 2.1.2). In this work, two types of DHICA-melanin in the voltammograms are observed. The oxidation peaks H2Q/SQ and SQ/Q exist in both types of DHICA-melanin. The major difference between Type 1 and Type 2 DHICA-melanin is the additional oxidation peak HQI/H2Q in Type 2 DHICA-melanin (Section 7.2.2). The supramolecular structure of Type 1 DHICA-melanin does not allow the deprotonation of the amine group by the anions CH_3COO^-. Therefore, in the rod-shaped structure of DHICA-melanin, Type 2 DHICA-melanin has the amine and $-COO^-$ groups facing outward and Type 1 has them inward forming hydrogen bonds between the oligomers.

Based on our discussions of altering of supramolecular structure of DHICA-melanin, we can consider controlling its supramolecular structure with the following points:

- Synergetic effect of multivalent metal ions and pH. pH controls which functional groups to deprotonate and chelate. The multivalent metal ion can serve as a center for the chelated functional groups to face inward to form a rod-shaped structure. For example, at pH 4, Fe^{3+} only chelates on $-COO^-$ and therefore have $-COO^-$ facing inward (Section 7.2.3.4).
- Polarity of the surrounding anions/molecules vs. polarity of the functional groups during the synthesis (Section 7.2.3).

8.1.8 Light irradiation vs. polymerization of DHI-melanin

Fully-polymerized DHI-melanin is found to have enhanced capacity/capacitance (up to ca 50%) and cycling stability under light irradiation. Part of such enhancement is persistent and is probably created by light-induced oxidative and reductive polymerization of DHI-melanin (Section 7.5.3). Such polymerization increases the numbers of building blocks in the π-π stacked oligomers and the area for the delocalization of electrons. Such polymerization is also the reason for the improved adhesion of DHI-melanin, where a higher degree of networked structure of DHI-melanin is formed than before.

We need to examine the change of structure of DHI-melanin under light irradiation by 1) the techniques that evaluate the molecular weight, such as gel permeation chromatography; 2) the techniques that evaluate the degree of cross-linking, such as cross-linking mass spectrometry; 3) the techniques that characterize the morphology, such as atomic force microscopy (AFM).

8.1.9 Transition metal ions vs. antioxidant/prooxidant properties

Transition metal ions at physiological concentrations do not affect the redox activities of eumelanin significantly, and consequently, the antioxidant/prooxidant properties (Section 7.3.2.3). However, if concentrations of the transition metal ions are increased over physiological concentrations, the cathodic shift of the redox potentials will be very high, and therefore, both antioxidant/prooxidant properties increased, which may be harmful to the human body.

On the other hand, the synergetic effect of transition metal ions and eumelanin that produces $^{\bullet}OH$ is prooxidant (Section 1.2.2.2). Such prooxidant properties will also increase due to the increase in the concentration of transition metal ions.

8.1.10 Buffered vs. unbuffered electrolytes

The difference of electrochemical potentials between buffered (acetate buffer) and unbuffered electrolytes is up to ca 0.53 V. Due to the effect of local pH, this value is estimated from the different ability to dissociate protons and anions of the weak acid CH_3COOH and water, that is, their different pK_a values (Section 2.2.3.1). With the same logic, other buffered electrolytes should have potential shifts by the difference of pK_a from that of CH_3COOH (Section 2.2.3.4). To further test this hypothesis, cyclic voltammetry of DHICA-melanin should be conducted in electrolytes composed of different buffering salts.

Furthermore, in buffered electrolytes, we expect a *buffered potential range* vs. *unbuffered potential range* that can be estimated from the concentration of the buffering salt (Section 2.2.3.4). To further test this hypothesis, different concentration of buffering salts and buffering salts with different pK_a values should be used.

8.1.11 Effect of sweeping rates

The electrochemical potentials have a certain dependency on the sweeping rates. This phenomenon supports the hypothesis that the PAET processes of eumelanin are controlled by local pH (Section 7.1.4.5). Other quinone-based materials, such as tannin, show similar dependence of electrochemical potentials on the sweeping rates [15]. This hypothesis, to a certain degree, can apply to other materials with PAET processes. Furthermore, the presence of multivalent metal ions may result in different degrees of such dependence (Figure S4 in Appendix A). Therefore, studies on the relation between the effect of the multivalent metal ions and the change of local pH should be conducted.

8.1.12 Effect of monovalent metal ions

Monovalent metal ions such as Na^+, K^+, NH_4^+ do not seem to affect the electrochemical potentials of eumelanin significantly above a certain negative potential. This conclusion does not include other monovalent metal ions, such as Li^+ (Section 2.2.2).

8.1.13 Current collectors vs. Cycling stability

The term *cycling stability* is often used for energy storage, meaning how much capacity/capacitance remains after a given number of cycles of cyclic voltammetry or galvanostatic charge-discharge are conducted. In fundamental electrochemical studies, cycling stability is also important for obtaining solid results.

Adhesion properties between eumelanin and current collectors that affect cycling stability partly depend on the current collectors. Three-dimensional carbon paper like the current collector offers better adhesion to eumelanin than the two-dimensional ITO glass (Article 2 and [20]). The high adhesion of eumelanin on carbon paper is probably due to the capillary effect or surface tension produced by the small spaces between carbon fibers (Section 7.5.4.1). We suggest effort be made to develop the rough surface on the current collector that can provide the capillary effect or surface tension of the electrode material.

8.1.14 Potential limit vs. Cycling stability

Potential limit, within which cycling stability seems to be high, is another factor for cycling stability of eumelanin. The potential limit seems to be related to the local pH that depolymerizes eumelanin (Section 7.5.2). Therefore, the potential limit can be increased in unbuffered electrolytes [50]. To verify such a hypothesis, we suggest that cycling by cyclic voltammetry and galvanostatic charge-discharge be conducted on DHI-melanin at the same polymerization state in buffered and unbuffered electrolytes.

8.2 Impacts on quinone-based energy storage field

8.2.1 Electrochemical potentials for batteries

The effect of local pH and transition metal ions on the electrochemical potentials can inspire the studies on other quinone-based materials.

8.2.2 Light-induced polymerization as a novel synthetic method for quinone-based materials

The use of light irradiation that induces further polymerization of DHI-melanin can be regarded as a chemical synthesis method for quinone-based materials, or even other redox- active organic materials. Having light irradiation for a long time means that the degree of polymerization increases dramatically. Under such long-term light-irradiation, eumelanin or other materials can form chemical structures that do not exist in normal conditions. Such chemical structures can enable very high electron transport, electron transfer properties as well as cycling stability for energy storage purposes. DHI-melanin should be investigated with light irradiation for up to 48 h or even 72 hours. Investigating with specific wavelengths for DHI-melanin can offer directional polymerization because the same light energy can activate the oligomers with the same structure. Materials with low visible optical absorption can also be considered with the light of UV or infrared range.

8.2.3 Enhanced capacity/capacitance by transition metal ions

This work also shows that transition metal ions at high concentrations in the electrolyte enhance the capacity/capacitance of eumelanin due to their synergetic effect. In this work, the capacity and

capacitance of eumelanins (DHI-, DHICA- and Sepia melanin) enhanced ca two orders of magnitude after adding Cu^{2+} (Section 7.3.2.1). The synergetic effect results in electrochemical currents higher than the sum of both Cu^{2+} and eumelanin. The reasons for such a synergetic effect are not totally understood. We suggest that this synergetic effect be confirmed using a proper degassing procedure that excludes the effect of oxygen reduction reaction (ORR) (Section 3.2.4).

This part of work can initiate a broad study of how transition metal ions can enhance the energy storage properties of redox-active organic materials and accelerate their commercialization. In perspective, wastewater usually contains various kinds of transition metal ions, therefore can be used as the electrolyte that enables high capacity/capacitance of the device. This innovative concept could also impact the fields of wastewater treatment and electrochemical energy storage.

8.3 Impacts on biological fields

From a biological point of view, eumelanin is present in most organs/tissues of the human body and its redox activities vary depending on the pH of the organ/tissue. The organs/tissues use pH to regulate the redox activities of its biomacromolecules. For example, normal blood pH is 7.4 but varies between 0 and 14. At pH < 6.3, eumelanin or its precursors are not reductive. At pH = pK_a, the redox properties of eumelanin are switched on/off. At pH between these pK_a values, the amount of electron transfer increases due to the rise of pH, and vice versa. Therefore, the redox activities of the same biomacromolecule vary in different organs/tissues due to different pH. There are other biomacromolecules (protein, enzyme, peptides and biopigments) that also have proton-assisted electron transfer processes, such as superoxide dismutase (SOD) [188][189]. It means that these biomacromolecules can also have their redox activities regulated by the pH of the organs/tissues.

8.4 Challenges and impacts on other electrochemical fields

There are other proton-assisted electron transfer processes uncovered in this thesis, such as oxygen reduction reaction (ORR), oxygen evolution reaction (OER) and hydrogen evolution reaction (HER). For example, ORR catalytic activity of eumelanin has a few unanswered questions:

- the onset potentials of ORR at each pH;
- the mechanism of ORR: whether it has a 2-electron process, generating H_2O_2, or a 4-electron process, generating H_2O.

The use of the concept local pH can potentially shed light on these two questions. The key to understanding the onset potentials can be that these reactions are triggered at certain local pHs. Therefore, applying the concept local pH will give a whole new perspective on the voltammograms. It can thus challenge the conventional electrochemical knowledge and methodology. Future researchers would need to deduce new equations or to modify the conventional functions due to simple changes of the basic hypotheses.

REFERENCES

[1] International Energy Agency, “World Energy Outlook 2019,” 2019.

[2] L. Tong, Y. Jing, R. G. Gordon, and M. J. Aziz, “Symmetric all-quinone aqueous battery,” *ACS Appl. Energy Mater.*, vol. 2, pp. 4016–4021, 2019.

[3] D. Larcher and J. M. Tarascon, “Towards greener and more sustainable batteries for electrical energy storage,” *Nat. Chem.*, vol. 7, no. 1, pp. 19–29, 2015.

[4] Z. Song and H. Zhou, “Towards sustainable and versatile energy storage devices: an overview of organic electrode materials,” *Energy Environ. Sci.*, vol. 6, no. 8, pp. 2280–2301, 2013.

[5] Y. Xu, M. Zhou, and Y. Lei, “Organic materials for rechargeable sodium-ion batteries,” *Mater. Today*, vol. 21, no. 1, pp. 60–78, 2018.

[6] M. Irimia-Vladu, “‘Green’ electronics: biodegradable and biocompatible materials and devices for sustainable future.,” *Chem. Soc. Rev.*, vol. 43, no. 2, pp. 588–610, 2014.

[7] Y. Zhou, B. Wang, *et al.*, “Polyanthraquinone-based nanostructured electrode material capable of high-performance pseudocapacitive energy storage in aprotic electrolyte,” *Nano Energy*, vol. 15, pp. 654–661, 2015.

[8] Z. Song, Y. Qian, *et al.*, “A quinone-based oligomeric lithium salt for superior Li-organic batteries,” *Energy Environ. Sci.*, vol. 7, no. 12, pp. 4077–4086, 2014.

[9] C.-Y. Gao, L. Zhao, and M.-X. Wang, “Stabilization of a reactive polynuclear silver carbide cluster through the encapsulation within a supramolecular cage.,” *J. Am. Chem. Soc.*, vol. 134, no. 2, pp. 824–7, Jan. 2012.

[10] Y. Liang, Y. Jing, *et al.*, “Universal quinone electrodes for long cycle life aqueous rechargeable batteries,” *Nat. Mater.*, vol. 16, pp. 841–850, 2017.

[11] T. Janoschka, N. Martin, *et al.*, “An aqueous, polymer-based redox-flow battery using non-corrosive, safe, and low-cost materials,” *Nature*, vol. 527, no. 7576, pp. 78–81, 2015.

[12] M. R. Gerhardt, C. J. Galvin, *et al.*, “A metal-free organic-inorganic aqueous flow

battery," *Nature*, vol. 505, pp. 195–198, 2014.

[13] K. Naoi, S. Suematsu, M. Hanada, and H. Takenouchi, "Enhanced cyclability of π-π stacked supramolecular (1, 5-diaminoanthraquinone) oligomer as an electrochemical capacitor material," *J. Electrochem. Soc.*, vol. 149, no. 4, pp. 472–477, 2002.

[14] T. Sun, Z. Li, *et al.*, "A biodegradable polydopamine-derived electrode material for high-capacity and long-life lithium-ion and sodium-ion batteries," *Angew. Chemie*, vol. 128, no. 36, pp. 10820–10824, 2016.

[15] A. Mukhopadhyay, Y. Jiao, *et al.*, "Heavy metal-free tannin from bark for sustainable energy storage," *Nano Lett.*, vol. 17, no. 12, pp. 7897–7907, 2017.

[16] Y. J. Kim, W. Wu, *et al.*, "Biologically derived melanin electrodes in aqueous sodium-ion energy storage devices," *Proc. Natl. Acad. Sci. U. S. A.*, vol. 110, no. 52, pp. 20912–7, 2013.

[17] Y. Liang, Z. Tao, and J. Chen, "Organic electrode materials for rechargeable lithium batteries," *Adv. Energy Mater.*, vol. 2, no. 7, pp. 742–769, 2012.

[18] C. Wang, Z. Yang, *et al.*, "High-performance alkaline organic redox flow batteries based on 2-hydroxy-3-carboxy-1,4-naphthoquinone," *ACS Energy Lett.*, vol. 3, no. 10, pp. 2404–2409, 2018.

[19] D. Hardee, Q. Chen, *et al.*, "Alkaline quinone flow battery," *Science*, vol. 349, no. 6255, pp. 1529–1532, 2015.

[20] R. Xu, A. Gouda, *et al*, "Melanin: a greener route to enhance energy storage under solar light," *ACS Omega*, vol. 4, no. 7, pp. 12244–12251, 2019.

[21] A. B. Mostert, B. J. Powell, *et al.*, "Role of semiconductivity and ion transport in the electrical conduction of melanin," *Proc. Natl. Acad. Sci. U. S. A.*, vol. 109, no. 23, pp. 8943–8947, 2012.

[22] L. Zecca, A. Stroppolo, *et al.*, "The role of iron and copper molecules in the neuronal vulnerability of locus coeruleus and substantia nigra during aging.," *Proc. Natl. Acad. Sci. U. S. A.*, vol. 101, no. 26, pp. 9843–9848, 2004.

[23] E. Di Mauro, R. Xu, G. Soliveri, and C. Santato, "Natural melanin pigments and their

interfaces with metal ions and oxides : emerging concepts and technologies," *MRS Commun.*, vol. 7, no. 2, pp. 141–151, 2017.

[24] H. M. Swartz, T. Sarna, and L. Zecca, "Modulation by neuromelanin of the availability and reactivity of metal ions," *Ann. Neurol. Off. J. Am. Neurol. Assoc. Child Neurol. Soc.*, vol. 32, no. S1, pp. S69–S75, 1992.

[25] A. Pezzella, M. Barra, *et al.*, "Stem cell-compatible eumelanin biointerface fabricated by chemically controlled solid state polymerization," *Mater. Horizons*, vol. 2, no. 2, pp. 212–220, 2015.

[26] R. Micillo, L. Panzella, *et al.*, "'Fifty shades' of black and red or how carboxyl groups fine tune eumelanin and pheomelanin properties," *Int. J. Mol. Sci.*, vol. 17, no. 5, p. 746, 2016.

[27] S. Ito, "A chemist's view of melanogenesis," *Pigment Cell Res.*, vol. 16, no. 3, pp. 230–236, 2003.

[28] J. Wünsche, Y. Deng, *et al.*, "Protonic and electronic transport in hydrated thin films of the pigment eumelanin," *Chem. Mater.*, vol. 27, no. 2, pp. 436–442, 2015.

[29] M. Ambrico, P. F. Ambrico, *et al.*, "From commercial tyrosine polymers to a tailored polydopamine platform: concepts, issues and challenges en route to melanin-based bioelectronics," *J. Mater. Chem. C*, vol. 3, pp. 6413–6423, 2015.

[30] R. Powell and B. Rosenberg, "The nature of the charge carriers in solvated biomacromolecules," *Bioenergies*, vol. 1, pp. 493–509, 1970.

[31] J. McGinness, P. Corry, and P. Proctor, "Amorphous semiconductor switching in melanins," *Science*, vol. 183, no. 4127, pp. 853–855, 1974.

[32] S. B. Rienecker, A. B. Mostert, *et al.*, "Heavy water as a probe of the free radical nature and electrical conductivity of melanin," *J. Phys. Chem. B*, vol. 119, no. 48, pp. 14994–15000, 2015.

[33] F. H. J. Figge, "Melanin : a natural reversible oxidation-reduction system," *Exp. Biol. Med.*, vol. 41, no. 1, p. 127, 1939.

[34] K. Hernandez-Burgos, G. G. Rodriguez-Calero, W. Zhou, and S. E. Burkhardt, "Increasing the gravimetric energy density of organic based secondary battery cathodes using small

radius cations (Li^+ and Mg^{2+}),” *J. Am. Chem. Soc.*, vol. 135, pp. 14532–14535, 2013.

[35] M. L. Tran, B. J. Powell, and P. Meredith, “Chemical and structural disorder in eumelanins - a possible explanation for broad band absorbance,” *Biophys. J.*, vol. 90, no. 3, p. 28, 2005.

[36] P. Díaz, Y. Gimeno, *et al.*, “Electrochemical self-assembly of melanin films on gold,” *Langmuir*, vol. 21, no. 13, pp. 5924–5930, 2005.

[37] A. Antidormi, C. Melis, E. Canadell, and L. Colombo, “Understanding the polymerization process of eumelanin by computer simulations,” *J. Phys. Chem. C*, vol. 122, no. 49, pp. 28368–28374, 2018.

[38] S. Meng and E. Kaxiras, “Theoretical models of eumelanin protomolecules and their optical properties,” *Biophsical J.*, vol. 94, pp. 2095–2105, 2008.

[39] E. Kaxiras, A. Tsolakidis, G. Zonios, and S. Meng, “Structural model of eumelanin,” *Phys. Rev. Lett.*, vol. 97, no. 21, pp. 1–4, 2006.

[40] M. D’Ischia, A. Napolitano, *et al.*, “Chemical and structural diversity in eumelanins: unexplored bio-optoelectronic materials,” *Angew. Chemie - Int. Ed.*, vol. 48, no. 22, pp. 3914–3921, 2009.

[41] C. Chen, C. Chuang, *et al.*, “Excitonic effects from geometric order and disorder explain broadband optical absorption in eumelanin.,” *Nat. Commun.*, vol. 5, p. 3859, 2014.

[42] P. Ghosh and D. Ghosh, “Elucidating the photoprotection mechanism of eumelanin monomers,” *J. Phys. Chem. B*, vol. 121, no. 24, pp. 5988–5994, 2017.

[43] E. Vahidzadeh, A. P. Kalra, and K. Shankar, “Melanin-based electronics: from proton conductors to photovoltaics and beyond,” *Biosens. Bioelectron.*, vol. 122, pp. 127–139, 2018.

[44] W. J. D. Beenken and T. Pullerits, “Excitonic coupling in polythiophenes: comparison of different calculation methods,” *J. Chem. Phys.*, vol. 120, no. 5, p. 2490, 2004.

[45] K. Y. Ju, M. C. Fischer, and W. S. Warren, “Understanding the role of aggregation in the broad absorption bands of eumelanin,” *ACS Nano*, vol. 12, no. 12, pp. 12050–12061, 2018.

[46] J. Cheng, S. C. Moss, M. Eisner, and P. Zshack, “X-ray characterization of melanins—I,”

Pigment Cell Melanoma Res., vol. 7, no. 14, pp. 255–262, 1994.

[47] C. Jin, S. C. Moss, and M. Eisner, "X-ray characterization of melanins—II," *Pigment Cell Res.*, vol. 7, no. 4, pp. 263–273, 1994.

[48] D. R. Dreyer, D. J. Miller, *et al.*, "Elucidating the structure of poly(dopamine)," *Langmuir*, vol. 28, no. 15, pp. 6428–6435, 2012.

[49] B. Szpoganicz, S. Gidanian, P. Kong, and P. Farmer, "Metal binding by melanins: studies of colloidal dihydroxyindole-melanin, and its complexation by Cu(II) and Zn(II) ions," *J. Inorg. Biochem.*, vol. 89, no. 1–2, pp. 45–53, 2002.

[50] Y. J. Kim, W. Wu, *et al.*, "Catechol-mediated reversible binding of multivalent cations in eumelanin half-cells," *Adv. Mater.*, vol. 26, no. 38, pp. 6572–6579, 2014.

[51] P. Kumar, E. Di Mauro, *et al.*, "Melanin-based flexible supercapacitors," *J. Mater. Chem. C*, vol. 4, no. 40, pp. 9516–9525, 2016.

[52] H.-A. Park, Y. J. Kim, *et al.*, "Lithium purification from aqueous solutions using bioinspired redox active melanin membranes," *Polym. Int.*, vol. 65, no. 11, pp. 1331–1338, 2016.

[53] A. J. Bard and L. R. Faulker, *Electrochemical Methods: Fundamentals and Applications*. New York: John Wiley & Sons, 2001.

[54] T. Brousse, D. Bélanger, and J. W. Long, "To be or not to be pseudocapacitive?," *J. Electrochem. Soc.*, vol. 162, no. 5, pp. A5185–A5189, 2015.

[55] P. Palladino, F. Bettazzi, and S. Scarano, "Polydopamine: surface coating, molecular imprinting, and electrochemistry—successful applications and future perspectives in (bio)analysis," *Anal. Bioanal. Chem.*, vol. 411, no. 19, pp. 4327–4338, 2019.

[56] L. Panzella, L. Leone, *et al.*, "Red human hair pheomelanin is a potent pro-oxidant mediating UV-independent contributory mechanisms of melanomagenesis," *Pigment Cell Melanoma Res.*, vol. 27, pp. 244–252, 2013.

[57] W. D. Bush, J. Garguilo, *et al.*, "The surface oxidation potential of human neuromelanin reveals a spherical architecture with a pheomelanin core and a eumelanin surface," *Proc. Natl. Acad. Sci.*, vol. 103, no. 40, pp. 14785–14789, 2006.

[58] H. Sies, “What is oxidative stress?,” in *Oxidative Stress and Vascular Disease*, J. F. KeaneyJr., Ed. Boston, MA: Springer, 2000, pp. 1–8.

[59] A. Rahal, A. Kumar, *et al.*, “Oxidative Stress, Prooxidants, and Antioxidants: The Interplay,” *Biomed Res. Int.*, vol. 2014, pp. 1–19, 2014.

[60] R. Apak, M. Ozyurek, K. Guclu, and E. Capanoglu, “Antioxidant activity/capacity measurement . 1. classification, physicochemical principles, mechanisms, and electron transfer (et)-based assays,” *J. Agr. Food Chem.*, vol. 64, pp. 997–1027, 2016.

[61] B. Halliwell and J. M. C. Gutteridge, “The definition and measurement of antioxidants in biological systems,” *Free Radic. Biol. Med.*, vol. 18, no. I, pp. 125–126, 1995.

[62] B. Halliwell, M. A. Murcia, S. Chirico, and O. I. Aruoma, “Free radicals and antioxidants in food and in vivo: what they do and how they work,” *Crit. Rev. Food Sci. Nutr.*, vol. 35, no. 1–2, pp. 7–20, 1995.

[63] E. G. Yordi, E. M. Perez, M. J. Matos, and E. U. Villares, “Antioxidant and pro-oxidant effects of polyphenolic compounds and structure-activity relationship evidence,” *Intech*, vol. i, p. 13, 2016.

[64] M. Carocho and I. C. F. R. Ferreira, “A review on antioxidants, prooxidants and related controversy: natural and synthetic compounds, screening and analysis methodologies and future perspectives,” *Food Chem. Toxicol.*, vol. 51, no. 1, pp. 15–25, 2013.

[65] E. Kim, Y. Liu, *et al.*, “Context-dependent redox properties of natural phenolic materials,” *Biomacromolecules*, vol. 15, no. 5, pp. 1653–1662, 2014.

[66] A. G. Orive, A. H. Creus, *et al.*, “Oxygen reduction on iron - melanin granular surfaces,” *J. Phys. Chem. C*, vol. 113, pp. 17097–17103, 2009.

[67] L. Migliaccio, M. Gryszel, *et al.*, “Aqueous photo(electro)catalysis with eumelanin thin films,” *Mater. Horizons*, vol. 5, no. 5, pp. 984–990, 2018.

[68] T. Nagaoka, T. Sakai, K. Ogura, and T. Yoshino, “Oxygen reduction at electrochemically treated glassy carbon electrodes,” *Anal. Chem.*, vol. 58, pp. 1953–1955, 1986.

[69] T. Nagaoka, T. Sakai, K. Ogura, and T. Yoshino, “Oxygen reduction with hydroxy-1,4-naphthoquinones immobilized at carbon electrodes,” *J. Chem. Soc. Faraday Trans. 1*

Phys. Chem. Condens. Phases, vol. 83, no. 6, pp. 1823–1833, 1987.

[70] E. Kim, M. Kang, *et al.*, "Spectroelectrochemical reverse engineering demonstrates that melanin's redox and radical scavenging activities are linked," *Biomacromolecules*, vol. 18, pp. 4084–4098, 2017.

[71] H. Liu, X. Qu, *et al.*, "Role of polydopamine's redox-activity on its pro-oxidant, radical-scavenging, and antimicrobial activities," *Acta Biomater.*, vol. 88, pp. 181–196, 2019.

[72] E. Kim, L. Panzella, *et al.*, "Reverse engineering applied to red human hair pheomelanin reveals redox-buffering as a pro-oxidant mechanism," *Sci. Rep.*, vol. 5, no. November, p. 18447, 2015.

[73] M. Kang, E. Kim, *et al.*, "Reverse engineering to characterize redox properties: revealing melanin's redox activity through mediated electrochemical probing," *Chem. Mater.*, vol. 30, no. 17, pp. 5814–5826, 2018.

[74] D. Erudaitius, A. Huang, *et al.*, "Peroxiporin expression is an important factor for cancer cell susceptibility to therapeutic H_2O_2: Implications for pharmacological ascorbate therapy," *PLOS One*, vol. 12, no. 1, pp. 1–14, 2017.

[75] U. G. Knaus, R. Hertzberger, *et al.*, "Pathogen control at the intestinal mucosa – H_2O_2 to the rescue," *Gut Microbes*, vol. 0976, pp. 1–8, 2017.

[76] C. C. Winterbourn, "Toxicity of iron and hydrogen peroxide: the Fenton reaction," *Toxicol. Lett.*, vol. 82–83, no. C, pp. 969–974, 1995.

[77] M. Zareba, A. Bober, *et al.*, "The effect of a synthetic neuromelanin on yield of free hydroxyl radicals generated in model systems," *Biochim. Biophys. Acta*, vol. 1271, pp. 343–348, 1995.

[78] B. Pilas, T. Sarna, B. Kalyanaraman, and S. H. M., "The effect of melanin on iron associated decomposition of hydrogen peroxide," *Free Radic. Biol. Med.*, vol. 4, pp. 285–293, 1988.

[79] M. J. Laughton, B. Halliwell, *et al.*, "Antioxidant and pro-oxidant actions of the plant phenolics quercetin, gossypol and myricetin," *Biochem. Pharmacol.*, vol. 38, no. 17, pp. 2859–2865, 2002.

[80] B. Halliwell, “How to characterize a biological antioxidant,” *Free Radic. Res. Commun.*, vol. 9, no. I, pp. 1–32, 1990.

[81] B. Halliwell, “Ascorbic acid, iron overload, and desferrioxamine.,” *Br. Med. J.*, vol. 285, no. 6337, pp. 296–296, 2009.

[82] C. Villanueva and R. D. Kross, “Antioxidant-induced stress,” *Int. J. Mol. Sci.*, vol. 13, no. 2, pp. 2091–2109, 2012.

[83] E. Di Mauro, “The Biopigment Eumelanin in the Sustainability Challenge: Interfaces with Metal Electrodes , UV-Absorption Enhancement of Plastics and its Biodegradability,” Polytechnique Montreal, 2019.

[84] D. Huang, O. U. Boxin, and R. L. Prior, “The chemistry behind antioxidant capacity assays,” *J. Agr. Food Chem.*, vol. 53, no. 6, pp. 1841–1856, 2005.

[85] L. Barros, S. Falcão, *et al.*, “Antioxidant activity of Agaricus sp. mushrooms by chemical, biochemical and electrochemical assays,” *Food Chem.*, vol. 111, no. 1, pp. 61–66, 2008.

[86] J. Sochor, J. Dobes, *et al.*, “Electrochemistry as a tool for studying antioxidant properties,” *Int. J. Electrochem. Sci.*, vol. 8, no. 6, pp. 8464–8489, 2013.

[87] R. Keyrouz, M. L. Abasq, *et al.*, “Total phenolic contents, radical scavenging and cyclic voltammetry of seaweeds from Brittany,” *Food Chem.*, vol. 126, no. 3, pp. 831–836, 2011.

[88] G. K. Ziyatdinova and H. C. Budnikov, “Evaluation of the antioxidant properties of spices by cyclic voltammetry,” *J. Anal. Chem.*, vol. 69, no. 10, pp. 990–997, 2014.

[89] T. Cecchi, A. Pezzella, *et al.*, “On the antioxidant activity of eumelanin biopigments : a quantitative comparison between free radical scavenging and redox properties,” *Nat. Prod. Res.*, pp. 1–9, 2019.

[90] K. L. Double, M. Gerlach, *et al.*, “Iron-binding characteristics of neuromelanin of the human substantia nigra,” *Biochem. Pharmacol.*, vol. 66, no. 3, pp. 489–494, 2003.

[91] R. L. Schroeder, K. L. Double, and J. P. Gerber, “Using Sepia melanin as a PD model to describe the binding characteristics of neuromelanin - a critical review,” *J. Chem. Neuroanat.*, vol. 64–65, pp. 20–32, 2015.

[92] T. E. Young, B. W. Babbitt, and L. A. Wolfe, “Melanin. 2. Electrochemical study of the

oxidation of a-methyldopa and 5,6-dihydroxy-2-methylindole," *J. Org. Chem.*, vol. 45, pp. 2899–2902, 1980.

[93] M. D'Ischia, A. Napolitano, *et al.*, "5,6-Dihydroxyindoles and indole-5,6-diones," *Adv. Heterocycl. Chem.*, vol. 89, no. December 2014, pp. 1–63, 2005.

[94] A. Palumbo, M. d'Ischia, *et al.*, "Structural modifications in biosynthetic melanins induced by metal ions," *Biochim. Biophys. Acta.*, vol. 964, no. 2, pp. 193–199, 1988.

[95] A. Palumbo, F. Solano, *et al.*, "Comparative action of dopachrome tautomerase and metal ions on the rearrangement of dopachrome," *Biochim. Biophys. Acta.*, vol. 1115, no. 1, pp. 1–5, 1991.

[96] M. Xiao, W. Chen, *et al.*, "Elucidation of the hierarchical structure of natural eumelanins," *J. R. Soc. Interface*, vol. 15, no. 140, p. 20180045, 2018.

[97] A. A. R. Watt, J. P. Bothma, and P. Meredith, "The supramolecular structure of melanin," *Soft Matter*, vol. 5, no. 19, p. 3754, 2009.

[98] C.-T. Chen, V. Ball, *et al.*, "Self-Assembly of tetramers of 5,6-dihydroxyindole explains the primary physical properties of eumelanin: experiment, simulation, and design," *ACS Nano*, vol. 7, no. 2, pp. 1524–1532, 2013.

[99] A. Büngeler, B. Hämisch, and O. Strube, "The supramolecular buildup of eumelanin: structures, mechanisms, controllability," *Int. J. Mol. Sci.*, vol. 18, no. 9, p. 1901, Sep. 2017.

[100] A. Büngeler, B. Hämisch, *et al.*, "Insight into the final step of the supramolecular buildup of eumelanin," *Langmuir*, vol. 33, no. 27, 2017.

[101] L. Novellino, A. Napolitano, and G. Prota, "5,6-Dihydroxyindoles in the fenton reaction: A model study of the role of melanin precursors in oxidative stress and hyperpigmentary processes," *Chem. Res. Toxicol.*, vol. 12, no. 10, pp. 985–992, 1999.

[102] M. Arzillo, G. Mangiapia, *et al.*, "Eumelanin buildup on the nanoscale: aggregate growth/assembly and visible absorption development in biomimetic 5,6-dihydroxyindole polymerization," *Biomacromolecules*, vol. 13, no. 8, pp. 2379–2390, 2012.

[103] L. Panzella, G. Gentile, *et al.*, "Atypical structural and π-electron features of a melanin

polymer that lead to superior free-radical-scavenging properties," *Angew. Chemie*, vol. 52, no. 48, pp. 12684–12687, 2013.

[104] A. Pezzella, L. Panzella, *et al.*, "Lack of visible chromophore development in the pulse radiolysis oxidation of 5,6-dihydroxyindole-2-carboxylic acid oligomers: DFT investigation and implications for eumelanin absorption properties," *J. Org. Chem.*, vol. 74, no. 10, pp. 3727–3734, 2009.

[105] I. G. Kim, H. J. Nam, H. J. Ahn, and D. Y. Jung, "Electrochemical growth of synthetic melanin thin films by constant potential methods," *Electrochim. Acta*, vol. 56, no. 7, pp. 2954–2959, 2011.

[106] Z. Tian, W. Hwang, and Y. J. Kim, "Mechanistic understanding of monovalent cation transport in eumelanin pigments," *J. Mater. Chem. B*, vol. 7, no. 41, pp. 6355–6361, 2019.

[107] C. Serpentini, C. Gauchet, *et al.*, "First electrochemical investigation of the redox properties of DOPA – melanins by means of a carbon paste electrode," *Electrochim. Acta*, vol. 45, pp. 1663–1668, 2000.

[108] L. G. S. Albano, E. Di Mauro, *et al.*, "Novel insights on the physicochemical properties of eumelanins and their DMSO derivatives," *Polym. Int.*, vol. 65, no. 11, pp. 1315–1322, 2016.

[109] P. Borghetti, A. Goldoni, *et al.*, "Effects of potassium on the supramolecular structure and electronic properties of eumelanin thin films," *Langmuir*, vol. 26, no. 24, pp. 19007–19013, 2010.

[110] Y. J. Kim, A. Khetan, *et al.*, "Evidence of porphyrin-like structures in natural melanin pigments using electrochemical fingerprinting," *Adv. Mater.*, vol. 28, no. 16, pp. 3173–3180, 2016.

[111] L. K. Charkoudian and K. J. Franz, "Fe(III)-coordination properties of neuromelanin components: 5,6-dihydroxyindole and 5,6-dihydroxyindole-2-carboxylic acid," *Inorg. Chem.*, vol. 45, no. 9, pp. 3657–3664, 2006.

[112] J. Nordlund, R. Boissy, V. Hearing, and R. King, *The Pigmentary System: Physiology and Pathophysiology*. New York: Oxford University Press, 1998.

[113] K. Wakamatsu and I. Shosuke, “Preparation of eumelanin-related dihydroxyindole-2-carboxylic acid, and their o-methyl derivatives,” *Anal. Biochem.*, vol. 170, pp. 335–340, 1988.

[114] T. E. Young, J. R. Griswold, and M. H. Hulbert, “Melanin. I. Kinetics of the oxidative cyclization of dopa to dopachrome,” *J.Org.Chem.*, vol. 39, no. 13, pp. 1980–1982, 1974.

[115] G. Kortüm, W. Vogel, and K. Andrussow, “Dissociation constants of organic acids in aqueous solution,” *Pure Appl. Chem.*, vol. 1, no. 2–3, pp. 187–536, 1960.

[116] K. Y. Ju, J. Kang, J. H. Chang, and J. K. Lee, “Clue to understanding the janus behavior of eumelanin: investigating the relationship between hierarchical assembly structure of eumelanin and its photophysical properties,” *Biomacromolecules*, vol. 17, no. 9, pp. 2860–2872, 2016.

[117] N. Elgrishi, K. J. Rountree, *et al.*, “A practical beginner’s guide to cyclic voltammetry,” *J. Chem. Educ.*, vol. 95, no. 2, pp. 197–206, 2018.

[118] M. E. Orazem and B. Tribollet, *Electrochemical Impedance Spectroscopy*. John Wiley and Sons, 2011.

[119] J. Goldstein, *Practical Scanning Electron Microscopy: Electron and Ion Microprobe Analysis*. Springer Science & Business Media, 2012.

[120] D. B. Holt and D. Joy, *SEM Microcharacterization of Semiconductors*. Academic Press, 2013.

[121] Y. Liu, L. Hong, *et al.*, “Ion-exchange and adsorption of Fe(III) by Sepia melanin,” *Pigment Cell Res.*, vol. 17, no. 3, pp. 262–269, 2004.

[122] J. Goldstein, D. Newbury, *et al.*, *Scanning Electron Microscopy and X-Ray Microanalysis*, vol. 215, no. 4532. 2003.

[123] S. Hofmann, *Auger-and X-ray Photoelectron Spectroscopy in Materials Science: A User-Oriented Guide*. Springer Science & Business Media, 2012.

[124] P. S. Bagus, E. S. Ilton, and C. J. Nelin, “The interpretation of XPS spectra: insights into materials properties,” *Surf. Sci. Rep.*, vol. 68, no. 2, pp. 273–304, 2013.

[125] N. S. Faradzhev, S. B. Hill, and C. J. Powell, “Quantitative analysis of trace levels of

surface contamination by X-ray photoelectron spectroscopy. Part II: systematic uncertainties and absolute quantification," *Surf. Interface Anal.*, vol. 49, no. 12, pp. 1214–1224, 2017.

[126] H. J. Guzmán, F. Isquierdo, *et al.*, "X-ray photoelectron spectroscopy analysis of hydrotreated athabasca asphaltenes," *Energy and Fuels*, vol. 31, no. 10, pp. 10706–10717, 2017.

[127] V. Esen, S. Saglam, and B. Oral, "Light sources of solar simulators for photovoltaic devices : a review," *Renew. Sustain. Energy Rev.*, vol. 77, pp. 1240–1250, 2017.

[128] A. K. Gaigalas and L. Wang, "Measurement of the fluorescence quantum yield using a spectrometer with an integrating sphere detector," *J. Res. Natl. Inst. Stand. Technol.*, vol. 113, no. 1, pp. 17–28, 2008.

[129] P. Meredith, B. J. Powell, *et al.*, "Towards structure-property-function relationships for eumelanin," *Soft Matter*, vol. 2, no. 1, pp. 37–44, 2006.

[130] R. Xu, C. T. Prontera, *et al.*, "An electrochemical study of natural and chemically controlled eumelanin," *APL Mater.*, vol. 5, no. 12, p. 126108, 2017.

[131] G. Prota, *Melanins and Melanogenesis*. San Diego: Academic Press, 1992.

[132] M. D'Ischia, K. Wakamatsu, *et al.*, "Melanins and melanogenesis: from pigment cells to human health and technological applications," *Pigment Cell Melanoma Res.*, vol. 28, no. 5, pp. 520–544, Sep. 2015.

[133] P. Meredith, K. Tandy, and A. Mostert, "A hybrid ionic-electronic conductor: melanin, the first organic amorphous semiconductor?," in *Organic Electronics: Emerging Concepts and Technologies*, Wiley, 2013, pp. 91–111.

[134] B. Larsson and H. Tjälve, "Studies on the melanin-affinity of metal ions," *Acta Physiol. Scand.*, vol. 104, no. 4, pp. 479–484, Dec. 1978.

[135] L. Hong and J. D. Simon, "Current understanding of the binding sites, capacity, affinity, and biological significance of metals in melanin," *J. Phys. Chem. B*, vol. 111, no. 28, pp. 7938–7947, 2007.

[136] S. Gidanian and P. J. Farmer, "Redox behavior of melanins : direct electrochemistry of

dihydroxyindole-melanin and its Cu and Zn adducts," *J. Inorg. Biochem.*, vol. 89, pp. 54–60, 2002.

[137] A. Pezzella, M. D'Ischia, *et al.*, "An integrated approach to the structure of sepia melanin. evidence for a high proportion of degraded 5, 6-dihydroxyindole-2-carboxylic acid units in the pigment backbone," *Tetrahedron*, vol. 53, no. 24, pp. 8281–8286, 1997.

[138] Y. Liu and J. D. Simon, "The effect of preparation procedures on the morphology of melanin from the ink sac of Sepia officinalis," *Pigment Cell Res.*, vol. 16, pp. 72–80, 2003.

[139] T. Sakaguchi and A. Nakajima, "Accumulation of uranium by biopigments," *Chem. Technol. Biotechnol.*, vol. 40, no. 2, pp. 133–141, 1987.

[140] J. Mähler and I. Persson, "A study of the hydration of the alkali metal ions in aqueous solution," *Inorg. Chem.*, vol. 51, pp. 425–438, 2012.

[141] P. Prem, K. Dube, S. Madison, and J. Bartolone, "New insights into the physicochemical effects of ammonia/peroxide bleaching of hair and Sepia melanins," *J. Cosmet. Sci.*, vol. 54, p. 4395, 2003.

[142] A. Napolitano and A. Peuella, "New pyrrole acids by oxidative degradation of eumelanins with hydrogen peroxide. Further hints to the mechanism of pigment breakdown," *Tetrahedron*, vol. 52, no. 26, pp. 8775–8780, 1996.

[143] E. Di Mauro, O. Carpentier, *et al.*, "Resistive switching controlled by the hydration level in thin films of the biopigment eumelanin," *J. Mater. Chem. C*, vol. 4, no. 40, pp. 9544–9553, 2016.

[144] R. Xu, A. Gouda, *et al.* "Light-enhanced electrochemical energy storage of synthetic melanin on conductive glass substrates," *MRS Adv.*, vol. 5, no. 27–28, pp. 1441–1448, 2020.

[145] International Energy Agency, "World Energy Outlook 2017," 2017.

[146] N. Armaroli and V. Balzani, *Powering planet Earth: Energy Solutions For the Future*. John Wiley and Sons, 2012.

[147] A. S. Arico, P. Bruce, *et al.*, "Nanostructured materials for advanced energy conversion and storage devices," in *Materials for Sustainable Energy: A Collection of Peer-Reviewed*

Research and Review Articles from Nature Publishing Group, 2011, pp. 148–159.

[148] N. Vlachopoulos and A. Hagfeldt, "Photobatteries and photocapacitors," in *Molecular Devices for Solar Energy Conversion and Storage*, Springer, 2018, pp. 281–325.

[149] D. Vonlanthen, P. Lazarev, *et al.*, "A stable polyaniline-benzoquinone-hydroquinone supercapacitor," *Adv. Mater.*, vol. 26, no. 30, pp. 5095–5100, 2014.

[150] M. Jastrzebska, A. Kocot, and L. Tajber, "Photoconductivity of synthetic dopa-melanin polymer," *J. Photochem. Photobiol. B Biol.*, vol. 66, no. 3, pp. 201–206, 2002.

[151] P. Meredith, C. J. Bettinger, *et al.*, "Electronic and optoelectronic materials and devices inspired by nature," *Rep. Prog. Phys.*, vol. 76, no. 3, p. 034501, 2013.

[152] G. Mula, L. Manca, S. Setzu, and A. Pezzella, "Photovoltaic properties of PSi impregnated with eumelanin," *Nanoscale Res. Lett.*, vol. 7, pp. 1–21, 2012.

[153] A. Antidormi, C. Melis, E. Canadell, and L. Colombo, "Assessing the performance of eumelanin/Si interface for photovoltaic applications," *J. Phys. Chem. C*, vol. 121, no. 21, pp. 11576–11584, 2017.

[154] L. K. Povlich, J. Le, J. Kim, and D. C. Martin, "Poly(5,6-dimethoxyindole-2-carboxylic acid) (PDMICA): a melanin-like polymer with unique electrochromic and structural properties," *Macromolecules*, vol. 43, pp. 3770–3774, 2010.

[155] R. Xu, F. Soavi, C. Santato, and M. D. Monte, "An electrochemical study on the effect of metal chelation and reactive oxygen species on a synthetic neuromelanin model," *Front. Bioeng. Biotechnol.*, vol. 7, pp. 1–11, 2019.

[156] C. D. Marsden, "Pigmentation in the nucleus substantiae nigrae of mammals.," *J. Anat.*, vol. 95, pp. 256–61, 1961.

[157] L. Zecca, R. Fariello, *et al.*, "The absolute concentration of nigral neuromelanin, assayed by a new sensitive method, increases throughout the life and is dramatically decreased in Parkinson's disease," *FEBS Lett.*, vol. 510, no. 3, pp. 216–220, 2002.

[158] K. L. Double, V. N. Dedov *et al.*, "The comparative biology of neuromelanin and lipofuscin in the human brain," *Cell. Mol. Life Sci.*, vol. 65, no. 11, pp. 1669–1682, 2008.

[159] L. Hong, Y. Liu, and J. D. Simon, "Binding of metal ions to melanin and their effects on

the aerobic reactivity.," *Photochem. Photobiol.*, vol. 80, no. 3, pp. 477–481, 2004.

[160] W. Korytowski and T. Sarna, "Bleaching of melanin pigments," *J. Biol. Chem.*, vol. 265, no. 21, pp. 12410–12416, 1990.

[161] R. A. W. Smith, B. Garrett *et al.*, "Mechanistic insights into the bleaching of melanin by alkaline hydrogen peroxide," *Free Radic. Biol. Med.*, vol. 108, pp. 110–117, 2017.

[162] T. Sarna, B. Pilas, E. J. Land, and T. G. Truscott, "Interaction of radicals from water radiolysis with melanin," *Biochim. Biophys. Acta.*, vol. 883, no. 1, pp. 162–167, 1986.

[163] F. A. Zucca, J. Segura-Aguilar *et al.*, "Interactions of iron, dopamine and neuromelanin pathways in brain aging and Parkinson's disease," *Prog. Neurobiol.*, vol. 155, pp. 96–119, 2017.

[164] E. Brillas, I. Sirés, and M. A. Oturan, "Electro-Fenton process and related electrochemical technologies based on fenton's reaction chemistry," *Chem. Rev.*, vol. 109, no. 12, pp. 6570–6631, 2009.

[165] L. Zecca, F. A. Zucca, H. Wilms, and D. Sulzer, "Neuromelanin of the substantia nigra: a neuronal black hole with protective and toxic characteristics," *Trends Neurosci.*, vol. 26, no. 11, pp. 578–580, 2003.

[166] B. Beverskog and I. Puigdomenech, "Revised pourbaix diagrams for iron at 25–300 °C," *Corros. Sci.*, vol. 38, no. 12, pp. 2121–2135, 1996.

[167] L. Zecca, C. Bellei, *et al.*, "New melanic pigments in the human brain that accumulate in aging and block environmental toxic metals.," *Proc. Natl. Acad. Sci. U. S. A.*, vol. 105, no. 45, pp. 17567–17572, 2008.

[168] B. T. Chen, M. V Avshalumov, *et al.*, "H_2O_2 is a novel, endogenous modulator of synaptic dopamine release," *J. Neurophysiol.*, vol. 85, no. 6, pp. 2468–2476, 2001.

[169] C. Kortleven, C. Fasano, *et al.*, "The endocannabinoid 2-arachidonoylglycerol inhibits long-term potentiation of glutamatergic synapses onto ventral tegmental area dopamine neurons in mice," *Eur. J. Neurosci.*, vol. 33, no. 10, pp. 1751–1760, 2011.

[170] J. F. Atherton, D. L. Wokosin, S. Ramanathan, and M. D. Bevan, "Autonomous initiation and propagation of action potentials in neurons of the subthalamic nucleus," *J. Physiol.*,

vol. 586, no. 23, pp. 5679–5700, 2008.

[171] T. G. Costa, R. Younger, *et al.*, “Studies on synthetic and natural melanin and its affinity for Fe(III) ion,” *Bioinorg. Chem. Appl.*, vol. 2012, no. Iii, pp. 1–9, 2012.

[172] W. Yang, C. Liu, and Y. Chen, “Stability of polydopamine coatings on gold substrates inspected by surface plasmon resonance imaging,” *Langmuir*, vol. 34, no. 12, pp. 3565–3571, 2018.

[173] E. J. Son, J. H. Kim, K. Kim, and C. B. Park, “Quinone and its derivatives for energy harvesting and storage materials,” *J. Mater. Chem. A*, vol. 4, no. 29, pp. 11179–11202, 2016.

[174] W. G. Cook and R. P. Olive, “Pourbaix diagrams for the iron-water system extended to high-subcritical and low-supercritical conditions,” *Corros. Sci.*, vol. 55, pp. 326–331, 2012.

[175] Y.-J. Oh, G.-S. Park, and C.-H. Chung, “Planarization of copper layer for damascene interconnection by electrochemical polishing in alkali-based solution,” *J. Electrochem. Soc.*, vol. 153, no. 7, p. G617, 2006.

[176] W. D. Bush and J. D. Simon, “Quantification of Ca^{2+} binding to melanin supports the hypothesis that melanosomes serve a functional role in regulating calcium homeostasis,” *Pigment Cell Res.*, vol. 20, no. 2, pp. 134–139, 2007.

[177] R. W. Style, A. Jagota, C.-Y. Hui, and E. R. Dufresne, “Elastocapillarity: surface tension and the mechanics of soft solids,” *Annu. Rev. Condens. Matter Phys.*, vol. 8, pp. 99–118, 2017.

[178] F. Wu, Y. Ye, *et al.*, “Gluing carbon black and sulfur at nanoscale: a polydopamine-based ‘nano-binder’ for double-shelled sulfur cathodes,” *Adv. Energy Mater.*, vol. 7, no. 3, pp. 1–10, 2017.

[179] E. Sato, S. Iki, *et al.*, “Dismantlable adhesion properties of reactive acrylic copolymers resulting from cross-linking and gas evolution,” *J. Adhes.*, vol. 93, no. 10, pp. 811–822, 2017.

[180] C. Wu, X. Tang, *et al.*, “High-adhesion stretchable electrode via cross-linking intensified

electroless deposition on a biomimetic elastomeric micropore film," *ACS Appl. Mater. Interfaces*, vol. 11, no. 22, pp. 20535–20544, 2019.

[181] J. Wang, Y. Chen, *et al.*, "Intelligent textiles with comfort regulation and inhibition of bacterial adhesion realized by cross-linking poly(n-isopropylacrylamide-co-ethylene glycol methacrylate) to cotton fabrics," *ACS Appl. Mater. Interfaces*, vol. 9, no. 15, pp. 13647–13656, 2017.

[182] M. J. Gidley and G. E. Yakubov, "Functional categorisation of dietary fibre in foods: Beyond 'soluble' vs 'insoluble,'" *Trends Food Sci. Technol.*, vol. 86, no. January 2018, pp. 563–568, 2019.

[183] Y. Liu and J. D. Simon, "Metal-ion interactions and the structural organization of Sepia eumelanin," *Pigment Cell Res.*, vol. 18, no. 1, pp. 42–48, 2005.

[184] S. Mane, S. Ponrathnam, and N. Chavan, "Effect of chemical crosslinking on properties of polymer microbeads: a review," *Can. Chem. Trans.*, vol. 3, no. 4, pp. 473–485, 2016.

[185] R. Kohen, E. Beit-Yannai, E. M. Berry, and O. Tirosh, "Overall low molecular weight antioxidant activity of biological fluids and tissues by cyclic voltammetry," *Methods Enzymol.*, vol. 300, no. 1985, pp. 285–296, 1999.

[186] A. S. Saini and J. S. Melo, "Biosorption of uranium by melanin: Kinetic, equilibrium and thermodynamic studies," *Bioresour. Technol.*, vol. 149, pp. 155–162, 2013.

[187] B. Yu, J. Liu, S. Liu, and F. Zhou, "Pdop layer exhibiting zwitterionicity: a simple electrochemical interface for governing ion permeability," *Chem. Commun.*, vol. 46, no. 32, p. 5900, 2010.

[188] H. A. Azab, C. Luchinat, *et al.*, "Redox chemistry of superoxide dismutase. cyclic voltammetry of wild-type enzymes and mutants on functionally relevant residues," *Inorg. Chem.*, vol. 31, no. 22, pp. 4649–4655, 1992.

[189] Y. Sheng, I. A. Abreu, *et al.*, "Superoxide dismutases and superoxide reductases," *Chem. Rev.*, vol. 114, no. 7, pp. 3854–3918, 2014.

[190] M. D'Ischia, A. Napolitano, and A. Pezzella, "5,6-Dihydroxyindole chemistry : unexplored opportunities beyond eumelanin," *European J. Org. Chem.*, vol. 28, pp. 5501–

5516, 2011.

APPENDIX A – SUPPORTING INFORMATION OF ARTICLE 1

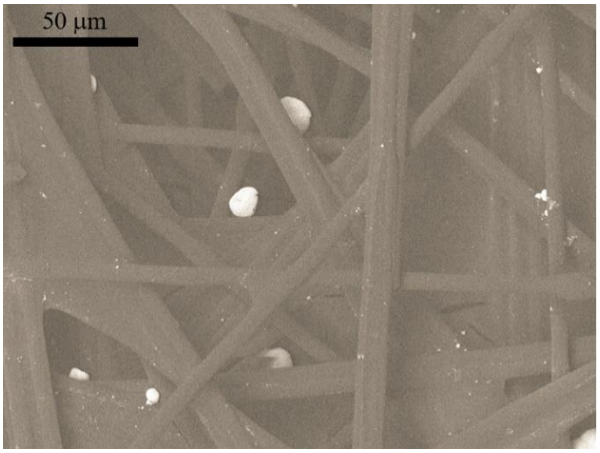

Figure S1 SEM images (backscattering mode, acceleration voltage 5 kV) of stained Sepia melanin on carbon paper. Bar size: 50 µm. Sepia melanin, with granules of different sizes and even debris, is mainly present at junctions of carbon fibers.

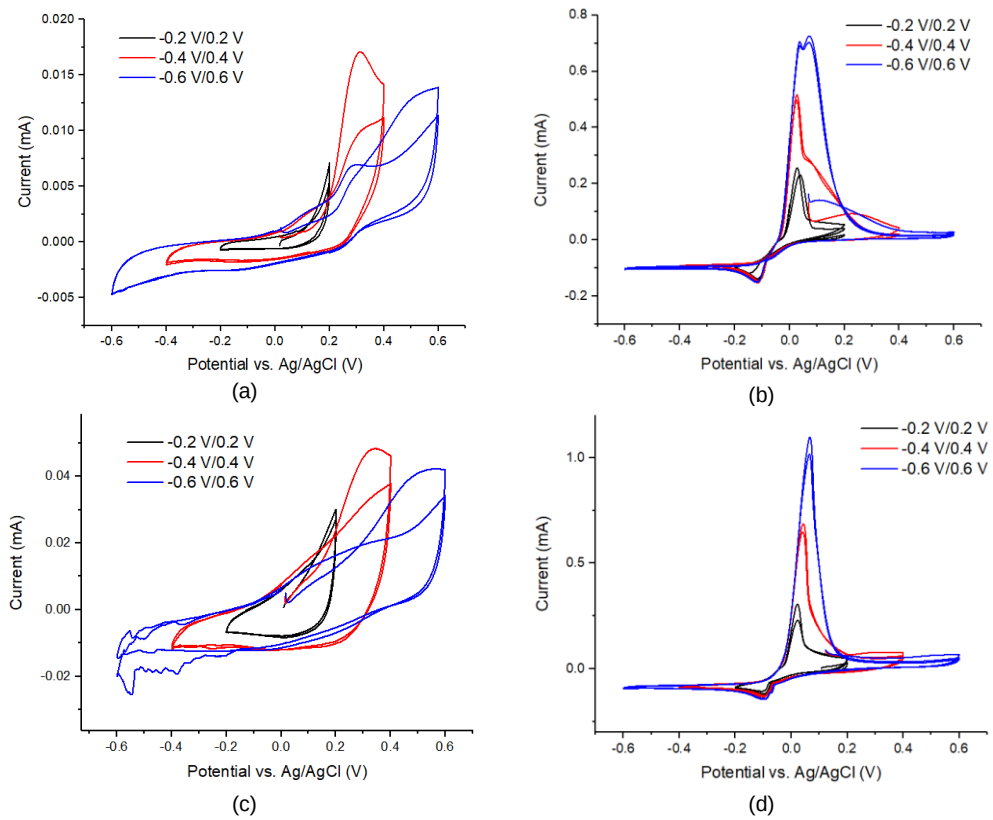

Figure S2 Early cycles at 1 mV/s for DHICA-melanin (a, b) and DHI-melanin (c, d) in $NaCH_3COO_{(aq)}$ (a, c) and $NH_4CH_3COO_{(aq)}$-including Cu(II) (b, d), for different ranges of the electrochemical potential. Instabilities are observables during the early cycles in DHI-melanin for the potential range -0.6 V/0.6 V, likely implying chemical changes.

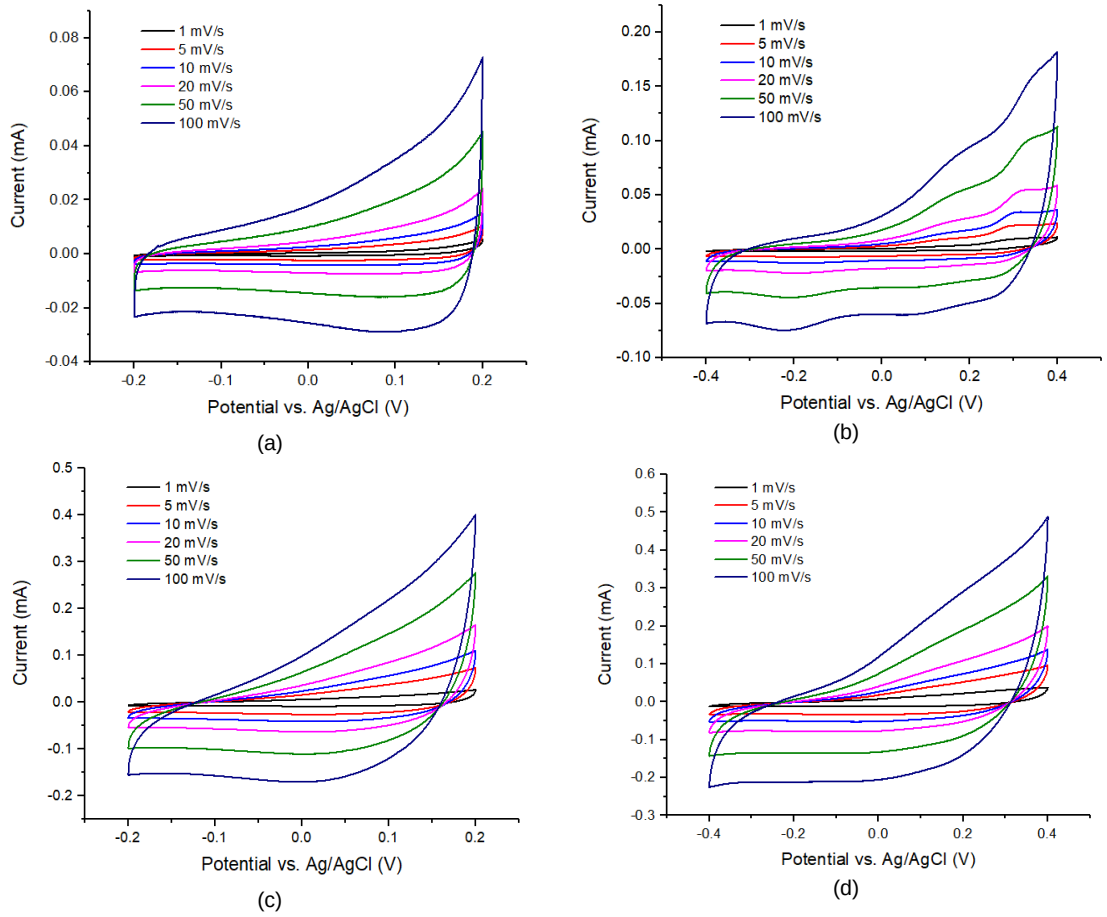

Figure S3 2nd cycle of a series of cyclic voltammograms obtained at different scan rates for DHICA-melanin (a, b) and DHI-melanin (c, d) in $NaCH_3COO_{(aq)}$, in the potential range -0.2/0.2 V (a, c) and -0.4/0.4 V (b, d).

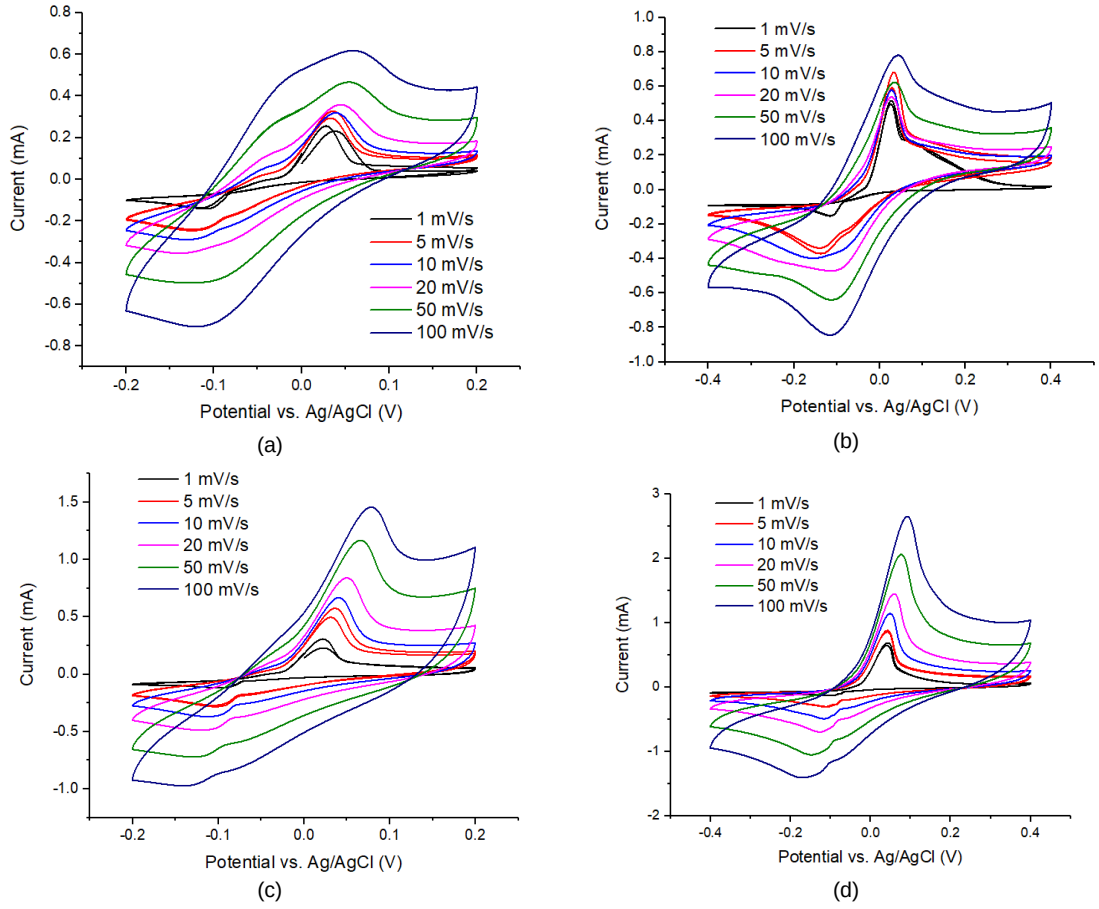

Figure S4 2nd and 3rd cycles (at 1 mV/s and 5 mV/s) and 2nd cycle (at the other scan rates) of a series of cyclic voltammograms of DHICA-melanin (a, b), DHI-melanin (c, d) in $Cu(CH_3COO)_2$-including $NH_4CH_3COO_{(aq)}$ in the potential range -0.2/0.2 V (a, c) and -0.4/0.4 V (b, d).

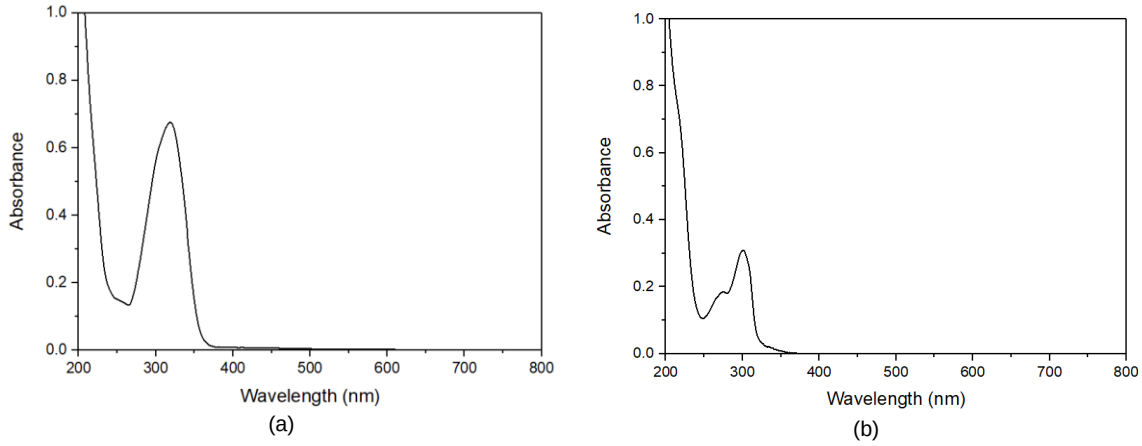

Figure S5 UV-vis spectra of monomers DHICA (a) and DHI (b) in methanol solution (50 μM).

The chemistry of DHI and DHICA monomers is discussed in [190]. The monomers were stored at -30 °C prior their use. The UV-vis spectra were obtained immediately after the monomers were dissolved in methanol (Sigma, anhydrous 99.8%) in ambient conditions, by a JASCO V-730 UV-visible spectrophotometer (Figure S5). The spectrum of DHI in methanol solution is similar to the solid-state monomers reported previously in the literature.[17] We cannot exclude the total absence of polymerization in solution prior to deposition on carbon and exposure to NH_3.

APPENDIX B – SUPPORTING INFORMATION OF ARTICLE 3

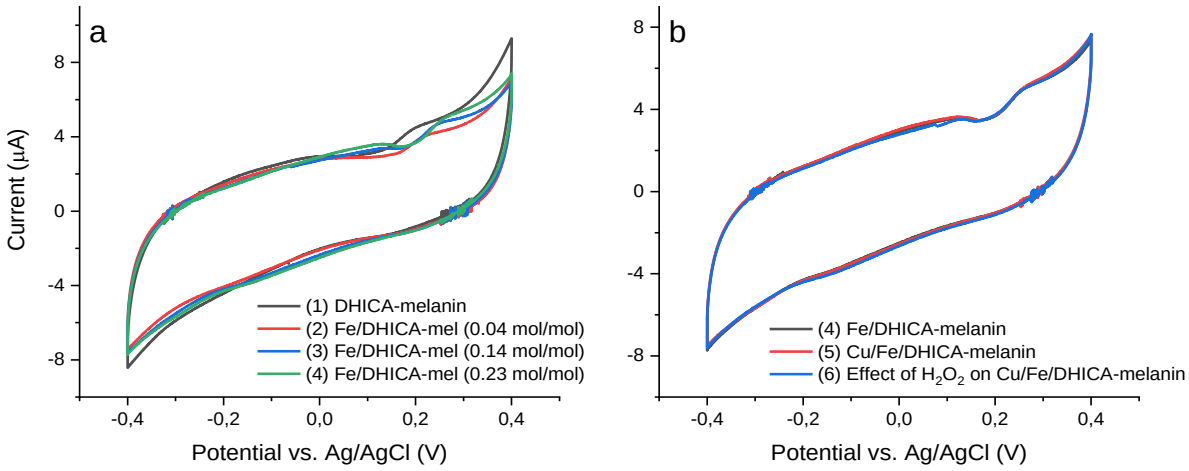

Figure S1 Effect of exposure to Fe^{3+}, Cu^{2+} and H_2O_2 on cyclic voltammograms of Type 1 DHICA-melanin (route ii, see main file and Table 6.1), at 5 mV/s, in the simulated neurological fluid pH 7. Protocol: 2 voltammetric cycles → add $Fe_2(SO_4)_3$ with Fe:DHICA-melanin 0.04 mol:mol → 2 voltammetric cycles → add $Fe_2(SO_4)_3$ with Fe:DHICA-melanin 0.14 mol:mol → 2 voltammetric cycles → add $Fe_2(SO_4)_3$ with Fe:DHICA-melanin 0.23 mol:mol → 2 voltammetric cycles → add $Cu(CH_3COO)_2$ with Cu:Fe:DHICA-melanin 0.002:0.23:1 mol:mol:mol → 2 voltammetric cycles → expose the Cu/Fe/DHICA-melanin complex sample in H_2O_2 solution (0.15 mM) → 2 voltammetric cycles. Only the second cycle is shown.

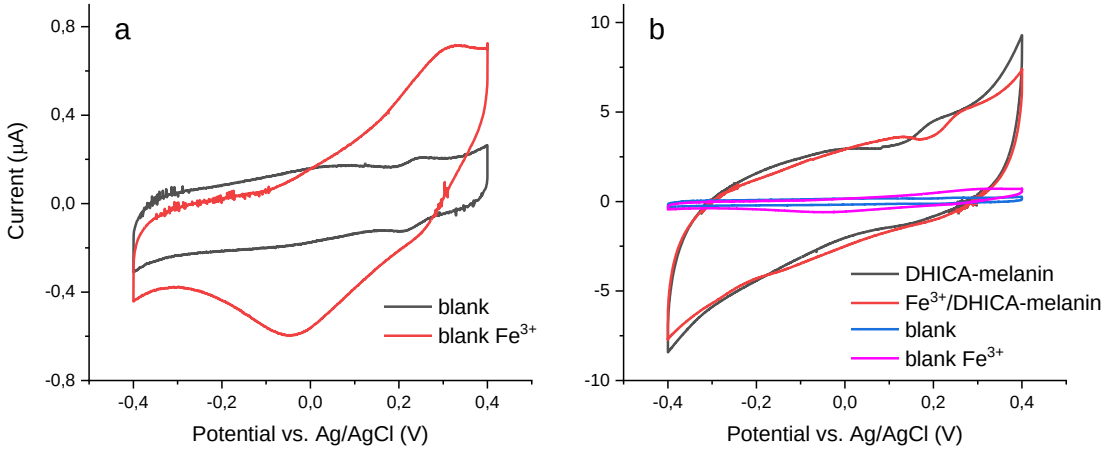

Figure S2 Effect of the presence of Fe^{3+} on cyclic voltammograms of (a) blank carbon paper and (b) Fe/DHICA-melanin (Type 1 DHICA-melanin, Fe^{3+}: DHICA-melanin (0.23 mol:mol) extracted from Figure S2) and blank carbon paper, each for two cycles, at 5 mV/s, in the simulated neurological fluid electrolyte (pH 7). The concentration of Fe^{3+} with blank carbon paper corresponds to Fe^{3+}: melanin (0.2 mol:mol). Only the second cycle is shown.

Without melanin, a blank carbon paper with Fe^{3+} in the electrolyte, corresponding to Fe: melanin 0.2 mol:mol, shows additional redox features with respect to carbon paper without Fe^{3+} in the electrolyte, i.e. an oxidation feature at ca 0.3 V vs. Ag/AgCl (3 M NaCl) and two reduction features at ca 0.3 V and ca 0 V (Figure S4). Therefore, even though the magnitude of currents of blank carbon is ca 10 times lower than Fe/DHICA-melanin, we cannot exclude the possibility that the anodic potential shift of the oxidation feature of Fe/DHICA-melanin can be partially due to the redox features of Fe^{3+} (Figure S2b).

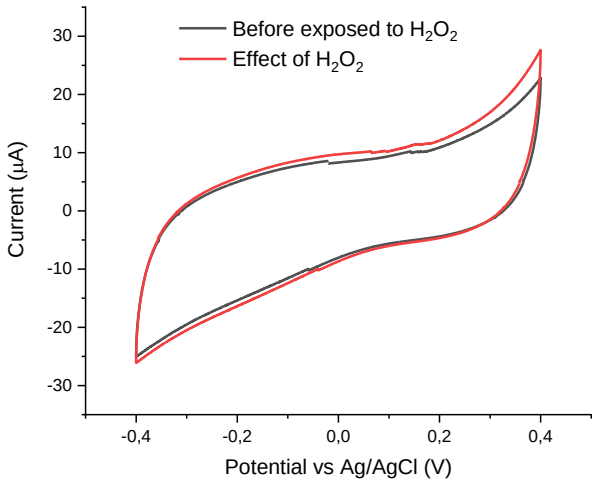

Figure S3 Effects of H_2O_2 on cyclic voltammograms of DHI-melanin at 5 mV/s, each for two cycles, in the simulated neurological fluid electrolyte (pH 7). Only the second cycle is shown.

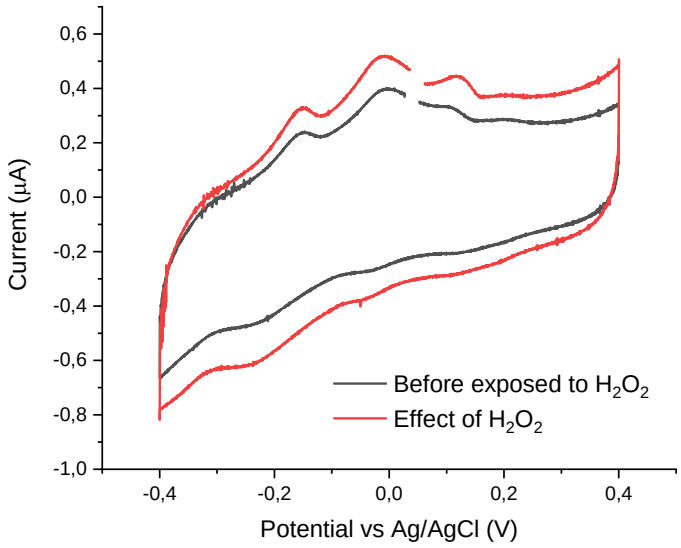

Figure S4 Effect of H_2O_2 on the cyclic voltammogram of bare carbon current collector at 5 mV/s, each for two cycles, in the simulated neurological fluid electrolyte (pH 7). Only the second cycle is shown.

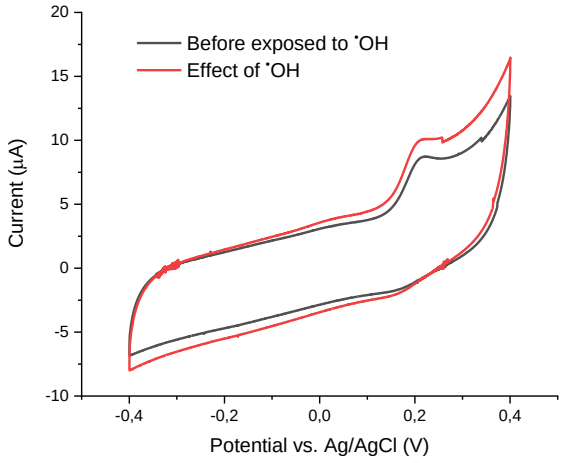

Figure S5 Effects of •OH on cyclic voltammograms of Type 1 DHICA-melanin at 5 mV/s, each for two cycles. •OH was obtained from the Fenton reaction ($3FeSO_4 + 3H_2O_2 \rightarrow Fe_2(SO_4)_3 + 3^{\bullet}OH + Fe(OH)_3$). The concentration of Fe^{2+} added corresponds to the molar ratio Fe:melanin 0.2 mol:mol, in the simulated neurological fluid electrolyte (pH 7). Only the second cycle is shown.

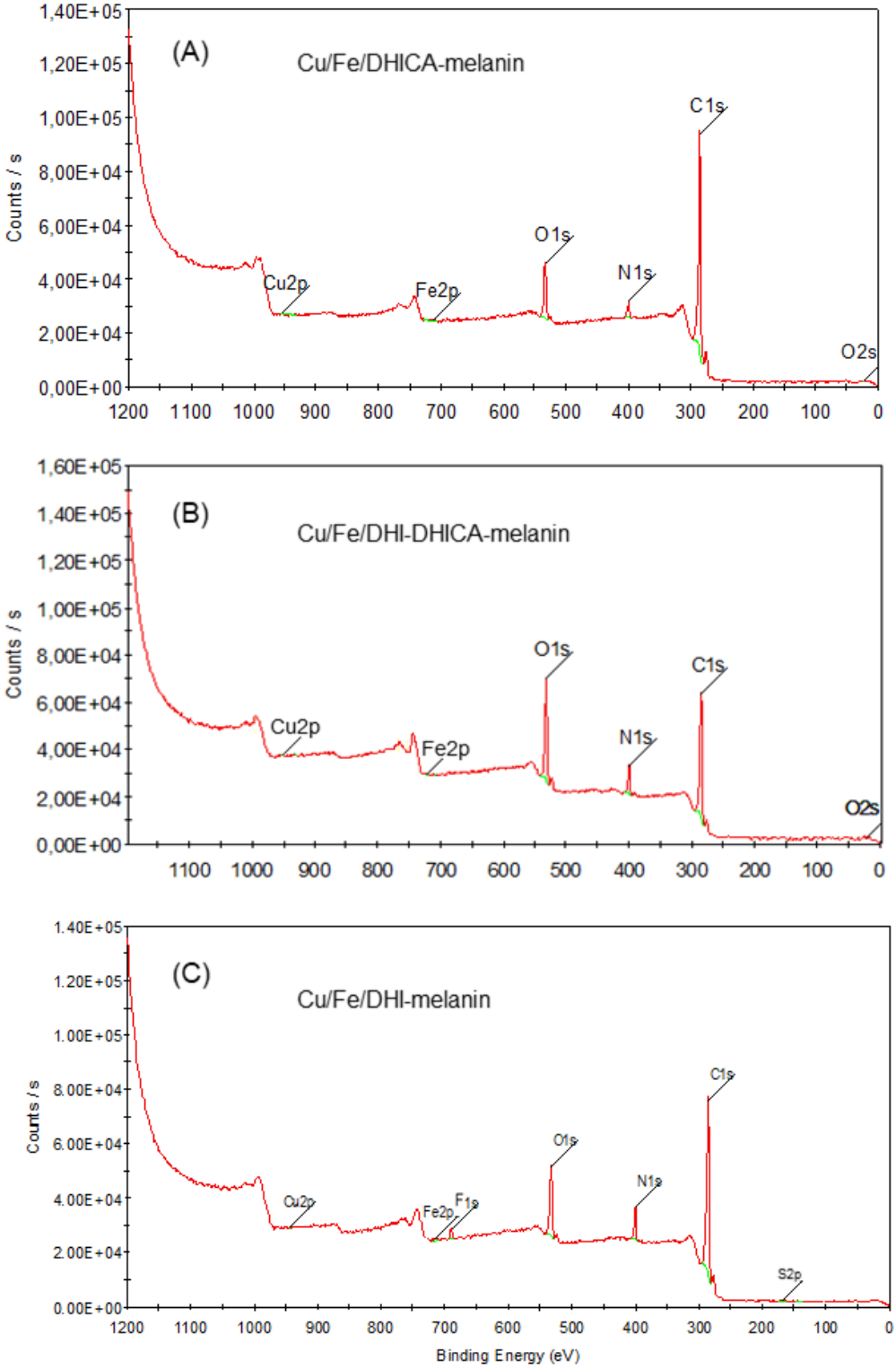

Figure S6 XPS survey scan of **(A)** Cu/Fe/DHICA-melanin, **(B)** Cu/Fe/DHI-DHICA-melanin and **(C)** Cu/Fe/DHI-melanin loaded on carbon paper prepared by pre-immersion (route i) (Table S1).

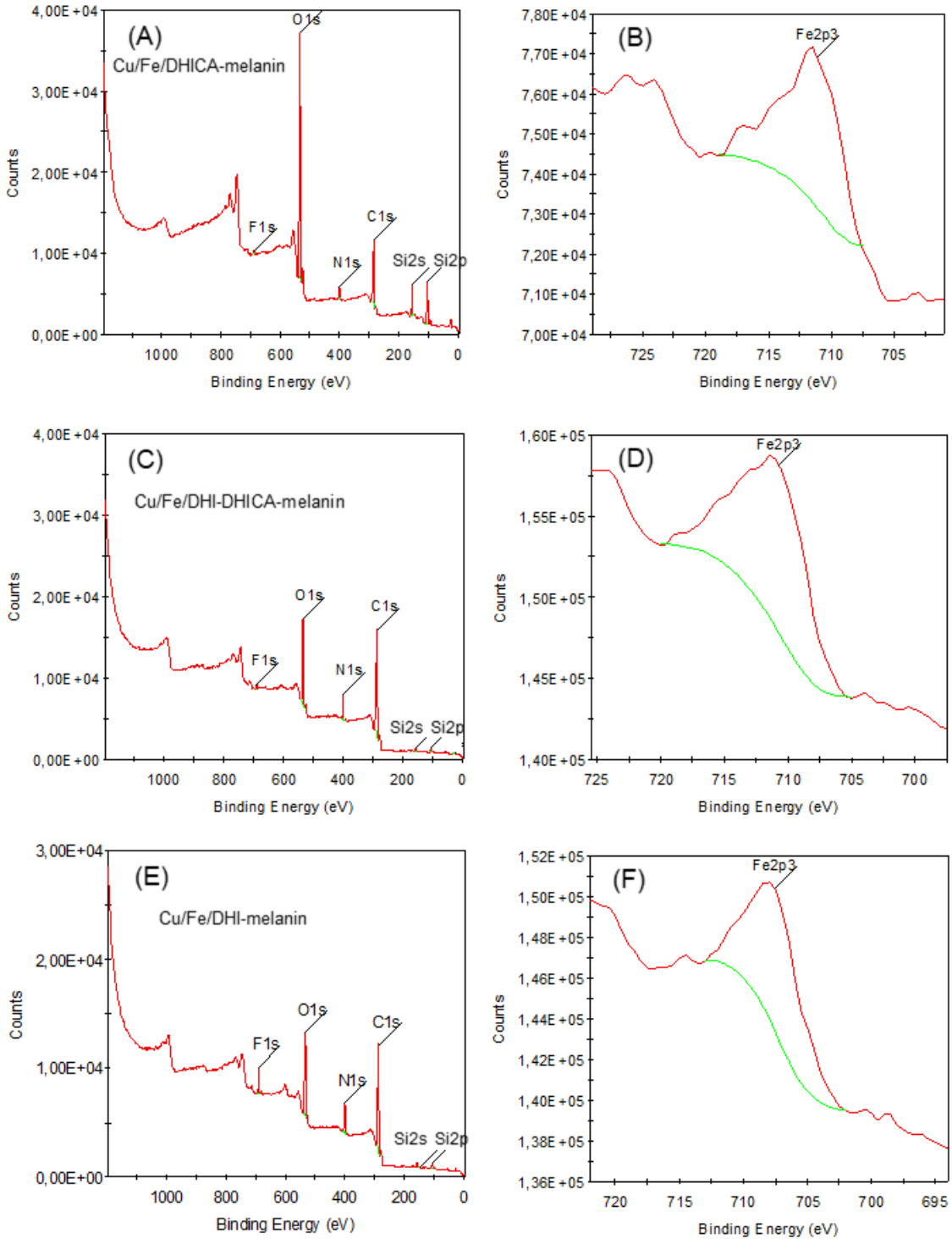

Figure S7 XPS survey scans of **(A) (B)** Cu/Fe/DHICA-melanin, **(C) (D)** Cu/Fe/DHI-DHICA-melanin and **(E) (F)** Cu/Fe/DHI-melanin loaded on fused silica (Table S2). **(B) (D) (F)** are survey scans on Fe 2p.

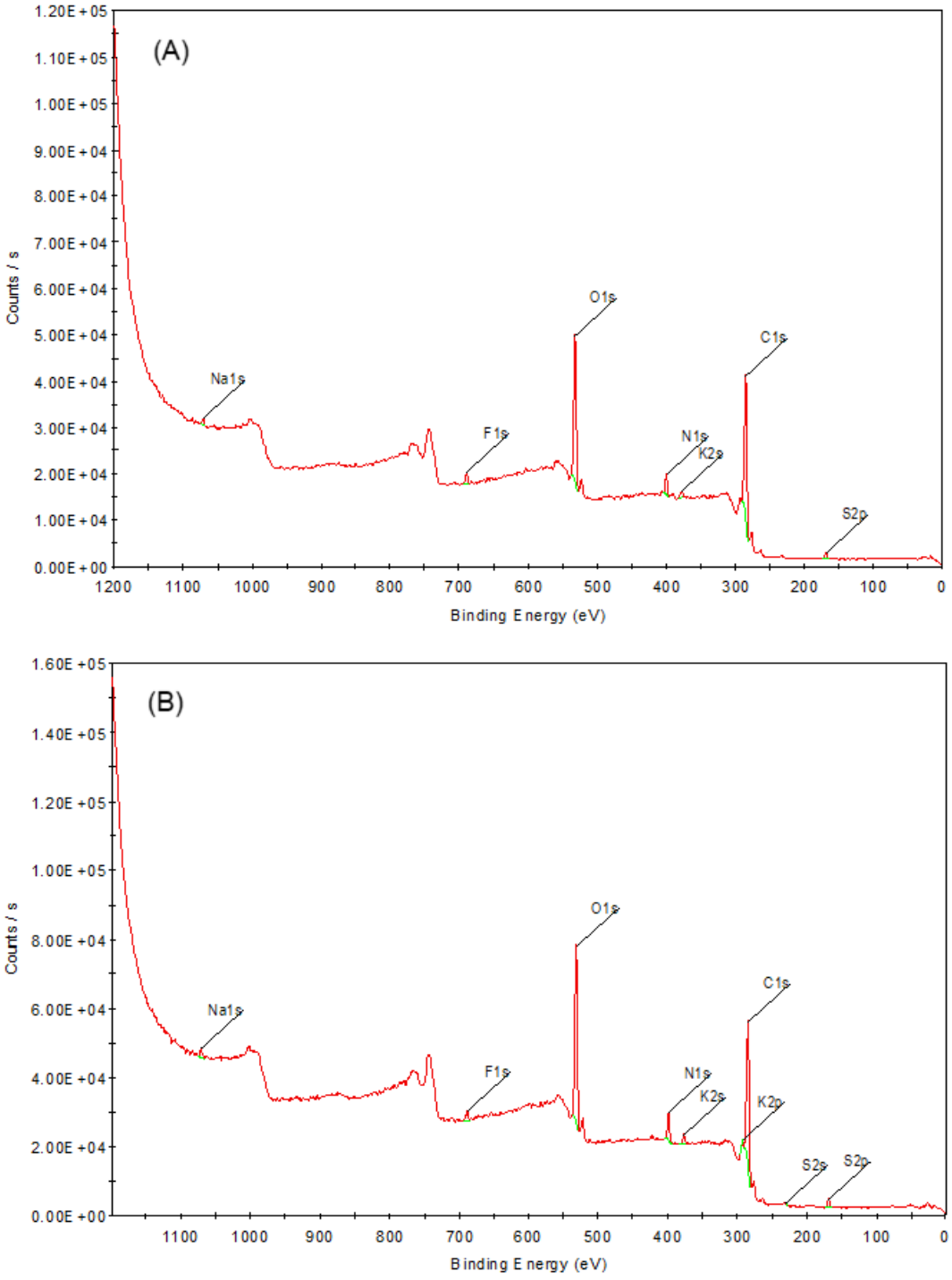

Figure S8 XPS survey scan of DHI-DHICA-melanin for C1s after (A) precycled, (B) cycled after effect of H_2O_2 (Figure S9 and Table S2), in the simulated neurological fluid electrolyte (pH 7).

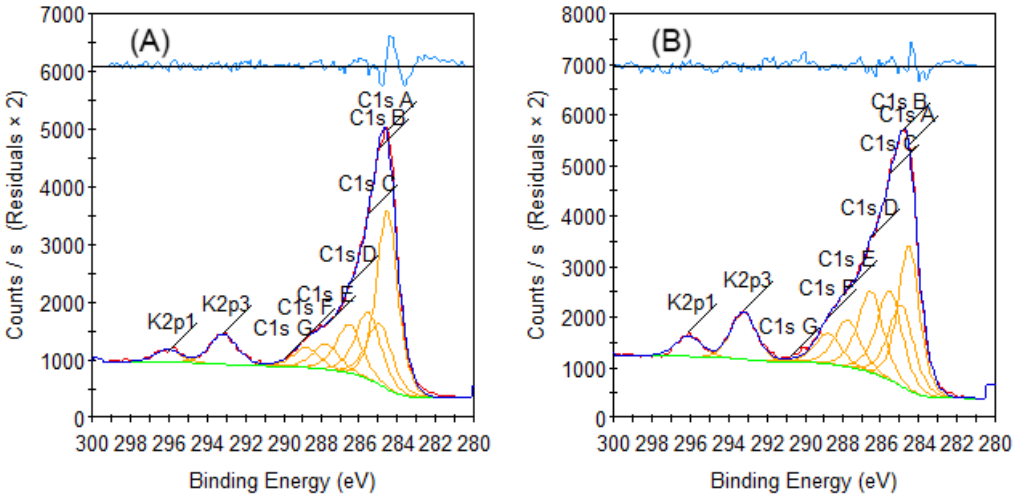

Figure S9 XPS spectra of DHI-DHICA-melanin for C1s after **(A)** precycled, **(B)** cycled after effect of H_2O_2 (Figure S8 and Table S2), in the simulated neurological fluid electrolyte (pH 7).

Table S1 Identification and quantification of elements in Cu/Fe/melanin samples loaded on carbon paper obtained by XPS survey scan (Figure S6).

Orbital of the atom	Binding Energy (eV)	Relative Atomic % (at%)		
		Cu/Fe/DHICA-melanin	Cu/Fe/DHI-DHICA-melanin	Cu/Fe/DHI-melanin
C 1s	285.0	86.3	68.1	77.6
N 1s	399.6	2.9	8.6	7.4
O 1s	531.9	10.8	23.3	13.3
Fe 2p3	711.2	-	-	0.2
Cu 2p3	934.7	Traces	-	-

Table S2 Identification and quantification of elements in Cu/Fe/melanin samples loaded on fused silica obtained by XPS survey scan (Figure S7). Results averaged over three spots.

Orbital of the atom	Binding Energy (eV)	Relative Atomic % (at%)		
		Cu/Fe/DHICA-melanin	Cu/Fe/DHI-DHICA-melanin	Cu/Fe/DHI-melanin
Si 2p	104.9	15.4	2.5	3.4
C 1s	284.8	35.2	62.4	62.4
N 1s	399.6	3.2	7.0	8.8
O 1s	531.9	45.4	26.9	22.2
F 1s	688.9	0.3	1.0	2.9
Fe 2p3	711.0	0.4	0.6	0.4
Cu 2p3	934.7	-	-	-

The DHICA-melanin sample shows ca half of the amount of C 1s and N 1s with respect to DHI-melanin and DHI-DHICA-melanin, possibly due to the experimentally observed partial dissolution of the DHICA-melanin component in the pre-immersed solution (Table S2).

Table S3 Identification of chemical bonding by high resolution XPS for DHI-DHICA-melanin (Figure S8 and S9).

Orbital of the atom	Binding Energy (eV)	Identification	Relative Atomic % (at%)	
			DHI-DHICA-melanin before exposure to H_2O_2	DHI-DHICA-melanin after exposure to H_2O_2
C 1s	284.6	C=C	26.0	16.3
	285.0	C-C	10.6	10.9
	285.5	C-N	11.7	12.0
	286.5	C-O	8.6	10.9
	287.7	C=O	4.4	6.3
	288.8	O-C=O	3.5	4.1
	290.7	$\pi \rightarrow \pi^*$ of C=C	0.3	0.2
N 1s	398.5	C=N	0.4	0.7
	400.2	C-N	5.3	5.1
O 1s	531.3	C=O	5.6	6.3
	531.6	O*=C-O	4.8	4.1
	532.3	C-OH aliphatic	7.8	10.3
	533.0	O=C-O*	4.9	4.1
	533.6	C-OH aromatic	5.4	7.2
	535.5	H_2O	0.7	1.3

*Indicates that the identification pertains to this atom.

APPENDIX C – PARTICIPATION TO CONFERENCES

1. R. Xu, C. T. Prontera, L. G. S. Albano, E. Di Mauro, S. Zhang, P. Kumar and C. Santato, “Shedding light on the hydration-dependent electrical conductivity in eumelanin thin films”, 2016 Materials Research Society (MRS) Fall Meeting and Exhibit, Materials Research Society, Poster; Boston, USA, 28/11/2016;

2. R. Xu, C. T. Prontera, L. E. Di Mauro, A. Pezzella, F. Soavi and C. Santato, “Electrochemical properties of chemically controlled eumelanin”, 2017 MRS Fall Meeting and Exhibit, Materials Research Society, Oral; Boston, USA, 29/11/2017;

3. R. Xu, F. Soavi and C. Santato, “Electrochemical studies on molecular models of neuromelanin”, 69th Annual Meeting of the International Society of Electrochemistry (ISE), Poster, Bologna, Italy, 2/9/2018.

4. R. Xu, A. Gouda, F. Soavi and C. Santato, “Solar light harvesting enhances the energy storage performance of melanin-based electrodes”, 69th Annual Meeting of the International Society of Electrochemistry (ISE), Poster, Bologna, Italy, 3/9/2018.